Computational Insights into the Antimicrobial Mechanism of Action of Class II Bacteriocins.

A DISSERTATION SUBMITTED TO THE FACULTY OF THE GRADUATE SCHOOL OF THE UNIVERSITY OF MINNESOTA

BY

PANAGIOTA KYRIAKOU

IN PARTIAL FULLFILLMENT OF THE REQUIREMENTS FOR THE DEGREE OF DOCTOR OF PHILOSOPHY.

YIANNIS KAZNESSIS, ADVISOR

MAY 2017

Acknowledgments

First, and foremost, thank you to my Advisor, Professor Yiannis Kaznessis, for giving me the opportunity to join his group and for his continuous support during my doctoral studies. Whether I had a question about research or my career, Yiannis's door was always open. The skills and knowledge I gained from working in the Kaznessis group will stay with me in all my future endeavors.

I am grateful to Prodromos Daoutidis, Joseph Zasadzinski, and Jonathan Sachs for their willingness to serve as my committee members and for their brilliant comments, suggestions, and advice. I also want to thank our collaborators in the Nissen-Meyer group at the University of Oslo, especially Dr. Per E. Kristiansen, for providing much-needed experimental insight into my work.

I would like to acknowledge the support of my current and previous groupmates in the Kaznessis group, particularly Brittany Forkus and Michael Vlysidis, who go far beyond being just colleagues and groupmates. Their support and friendship was indispensable throughout my studies. I would like to extend my thanks to all the people in CEMS who were a part of my life these past five years.

I was lucky to meet people who not only made my stay in Minneapolis enjoyable, but also contributed to my development as a person. Angelika, Sofia, and Smaro created a feeling of family for me here and I am eternally thankful for that. Moreover, I am grateful to the entire Greek community in Minneapolis, and to my friends back in Greece, for their tireless support. Special thanks to my close friend, Stavroula, who stayed with me in Minneapolis for three months to help me through a challenging time.

Finally, I would like to express my immense gratitude to my parents, my brother, and the rest of my family for the love and endless support with which they surround me. They were with me through every step, every challenge, and every success. Finally, I would like to thank my partner, Tyler, for making my life happier the last two years. His genuine support, love, and encouragement played a key role in achieving my goals.

To my family

Abstract

Antibiotic resistance is a global problem and poses an alarming threat to public health. Microorganisms resistant to all commercially available antibiotics have emerged, undermining the ability to fight infectious diseases. The antibiotic resistance crisis has been attributed to the overuse of antibiotics, as well as a lack of new drug development. Coordinated efforts are needed to overcome this challenge, including discovery of alternative drugs.

Bacteriocins are bacteria-produced, antimicrobial peptides that are potentially powerful antibiotic drug candidates. Despite considerable scientific interest around bacteriocins, and despite their promise as potent, latent antibiotics, their everyday medical value has been negligible. In order to more effectively utilize the full potential of bacteriocins as a platform to develop new antibacterial agents, a detailed understanding of their mechanism of action is required. This mechanistic insight will offer ways to control and optimize their activity and selectivity against specific pathogens, greatly enhancing their potential for medical applications. The goal of this work is to elucidate the mechanism of action of class II bacteriocins by employing a variety of computational methods that are built around atomistic molecular dynamics simulations.

First, we studied Plantaricin EF, a two-peptide class IIb bacteriocin. This bacteriocin was simulated in different environments including water, micelles, and lipid bilayers. The interaction between the two peptides that promotes dimerization, and the interaction between the dimer and the membrane were elucidated. Guided by experimental studies, a transmembrane model of the dimer embedded in the bilayer was additionally designed. Results obtained from a 1 μs long atomistic molecular dynamics simulation, demonstrated for the first time that a bacteriocin, with a narrow antimicrobial activity range, can by itself form a water (and potentially ion) permeable, toroidal pore in a lipid bilayer. This pore was characterized in detail.

It is not unlikely that the mechanism of action of bacteriocins can involve poration of the membrane as well as receptor-mediation. Therefore, the interaction of a bacteriocin with its putative receptor was also examined. Lacking the structure of a receptor, we employed structure-prediction techniques in combination with docking calculations, and

molecular dynamics simulations. For the first time a class II bacteriocin-receptor complex was built, setting the ground for investigating the role that receptors play in the bactericidal activity of these antimicrobial peptides.

We believe that our findings could be of importance to the designing of new antibiotic agents, as it would guide the search for better bacteriocins toward peptides with improved activity and specificity, that form stable pores, increase water or ion permeability, and interact more efficiently with a receptor.

Table of Contents

List of Figures

List of Tables

Abbreviations

AMR	AntiMicrobial Resistance
CDC	Center for Disease Control and prevention
AMP	AntiMicrobial Peptide
MOA	Mechanism Of Action
FDA	Food and Drug Administration
GAIN	Generating Antibiotic Incentives Now
IM	Inner Membrane
OM	Outer Membrane
LAB	Lactic Acid Bacteria
MRSA	Methicillin-Resistant *Staphylococcus aureus*
VRE	Vancomycin-Resistant *Enterococcus faecalis*
Man-PTS	Mannose PhosphoTransferase System
UppP	Undecaprenyl pyrophosphate Phosphatase
TFE	2,2,2-TriFluoroEthanol
DPPC	DiPalmitoylPhosphatidylCholine
POPG	PalmitoylOleoylPhosphatidylGlycerol
POPC	PalmitoylOleoylPhosphatidylCholine
PlnEF	Plantaricin EF
PlnE	Plantaricin E
PlnF	Plantaricin F
DPC	DodecylPhosphoCholine
DOPG	DioleoylPhosphoGlycerol
DOPC	DioleoylPhosphoCholine
NMR	Nuclear magnetic resonance
PDB	Protein DataBank
PCA	Principal Component Analysis
MP	Membrane Protein

Chapter 1

Introduction

1.1. Antibiotic resistance (AMR) on the rise

Alexander Fleming's 1928 discovery of penicillin and its introduction into clinical use in 1940 transformed modern medicine. Humanity entered a new era of improved public health and quality of life [1]. For a short while, deadly microbial infections were thought to be a problem of the past. It was not long, though, before the first signs of antimicrobial resistance (AMR) to antibiotics became apparent [2]. In response, new antibiotic agents were introduced that would, in turn, ultimately face the same fate of developed resistance. The circle of the development of new antibiotic drugs and the responding emergence of resistance to them has continued for the last 70 years. Now, however, the utility of antibiotics is diminishing more rapidly than ever because of the increasing frequency of resistance appearing in bacteria.

In our times, it is an unfortunate reality that resistance has been found to all commercially available antibiotics, even to the so-called "last resort" ones like colistin [2–4]. The Center for Disease Control and Prevention (CDC) estimates that antibiotic-resistant bacteria infect 2,000,000 people each year in the US, while the global death toll of such infections reaches 700,000 annually [5,6]. In 2014, the World Health Organization (WHO) released a global report on surveillance of AMR, warning that we are approaching a "post-antibiotic" era where even minor bacterial infections could be deadly [7,8]. According to a review on AMR commissioned by the UK, the worldwide fatalities due to antibiotic resistant infections could reach 10 million by 2050 if the world takes no action to reverse the spread of these infections [5].

The potential impact of AMR not only increases the lethality of infectious diseases, but it also compromises the efficacy of treatments, surgeries, and other therapeutic procedures, including chemotherapy and transplantation [9]. In addition, AMR is already having significant economic impacts. In 2013, in the United States alone, $20 billion in increased medical expenses is attributed to AMR to pay for prolonged hospital stays, expanded health care needs, and the additional use of medications [6]. With such a

heavy economic burden, AMR is likely to devastate disproportionately lower-income countries [10]. Yet another significant problem caused by AMR is the stress inflicted upon the agricultural sector. New regulations for the use of antibiotics in food animals have been introduced in both the EU and the US over the last decade since the extensive use of antibiotics in farming has been identified as one of the most impactful sources of AMR's ongoing evolution [11,12].

The debate over the appropriate use of antibiotics in the food production industry has been going on for several decades [13]. It comes as no surprise that bacteria would develop resistance to antibiotic-polluted environments, such as farms that extensively use antimicrobial drugs, or in healthcare where antibiotics are misused for ambiguous medical purposes [14,15]. Much of the widespread human consumption of antimicrobial agents is unnecessary [6]. The CDC estimates that 50% of antibiotics prescriptions are not needed, while 80% of consumed antibiotic drugs in the U.S. are used in livestock production [6,16]. Interestingly, 1 in 5 antibiotic resistant infections is caused by bacteria transferred to humans through the food chain [6].

Despite the alarming increase of AMR around the globe, there has been a steady decline in the introduction of new antibacterial drugs to consumers [2]. For many years, pharmaceutical companies have not considered the development of new antibiotics to be a primary goal. They have focused their research on more profitable drugs that treat chronic conditions, which offer better returns on investments [17]. An example is given by a cost-benefit analysis by the Office of Health Economics of London: it was estimated that developing a drug to be used to treat a chronic disease (in this case, a neuromuscular disease) would result in that drug having a net present value of $1 billion, compared to only a $50 million value for developing a new antibiotic [18]. Moreover, medical and scientific communities are not producing new knowledge regarding antibiotic drug development. Remarkably, most antibiotics introduced in the last 30 years are mere analogues of older drugs, with only two new classes of systemic antibacterial antibiotics being developed in that period of time [19].

To encourage and expand antibiotic discovery in this barren era, we need to rekindle basic research, identify alternative sources, and develop new routes that could provide potential antibiotic agents. One promising alternative source of fresh antibiotic drugs that has been investigated extensively of late is the use of antimicrobial peptides.

1.2. Antimicrobial peptides (AMPs) as a solution

Antimicrobial peptides are small proteins produced by virtually all forms of life. AMPs and are part of the innate immune response system of the producer organism, and they can be bacteriostatic (stopping bacterial growth) or bactericidal (killing bacteria) [20,21]. In the face of increasing antibiotic resistance, AMPs have attracted the interest of much research over the last 20 years. To date, more than 2600 naturally occurring AMPs have been identified [22]. Collectively they demonstrate a broad spectrum of antibacterial and antiviral activity; while some of them can be highly specific, others exhibit activity against a wide array of different organisms [23].

AMPs are often cationic and amphiphilic, and they are typically relatively short (12 to 100 amino acids) [24]. When compared to larger proteins or immune cells, they offer many attractive features, such as diverse bactericidal mechanisms and a smaller size that leads to shorter production time and more rapid diffusion [25]. Although all AMPs share a few common features, they have a wide range of secondary structures and limited sequence homology among different groups. Most AMPs consist of two to four β-sheets or amphiphilic α-helices, with occasional loop and coil regions [23].

Antimicrobial peptides are produced by single-celled microorganisms as well as by more complex ones, such as plants and humans [24]. Production of AMPs in bacteria has been extensively studied and is the focus of paragraph 2.3. In plants, numerous genes encoding AMPs are present in leaves, flowers, seeds, and tubers and it is believed they play a significant role in defense against bacteria and fungi [23]. Invertebrates are the source of many AMPS that have been very well studied. A few examples are melittin (the key component of bee venom), and tachyplesin and polyphemusin (which are found in horseshoe crabs). Polyphemusin exhibits remarkably high antibacterial and antifungal activity, and it is also active against the human immunodeficiency virus (HIV) [23,26]. The immune system defense against microbial infections of vertebrates is quite sophisticated as it involves an interplay among various components such as B-cells, T-cells, and antibodies [23].

Initially it was thought that the existence of AMPs in higher organisms is an evolutionary remnant of their primitive past; however, it is increasingly recognized that they play an integral part alongside the adaptive immune system [27]. In humans, in addition to direct bactericidal activity, AMPs are also involved in immunomodulatory

functions and are produced from a variety of cells and tissues, such as the epithelial cells and the ocular surface [27,28]. Amphibian skin is another rich source of AMPs, producing magainin, among others. Magainin was used as the first template of AMP-based formulations that moved to clinical trials [29].

When the magainin analogue, known as pexiganan, was rejected by the Food and Drug Administration (FDA) in 1999, the hope that AMPs could reach the pharmaceutical shelf was shaken [30]. [30]. In spite of many attempts since, all AMP-based drugs that have been developed and entered clinical trials have failed to produce fruitful results [31]. Manufacturing difficulties, toxicity in high doses, and failure to demonstrate better efficacy than conventional antibiotics are the main reasons behind these unsuccessful clinical trials [31].

However, recent developments bring back the hope in using AMPs as therapeutics. The Generating Antibiotic Incentives Now (GAIN) Act of 2012 aims to encourage antibiotic drug development in response to the rise of AMR [32]. It is expected to ease the regulation and demands that stopped AMPs from being approved and succeeding in clinical trials - such as removing the requirement to demonstrate superior activity when compared to currently used antibiotics [31].

Although AMPs may potentially be a powerful weapon in our fight against infections, bacterial resistance to AMPs could still appear [33]. However, resistance to antimicrobial peptides is expected to develop less rapidly, as their antibiotic activity is not susceptible to any known mechanisms of resistance to conventional antibiotics - rather, it has emerged mostly due to random mutations [25]. In order to create effective antibacterial drugs based on AMPs that would be better shielded against resistance, we need to develop an early understanding of their mechanism of action (MOA). There has been a significant amount of work over the last decade aiming to decipher the several, often complicated mechanisms of action of different AMPs.

1.2.1. Possible mechanism of action (MOA) of AMPs

A large number of studies have been dedicated to understanding the mechanism of action of AMPs (a recent, comprehensive review can be found here: [34]). The hypothesized MOA of a large group of AMPs includes cell membrane permeabilization, however, there is increasing evidence that some AMPs may interact with intracellular or membrane proteins [23,35–40]. Regardless of the final target of AMPs, their activity is

considered to be strongly dependent on their interactions with the cell membrane [23,41]. It is possible that some AMPs use more than one MOA depending on the particular target or their local concentration at the membrane surface [23,42].

AMPs often initially interact with the membrane surface through electrostatic attraction between the positively charged peptides and the negatively charged lipids, which are in abundance in bacterial membranes. Next, for some AMPs, permeabilization of the cell membrane might occur via the barrel-stave, the toroidal-pore or the carpet mechanisms (illustrated in Figure 1-1) [23]. In the barrel-stave model, the pore formation is created due to hydrophobic mismatch. The hydrophobic surface of the peptide faces toward the hydrophobic core of the membrane and the membrane's curvature or hydration do not change significantly.

Figure 1-1: Possible mechanisms of action of membrane active AMPs

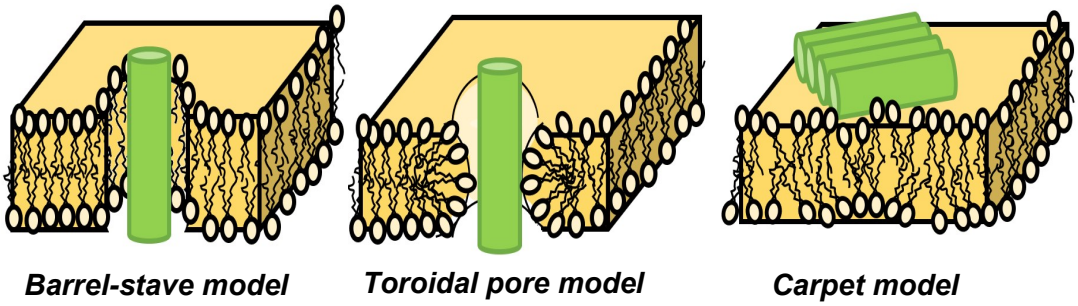

Bacterial membranes primarily consist of lipids forming a bilayer. In the absence of AMPs, the hydrophobic tails of the lipids face the center of the bilayer while the hydrophilic heads of the lipids face outwards. In the barrel-stave model, the peptide is inserted through the membrane without much alteration of the membranes structure. In the toroidal model, the peptide causes the bending of the head groups toward the center of the bilayer. In the carpet model, peptides accumulate on the surface where they form a carpet-like structure that disrupts the continuity of the surface of the membrane.

In the toroidal model, the AMP interacts with the membrane electrostatically. A breach is induced in the hydrophobic region as the polar head groups of the lipids are dragged into the core region and surround the peptide, causing their displacement and the thinning of the membrane. This leads to increased membrane hydration and water permeation through the breach. In the carpet mechanism, the peptides lie on the surface of the membrane parallel to the lipid bilayer, with their hydrophilic surface facing the solvent and the hydrophobic one facing the lipids. At high concentrations, the AMPs that employ the carpet mechanism could act as a detergent, disrupting the membrane

stability and cause holes in the surface or patches of the membrane to break up and then form micelles.

Figure 1-2: Suggested Mechanism of Action of Microcin J25

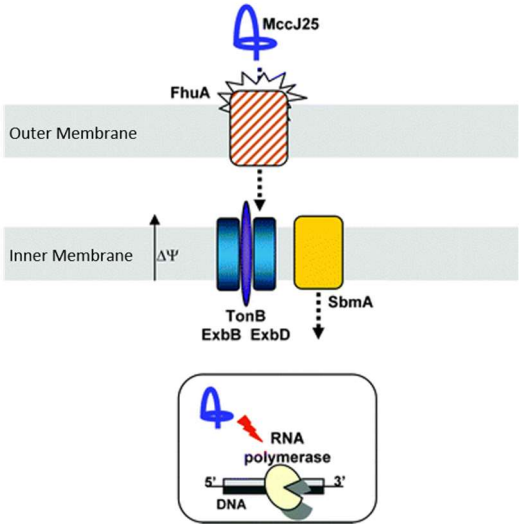

Microcin J25, is initially recognized by the iron-sideophore receptor, FhuA, at the outer membrane (OM) of target cells. The internalization of MccJ25 requires the inner membrane (IM) proteins, SbmA, TonB, ExbD, and ExbD. The TonB/ExbD/ExbD complex uses the proton-motive force from the IM to transduce energy to the OM to allow MccJ25 translocation. SbmA then transports MccJ25 across the IM. Once inside, MccJ25 inhibits RNA polymerase by binding to the nucleotide uptake channel. (adapted from [43]).

It has been established that some AMPs that are usually active at lower concentrations might not form pores on their own, but achieve their bactericidal function through interacting with one or more components of the membrane. Some peptides act via a receptor-mediated mode of action which involves the so-called membrane catalysis model [44]. This model suggests that the peptides interact with a membrane protein receptor via multiple steps, including the initial interaction of the peptide with the membrane, surface adsorption, translocation, and final binding to the receptor. Peptides that use this MOA could induce cell death by interacting with the receptor and either changing its structure in a way that induces water or ion leakage, or hindering some important function that the receptor was involved in [23]. Alternatively, an AMP could use the membrane protein receptor as a Trojan Horse to cross the membrane barrier and get imported in the cell, where it might disrupt essential cellular processes that would lead to the cell death. Different intracellular targets have been identified which includes

molecules involved in the nucleic acid synthesis, protein synthesis, enzymatic activity, and cell wall synthesis. A well-characterized peptide that exhibits a MOA involving several components is the lasso-peptide Microcin J25, and its mode of action is pictured in Figure 1-2.

1.3. Bacteriocins: An interesting group of AMPs

AMPs produced by bacteria are called bacteriocins and show a tremendous potential as novel antibiotic agents [45]. They are ribosomally synthesized by numerous prokaryotic microorganisms, including lactic acid bacteria (LAB), and are commonly active against closely related antagonistic strains, while a few exhibit a broader range of antibacterial activity [46,47]. Bacteriocins demonstrate a higher specificity against sensitive species than other AMPs, and they are active at picomolar to nanomolar concentrations [25]. While bacteriocins were among the first AMPs to be isolated, there is an increasing number of new bacteriocins being reported, which indicates that this reservoir of unused potential antibacterial therapeutics will continue growing [48].

The history of bacteriocins dates to the early 1920s. Nisin, the first bacteriocin (and antibiotic in general) to be used commercially in the food industry, was discovered in the late 1930s and approved as a food preservative in 1969 [30,49]. Today, Nisin is even used in Japan under the brand name Oralpeace™ as a hand wash and oral hygiene gel [50,51]. Despite numerous other bacteriocins having been isolated, 50 years later, nisin is still the only bacteriocin that has been approved for commercial use [48]. Nevertheless, the potential of bacteriocins in many applications has been well-documented [46,52,53]. Biopreservation might be the most well-established use of bacteriocins (a recent review can be found at [54]). However, numerous studies demonstrate the clinical potential of bacteriocins, as they are active against a variety of organisms, including antibiotic-resistant pathogens such as methicillin-resistant *Staphylococcus aureus* (MRSA) strains and vancomycin-resistant *Enterococcus faecalis* (VRE) strains [48]. The therapeutic application of bacteriocins is not limited just to antibiotics, though. In the last 15 years, there have been reports that colicins (a group of bacteriocins produced by *Escherichia coli*) have strong anti-cancer activity against numerous types of tumor cells [55].

In addition to high antimicrobial activity, bacteriocins share many positive attributes

that make them attractive for all the applications mentioned above. Perhaps the most remarkable advantage of bacteriocins is that they are amenable to bioengineering, due to their peptide nature and their relatively simple biosynthetic mechanisms, compared to conventional antibiotics [53]. Due to this advantage, probiotic bacterial strains that are safe to consume can been modified to produce bacterioicins inside the GI tract of hosts, potentially easing the production and delivery challenges that many protein drugs face, due to their their reduced bioavailability [56–58].

Even though it is undesirable, resistance is an unavoidable outcome of evolution. Resistance to bacteriocins that has been reported so far arises from random mutations or adaptation through changes in the cell membrane composition. Fortuitously, the types of resistance to bacteriocins are expected to have comparatively lower potential to become wide-spread. Resistance to conventional antibiotics can often occur as a result of the modifications on genetically-transferable components of the target bacterium, which can be transmitted horizontally between different strains and even species [48]. This mechanism of resistance has not been observed against bacteriocins.

Hereafter, we will focus on bacteriocins produced by lactic acid bacteria (LAB). These LAB bacteriocins are of particular interest since they have been characterized as food grade (or GRAS - generally recognized as safe) and thus are more likely to be approved as an antibiotic substitute [53]. Notably, toxicology studies have demonstrated that Nisin is not toxic to humans, which suggests that other LAB bacteriocins might not be toxic as well [46]. Moreover, LAB bacteriocins are colorless, odorless, tasteless, mostly heat-stable, and they are active under different pH, which further boosts their appeal as drug candidates [48].

1.3.1. Categories of bacteriocins produced by lactic acid bacteria (LAB)

Various classification schemes have been suggested for bacteriocins [59]. We, as many in the field, follow the classification proposed by Heng et al. in 2007 where bacteriocins, produced by LAB, can be classified into three categories [60].

Class I bacteriocins are called lantibiotics. They include small peptides that contain rare thermo-stable amino acids and post-translational modifications. The most important of these modifications is the introduction of a lanthionine non-natural amino acid, which results from cross-linkage of the β-carbon atoms of two alanine residues [25].

Class II contains peptides that do not undergo extensive posttranslational

modification. They can be divided into four subgroups: the pediocin-like bacteriocins (class IIa), the two-peptide bacteriocins (class IIb) , the circular bacteriocins (class IIc), and all the rest (class IId) [60].

Class III contains bacteriocins that are larger and heat-labile. They have complex structures and are often called “bacteriolysins” since studies have proposed that their mechanism is different from the other bacteriocins, in that they kill bacteria by promoting lysis of the cell wall as their N-terminal part is homologous to endopeptidases [61].

We focus on class II bacteriocins. In this group, four genes exist in the same operon in each case (five for those in class IIb) : one (or two) encoding for the peptides, one for an immunity protein (that protects the producer organism from the bactericidal activity of the peptide) and two that encode for transporting and secreting proteins [25]. Even though many of these immunity proteins have been isolated, it is not clear yet how they protect the host or how they interact with the peptides and/or the cell membrane. Paradoxically, even though all of these peptides share many characteristics, they demonstrate high selectivity against their targets. The simple explanations of cationic peptides forming pores in the anionic cell membranes cannot justify the extent of the diversity among their activities. Rather, they are assumed to interact at first with a target-specific membrane protein (through the receptor-mediated mechanism of action), likely driven by electrostatic forces [39,40]. This interaction presumably results in the uncontrollable ion transfer observed during experiments and facilitates the collapse of the membrane potential, leading to cell death. However, this interaction is blocked while in the presence of the immunity protein [39,40]

Class IIa bacteriocins

Class IIa - pediocin-like bacteriocins - consists of proteins below 10 kDa with 35-48 amino acids [62]. Their name is in reference to Pediocin PA1, the first peptide of this category that was well-characterized and identified [25]. The first class IIa peptides isolated were active only against Listeria species. However, there are numerous new class IIa peptides identified that are active against other bacteria such as *Enterococcus*, *Carnobacterium*, *Lactobacillus*, *Pediococcus* and *Clostridium* [62,63]. Some peptides belonging to this category are Enterocin A, Carnobacteriocin B2, Curvacin A, Leucocin A, and Sakacin P.

The peptides belonging to this category are highly homologous (40-60%) [64]. All of

them share common secondary structure domains, as well as sequence motifs. Their N-terminal region is conserved to a great degree and contains at least two cysteines, creating a disulfide bond, in the “Pediocin box” motif: -Y-G-N-G-V-x-C-x-K/N-x-x-C- (x is any amino acid) [25]. Class IIa peptides have at least one disulfide bridge and there are studies suggesting that the activity of the peptides is proportional to the number of its disulfide bridges [65]. The structure of several pediocin-like bacteriocins has been determined either by Circular Dichroism (CD) or with Nuclear Magnetic Resonance (NMR) studies in membrane-mimicking environments. Two conserved structural domains have been observed during these studies: an N-terminal β-sheet-like structure that is stabilized by a disulfide bridge, and a C-terminal containing one or two hydrophobic or amphiphilic α-helices [63]. The Pediocin box is located at the N-terminal domain, which is highly conserved [63]. On the other hand, the C-terminus helices vary considerably among class IIa bacteriocins, and there is evidence that suggests the C-terminal part is responsible for the high selectivity of class IIa bacteriocins [66,67].

Figure 1-3: Proposed MOA of class IIa bacteriocins

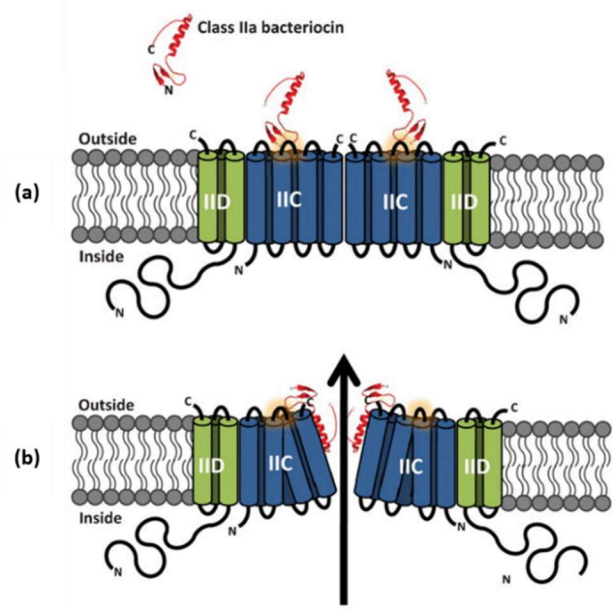

Proposed model for the MOA of class IIa bacteriocins: a) Initially the β-sheet N-terminal of the peptide interacts with the IIC domain extracellular loop (highlighted in yellow) of the Man-PTS IIC protein. b) Then the C-terminal helix binds to the transmembrane IIC and/or IID proteins, possibly causing conformational changes which lead to leakage of cellular components and the eventual cell death. (adapted from [63])

The mechanism of action of class IIa bacteriocins is the most well-characterized so far among all the class II bacteriocins. Studies reveal that bacteriocin-resistant mutants of otherwise susceptible strains share alterations on genes relative to the sugar transporter mannose phosphotransferase system (Man-PTS), which indicates that there should be some interaction between the bacteriocin and Man-PTS [63]. Diep et al. presented evidence that class IIa bacteriocins bind and form a complex with a subunit of Man-PTS [68]. The detailed hypothesized mechanism of action of class IIa bacteriocins is shown in Figure 1-3. The Man-PTS family is a large family of membrane proteins present in many bacteria, both Gram-negative and Gram-positive, but it is absent in eukaryotic cells, and therefore can serve as an ideal drug receptor that will allow selective targeting of the pathogen bacteria without demonstrating toxicity towards the mammalian cells [63].

Class IIb bacteriocins

Class IIb contains the two-peptide bacteriocins. Those heterodimeric bacteriocins require two different peptides, at an approximately equal concentration to exhibit their optimal activity [69]. Interestingly, each of the peptides from a two-peptide bacteriocin shows high bactericidal activity only when combined with its complementary peptide [70]. Moreover, there is only one immunity protein gene for every two-peptide bacteriocin, which strengthens the claim that the two peptides act as one antimicrobial unit [71]. The first two-peptide bacteriocin that was identified and well-studied was Lactococcin G, but other prominent peptides in the class IIb include Enterocin 7AB, Plantaricin EF, and Plantaricin JK [72–74]. Experiments have shown that these peptides form α-helical structures, however, their primary structures differ significantly [75].

An interesting structural characteristic of all class IIb bacteriocins characterized so far is that each contains GxxxG and GxxxG-like motifs. These are prevalent in transmembrane peptides and membrane proteins [75,76]. It has been suggested that these motifs facilitate helix-helix interactions and promote the oligomerization of transmembrane helical peptides or domains of membrane proteins. The hypothesis is that two glycine residues, when separated by three other amino acids, lie on the same face of the helix. Due to their small size, they create a relatively flat surface that may facilitate more pronounced helix-helix interactions (illustrated in Figure 1-4). Often, other small amino acids (like alanine or serine) replace either one or both glycines creating a

GxxxG-like motif [77]. Valine, leucine and isoleucine residue are frequently found neighboring the motifs [77].

It has been well-documented that class IIb bacteriocins induce cell death through membrane leakage [70]. However, the complete mechanism of action of class IIb bacteriocins is still unclear. Only recently (in 2014), Kjos et al. identified a possible receptor for Lactococcin G through whole genome sequencing of spontaneous resistant mutants [78]. All the mutations were in or near the *uppP* gene that encodes an undecaprenyl pyrophosphate phosphatase (UppP), which is a membrane-spanning protein involved in peptidoglycan synthesis. Moreover, they found that sensitivity to another class IIb bacteriocin, Enterocin 1071, which shows 57% identity to Lactococcin G, is directly linked to the expression of UppP in the target bacterium. However, we cannot assume that other class IIb bacteriocins use UppP as a target due to the significant differences in their sequences. Indeed, in 2016, Oppegård et al. identified the APC superfamily transporter as likely to serve as a receptor for Plantaricin JK [79]. In the same study, they concluded that the APC transporter is not the target of Plantaricin EF.

Figure 1-4: The GxxxG motif

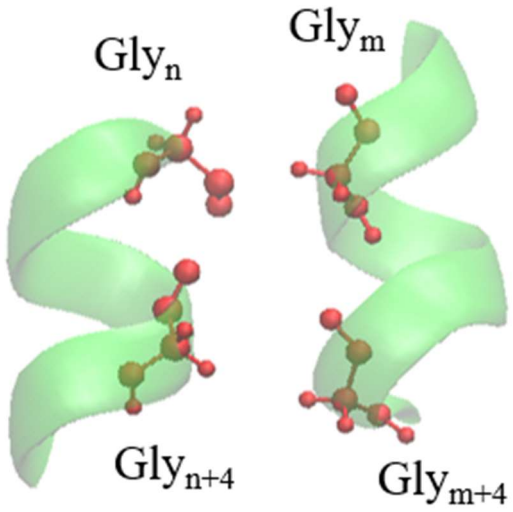

The GxxxG motif is hypothesized to induce high affinity in transmembrane helices [80]. Here the two helices are able to come into close proximity because the glycine residues, shown in red, create a flat surface due to their small size.

Class IIc bacteriocins

Class IIc bacteriocins are circular peptides, i.e. their C- and N- terminal backbones are covalently linked [81]. They show great stability, adopting a four- or five-α-helix

structure and encompassing a hydrophobic core [82]. It has been reported that they have high pH stability and are resistant to degradation, possibly due to their circular structure that increases their structural integrity [81]. Arguably, they are the most poorly understood subgroup of bacteriocins [48]. Nevertheless, the best-characterized class IIc bacteriocin is AS-48 [83].

Class IId

The remaining class II bacteriocins are allocated to class IId. Those are one-peptide, non-cyclic bacteriocins that do not contain the Pediocin box (as described at 0) in their primary structure [23]. The peptides in this category have a broad diversity, but some can be grouped further into two subgroups: the *sec*-dependent bacteriocins and the leaderless bacteriocins [84]. The former are peptides that contain a signal peptide (as almost all other bacteriocins) and are secreted through the general secretory (*sec*-) pathway; the latter do not have an N-terminal leader sequence or a signal peptide, which in other bacteriocins is cleaved off as they are transported outside the producer cell. It is speculated that the immunity protein for this peptide is involved in its secretion as well [85].

Figure 1-5: "Huge Toroidal Pore (HTP)" model of Lacticin Q

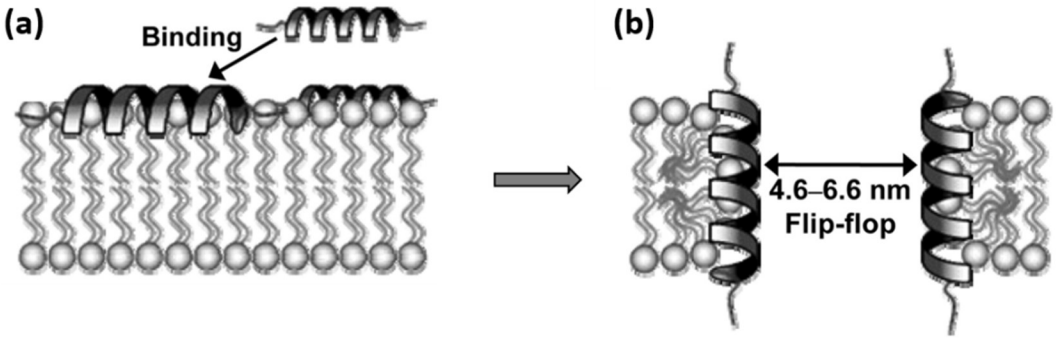

Lacticin Q interacts with the negatively-charged surface of the lipid bilayer (a). The peptides are inserted into the membrane and induce lipid flip-flop and pore formation (b). (adapted from [86])

The modes of action of class IId bacteriocins are as diverse as the primary sequence of these peptides. Lactococcin A, which cannot be included in either the *sec*-dependent bacteriocins or the leaderless bacteriocins group, is thought to behave similarly to class IIa bacteriocins and interact with Man-PTS [68]. Lactococcin 972, a *sec*-dependent bacteriocin, has been shown to interact with lipid II among others, inhibiting peptidoglycan biosynthesis in the same way that nisin does [84]. A Zn

Metallopeptidase, YvjB, has been identified as a possible receptor for the class IId leaderless bacteriocin LsbB through whole genome sequencing of resistant mutants to this bacteriocin [39]. Five more class IId peptides that share substantial sequence homology with LsbB, by having a conserved C-terminal KxxxGxxPWE (where x can be any amino acid) motif, are presumed to interact with YvjB as well [87]. On the other hand, Lacticin Q, another leaderless bacteriocin, has a broad range of bactericidal activity and does not appear to require a receptor. Indeed, the proposed MOA for Lacticin Q is that accumulation of peptides on the membrane surface lead to pore formation through the "Huge Toroidal Pore (HTP)" model (Figure 1-5) [86].

1.4. Molecular Simulation of Bacteriocins

Due to their variety and complexity, elucidating the mechanisms of action of bacteriocins is a major challenge. However, a better understanding of the structure-function relationship of their biological behavior could have a tremendous impact on the design of future antimicrobial agents. As computational power has increased dramatically in recent years, molecular simulations can now provide insights into the modes of activity and specificity of bacteriocins by studying them at atomistic resolution and nano- to millisecond timescales. Molecular dynamics (MD) simulations have evolved through the years, and as they now provide answers in an increasingly time and cost-effective manner, they have now become a tool of choice for many researchers [88]. In the paragraphs that follow, we present a brief introduction to the theory of MD and the potential of MD as a tool to explore the MOA of bacteriocins.

1.4.1. Theory on Molecular Dynamics (MD) Simulations

Molecular dynamics (MD) is a method that calculates the time evolution of a system [89]. In its classical form, Newton's equations of motion (which describe the interaction of *N* particles under a potential $U(\vec{r_i})$, *i* = 1,…,*N*) are solved numerically, propagating the system in time. A concise mathematical description could be the following:

$$\overrightarrow{F_i} = m_i \ddot{\vec{r}}_i \quad (1)$$

where m_i is the mass of particle *i,* $\overrightarrow{F_i}$ is the force acting on particle*,* and can be described as:

$$\overrightarrow{F_i} = -\frac{\partial U(\overrightarrow{r_i})}{\partial \overrightarrow{r_i}} \tag{2}$$

In atomistic MD simulations, each particle represents an atom as a point mass. The timestep for the integration should be sufficiently small to ensure numerical stability and thus is chosen to be smaller than the characteristic time of the fastest motion in the system (which typically is 1 fs). However, if constraints are applied to the bonds of this magnitude (which involves all covalent hydrogen bonds), the timestep can be increased to 2 fs, which reduces the computational resources and wall-clock time needed. The potential $U(\overrightarrow{r_i})$ is described empirically and is commonly called the force field. Many force fields exist for biomolecular simulations. For the work described here, we employ mostly the CHARMM force field that has the following functional form:

$$\begin{aligned} U(\overrightarrow{r_i}) = & \sum_{\text{bonds}} K_b(b - b_o)^2 + \sum_{\text{angles}} K_\theta(\theta - \theta_o)^2 \\ & + \sum_{\text{dihedrals}} K_\chi(1 + \cos(n\chi - \delta)) + \sum_{\substack{\text{improper} \\ \text{dihedrals}}} K_\varphi(\varphi - \varphi_o)^2 \\ & + \sum_{\substack{\text{nonbonded} \\ \text{VDW interactions}}} \varepsilon\left[\left(\frac{R_{ij}}{r_{ij}}\right)^{12} - \left(\frac{R_{ij}}{r_{ij}}\right)^{6}\right] + \sum_{\substack{\text{nonbonded} \\ \text{electrostatics}}} \frac{q_i q_j}{\varepsilon_1 r_{ij}} \end{aligned} \tag{3}$$

The bonds, angles and improper dihedrals are described as simple springs with constant K_y, and equilibrium length y_o (where y=b for bonds, θ for angles and φ for improper dihedrals). The dihedral angles are modeled with a periodic potential with force constant K_χ, which controls the rotation χ and a phase shift δ that corresponds to the equilibrium value. The non-bonded terms include the interaction between atoms that are separated by three or more covalent bonds and are described by Van der Waals dispersion forces and Coulombic interactions between point charges. The bonded interactions have been parameterized for each pair of atoms in a system, while the non-bonded have been parameterized for individual types of atoms. The calculation of the non-bonded interactions overwhelms the computational time needed, and thus various techniques are applied to reduce this cost. The Van der Waals forces are truncated to zero with a smoothing function after a specified distance. The Particle Mesh Ewald method is used for the electrostatics, in that it interpolates the reciprocal space Ewald

summation, which in turn is described as the sum between the short-range interactions that are calculated in real space and the longer-range ones that converge quickly in Fourier space.

To define the system, a unit “cell” is determined around the biomolecule, with boundaries set at a distance that will not influence its molecular behavior. The cell then repeats periodically at all edges, simulating a bulk system. It is important that the cell size is large enough so that each atom interacts with at most one copy of any other atom (this requirement is called minimum image convection). Energy is not conserved in a biological system of finite atoms (as Newton’s equation of motion dictates), rather, the pressure and the temperature are conserved (the so-called isothermal-isobaric ensemble, or NPT ensemble). Constant temperature and pressure simulations are possible with additional terms in the equation of motion.

1.4.2. Previous MD on bacteriocins

Molecular dynamics simulations have been employed over the past 15 years to elucidate the mechanism of action of numerous AMPs [90–93]. [90–93]. The majority of the peptides studied are pore-forming AMPs because significantly more is known about them, such as the structure of the peptides and, in some cases, the structure of the pore. In the case of bacteriocins, only the MOA of Nisin has been extensively investigated though MD simulations [94–96]. Both the structure of Nisin and the Nisin-lipid II complex have been solved experimentally, enabling their realistic representation in MD simulations [97]. Key interactions of the complex and its behavior in bacterial membrane models were revealed in these studies. The findings suggested that nisin interacts with the membrane as a first step for pore formation, which is mediated through the interaction with lipid-II [96]. In another study, researchers discussed how the degree of oligomerization of nisin affects the pore formation and the interaction with lipid-II [94].

Moreover, the behavior of a few class II bacteriocins was investigated through molecular dynamics simulations. First, in 2004, Kaur et al. explored the structural relationship of four class IIa bacteriocins at different temperatures [98]. As a membrane-mimicking model, they performed the simulation in TFE (2,2,2-trifluoroethanol), which is a common practice for experiments. Their simulations were 2 to 4 ns long. They concluded that the helical region is responsible for target recognition and it loses its structure at higher temperatures. The same group later studied the interaction between a

class IIa bacteriocin and its immunity protein in the presence of DPPC (dipalmitoylphosphatidycholine) or a POPG (palmitoyloleoylphosphatidylglycerol) lipid bilayer - this time, for up to 30 ns [99]. They observed that the peptide interacts with the immunity protein through specific ion-pair interactions. Later they investigated the possible dimer structures of the class IIb bacteriocin Plantaricin S in a mixed POPE (palmitoyloleoylphosphatidylethanolamine) and POPG bilayer for 400ns [100]. They found that the peptides interact strongly with each other when they are in an antiparallel orientation. Cruz et al. studied the binding of AS-48, a class IIc peptide, to a membrane and the resulting pore-formation dynamics; It is important to note that they used coarse-grained MD, where each particle of the system represents more than one atom. This way, the simulation can reach longer timescales, at the cost of losing spatial resolution. Finally, da Hora et al, demonstrated recently that a hybrid peptide of two class IIa bacteriocins induces negative curvature in the target cell membrane and disrupts its integrity, instead of forming a pore [101]. They performed the MD simulations in pure and mixed POPG POPC (palmitoyloleoylphosphatidylcholine) bilayers for up to 500 ns. Up to date, there has been no study of a class II bacteriocin in complex with its proposed receptor (like Man-PTS, UppP or YvjB) because we are lacking important information about the structure of these receptors.

1.5. Thesis Overview

The goal of this thesis is to shed light onto the mechanism of action (MOA) of class II bacteriocins. To achieve this, we employ different computational tools, focusing on molecular dynamics simulations. The thesis aims to investigate the nature of the interaction of a class II bacteriocin with a cell membrane and the possibility that a bacteriocin forms a transmembrane pore. We also address the challenge of studying a receptor without having prior knowledge of its structure. We focus mainly on the different aspects of the MOA of the class IIb bacteriocin PlnEF (Chapters 2-5), while in Chapter 6 we shift focus to the MOA of the class IId bacteriocin LsbB.

In 0, we introduce PlnEF, a class IIb, two-peptide bacteriocin, and we review the experimental information regarding its MOA. We then employ molecular dynamics simulations to study the behavior of this bacteriocin in water and in DPC micelles (a membrane-mimicking environment). To our knowledge, we are the first in the scientific

community to study the possible dimer structures and the peptide-peptide interactions of PlnEF from a computational perspective.

The initial interaction of a bacteriocin with a membrane plays a key role in its MOA, as we discuss in Chapter 3. We support this assertion by studying the PlnEF dimer on the surface of a model lipid bilayer. We go on to investigate the residues that are responsible for the peptide-peptide and peptide-membrane interactions. Then, we simulate different PlnEF-mutants of known activity in order to address the question of how the computational observations correlate with the experimental bactericidal activity of PlnEF. This study was published in the peer-reviewed journal, *Biochimica et Biophysica Acta (BBA) – Biomembranes* [102]; the experiments were conducted by our collaborators B. Ekblad and P.E. Kristiansen at the department of Biosciences in the University of Oslo, Norway.

In Chapter 4, we describe how we incorporated additional experimental studies into designing a transmembrane dimer model of PlnEF. We used extensive mutational analysis and fusion-peptide orientation experiments in order to computationally create the dimer model and position it in a lipid bilayer. Utilizing atomistic MD simulations, we studied the important motifs that were involved in the peptide association. The work described in Chapter 4, in combination with the experimental studies (presented in the appendix), led to a publication in the peer-reviewed journal, *Biochemistry* [103]. Our partners at the department of Biosciences in the University of Oslo, Norway, B. Ekblad, C. Oppegård, J. Nissen-Meyer, and P.E. Kristiansen, performed the experiments and coauthored the publication with us.

Chapter 5 extends the studies from Chapter 4 to further elucidate the behavior of the PlnEF transmembrane dimer. Through a 1 μs long atomistic MD simulation, we describe in detail the dimerization motifs of the dimer. We then analyze the effect of the dimer's presence in its environment, i.e. the membrane, water, and ions. Most importantly, we address the question about whether class IIb bacteriocins can form a transmembrane pore that allows water and ion permeation. We are preparing the submission of this study for publication in a peer-reviewed journal.

It has been suggested that the MOA of class II bacteriocins is associated with the presence of specific transmembrane receptors - therefore, we could not omit discussing the possibility of a receptor-mediated MOA. In Chapter 6, we introduce the idea of

employing protein structure prediction techniques to determine the structure of a bacteriocin receptor. We suggest a topology and we predict a structure for YvjB, which is a Zinc metallopeptidase that was identified as a possible receptor for the class IId bacteriocin LsbB. We proceed by designing an LsbB-YvjB complex through MD and docking calculations. We conclude Chapter 6 by detailing the next steps that are required to complete this study in the future.

In the last chapter (Chapter 7), we summarize the conclusions of this thesis, and we outline the future direction for further elucidating the mechanism of action of class II bacteriocins.

Chapter 2

Simulation of a Class IIb Bacteriocin in water and on micelles

The mechanism of action of class II bacteriocins is complex and diverse. Lacking information about their receptor or a pore structure renders it difficult to create an image of the system that would represent the direct bactericidal mechanism of the peptides. However, the interactions of the membrane with the peptides is another important, albeit indirect, aspect of the MOA that can be simulated. In the case of class IIb bacteriocins, one can additionally study through MD, the interactions between the peptides, which is presumed to be crucial for their activity. In this chapter, we start our journey of unraveling the mechanism of action of class IIb bacteriocins.

2.1. Introduction

The class IIb model bacteriocin we use is Plantaricin EF (PlnEF); that is comprised of Plantaricin E (PlnE) and Plantaricin F (PlnF). The sequence of Plantaricin EF can be found at Table 2-1. PlnE, a 34 residue peptide and PlnF, a 33 residue peptide are produced by *Lactobacillus plantarum* C11, alongside PlantaricinJK, another two-peptide bacteriocin [104]. *Lactobacillus plantarum* C11 was first isolated from a cucumber fermentation in 1990, while different *Lactobacillus plantarum* strains that produce PlnEF have been found in other fermented foods, such as meat and grains [105–107].

Table 2-1: Aminoacid sequence of the two peptide bacteriocin, Plantaricin EF

PlnE	**FNRGG YNFGK SVRHV VDAIG SVAGI RGILK SIR**
PlnF	**VFHAY SARGV RNNYK SAVGP ADWVI SAVRG FIHG**

Initially, the complementary antimicrobial action of Plantaricin E and Plantaricin F was studied against *L. plantarum* 965, and it was shown that they are 1000-fold more active when administrated together at equimolar concentrations (at 5 to 10 nM each) [73,104]. However, none of them is active in combination with Plantaricin J or K. PlnEF itself or strains producing PlnEF found to be active against a broader range of enteric

bacterial and fungal pathogens, such as *Escherichia Coli* [108,109] .

The hypothesis that they form pores in the cell membranes was tested by calculating the pH gradient (ΔpH) and the transmembrane electrical potential (Δψ) [73]. Through that study, it was found that they dissipate both ΔpH and Δψ and that PlnEF induces the conduction of small monocovalent cations, while PlnJK seems to lead to efflux of anions. Thus, it can be concluded that the mode of action of both PlnEF and PlnJK is connected to membrane permeabilization, which however is attained through different paths. Recently, Zhang et al. verified the membrane permeabilization hypothesis with scanning electron microscopy and transmission electron microscopy (Figure 2-1) [110].

Figure 2-1: Microscopy images of cells treated with PlnEF

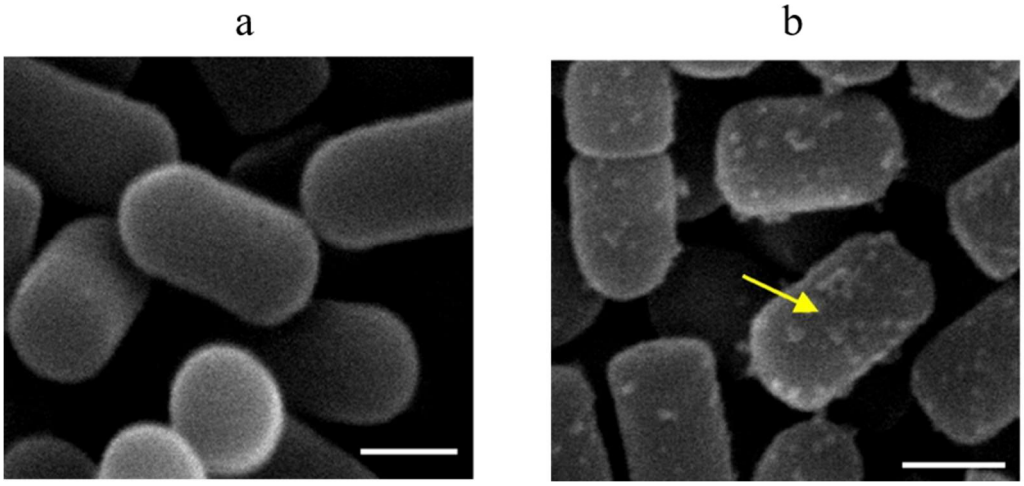

Scanning electron microscopy of bacterial cells treated without (a) or with (b) the class IIb bacteriocin, PlnEF for 30 min. It is evident that there is membrane disruption, while the yellow arrow points to blebs protruded in the cell surface. Scale bars: 500 nm. (Adapted from [110])

In order to explain the bactericidal mechanism and ion selectivity of PlnEF, structural analysis was conducted. Based on their aminoacid sequence, the Edmundson helical wheel representation suggests that both PlnE and PlnF have 18-24 residues, which will adopt α-helical structure, similar to other two-peptide bacteriocins [104,111]. CD studies provided a better insight in the secondary structure of PlnEF. The CD spectra of both peptides in aqueous solution has shown that they are unstructured with α-helical content less than 5%, while in presence of trifluoroethanol (TFE), that increases the hydrophobicity of the environment, the α-helical content of PlnE is 31%, while that of

PlnF 23%. In both cases, there was not any significant difference in the CD spectra of the individual peptides and when they were introduced together; indicating that adopting an α-helical structure precedes the interaction between the peptides [37].

The presence of membrane mimicking moieties, such as dodecylphosphocholine (DPC) micelles and anionic dioleoylphosphoglycerol (DOPG) liposomes induced the formation of α-helical structures. Specifically, the α-helical content reached a maximum of 41% in the case of DPC micelles and 38% in the case of DOPG liposomes. Interestingly thought, the average spectra in DPC micelles followed the same pattern as the ones in aqueous and TFE solutions, e.g. being similar for individual peptides and dimer complexes [37]. In contrast, the complementary peptides increased the helical structure of each other upon exposure to anionic liposomes; either when they are premixed before their introduction to DOPG or when mixing liposomes that already contain at least one of the peptides [37]. The simultaneous addition of complementary peptides extended the helical content of PlnEF by 9 to 12%, while this rise was independent to the peptide concentration. The structure of the peptides was also investigated in the presence of zwitterionic dioleoylphosphocholine (DOPC) liposomes. It was shown that DOPC liposomes do not induce structure and mixing with anionic lipids is needed [37]. Thus, it can be conjured, that the peptides adopt α-helical structures upon arrival at the target membrane, where they interact individually with anionic membrane components. Then the peptides interact with each other in a structure-inducing manner, possibly forming a membrane-associated dimer complex.

Recently the three dimension structures of the peptides PlnE and PlnF were analyzed by NMR spectroscopy in presence of DPC micelles [112]. Plantaricin E forms two α-helical-like regions (residues 10–21 and 25–31, pdb-id: 2jui, Figure 2-2a), while Plantaricin F forms one α-helix (residues 7 to 32, pdb-id: 2rlw, Figure 2-2b) with a kink around Pro-20, a common characteristic of many transmembrane proteins [112,113].

The analysis of the sequence and structure of the two peptides Plantaricin E and F has pointed out several pieces of information. The importance of helical conformation in the class IIb bacteriocins has been highlighted as it mediates the insertion inside the membrane [114]. It is hypothesized that the two peptides interact with each other through the well conserved GxxxG motifs [112], either by creating flat surfaces enabling the nearby polar residues to approach each other and thus interact strongly forming

hydrogen bonds or salt bridges, or by having increased presence of acidic α-carbon hydrogens of glycines that can participate in hydrogen bonding. PlnF has one GxxxG motif (G30xxxG34), while PlnE has two: one at its N-terminus (G5xxxG9) and one near its middle section but closer to its C-terminus (G20xxxG24). Both peptides have multiple possible GxxxG like motifs, e.g. the GxxxG-like motif S26xxxG30 at the C-terminus of PlnF. Two dimer complexes can be drawn based on the possible combination of the GxxxG motifs (shown in Figure 2-3), taking into account that we assume that the peptides will interact in a staggered fashion similarly to what was proposed for Lactococcin G before [112].

Figure 2-2: 3-D structure of Plantaricin E and F

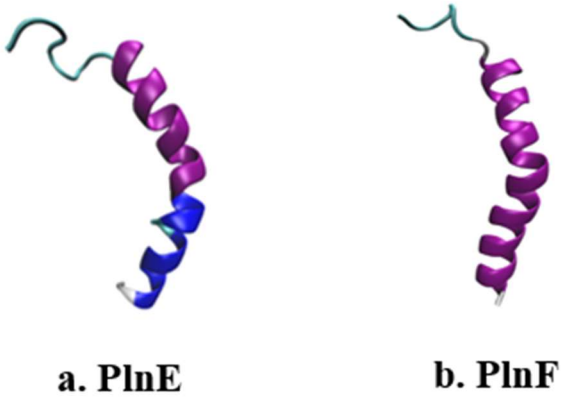

Cartoon representation of the NMR derived structures of PlnE (a) and PlnF (b) based on the STRIDE algorithm [151]. (magenta: α-helix, blue: 3-10-helix, cyan: turn, white: coil)

Despite the detailed studies, a proposed mechanism of action for the antimicrobial activity of the two-peptide bacteriocin PlantaricinEF cannot be concluded. In order to shed light to the molecular basis for the behavior of PlnEF, we have performed molecular simulations of the peptides individually and in dimers inside aqueous solution to investigate their possible interactions, as well as their proposed lack of stability. Next, the dynamics of the peptides in the presence of DPC micelles was examined, to enlighten which residues are responsible for the interaction with a membrane-like system and compare directly with the CD and NMR results.

2.2. Materials and methods

All the molecular dynamics simulations were carried out using the NAMD 2.9

simulation engine [115] with the CHARMM param36 force field [116]. The analysis and visualization were performed using the program VMD [117] and Origin (OriginLab, Northampton, MA). The initial coordinates for the peptides were obtained from the protein data bank http://www.rcsb.org/ (pdb entries: 2jui for PlnE and 2rlw for PlnF).

Figure 2-3: Possible models of the PlnEF

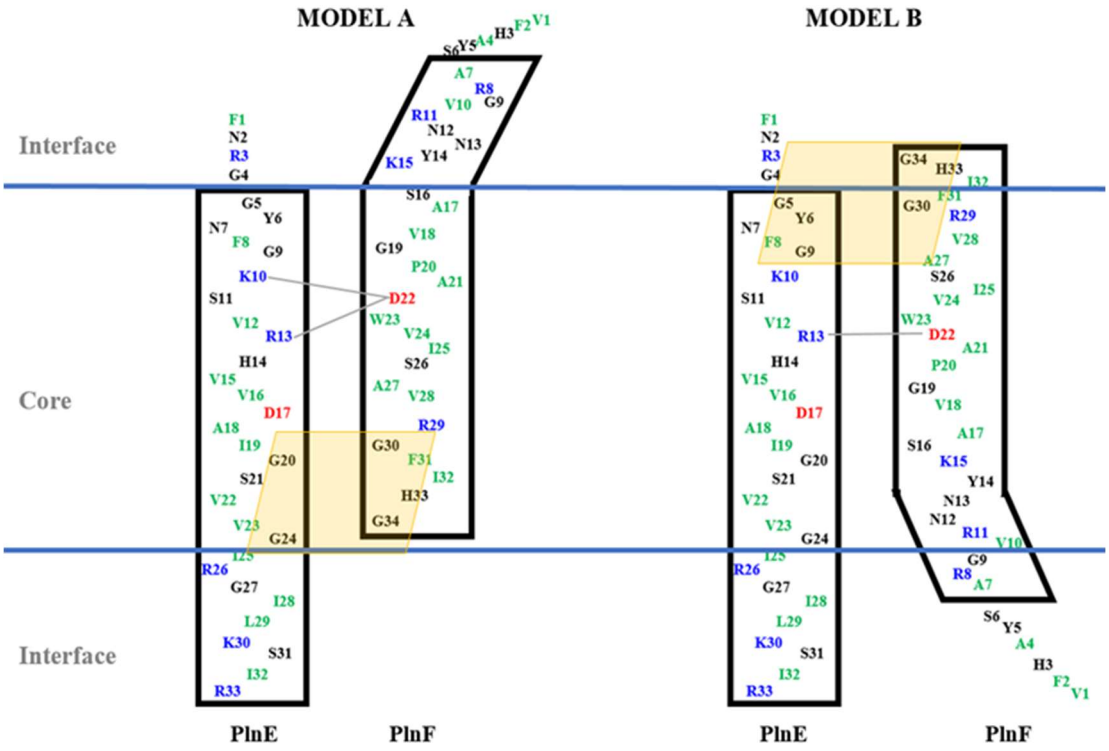

Illustration of possible dimer models of the PlnEF, designed dimer based on the GxxxG motifs present in the bacteriocin. Model A: the C-terminal GxxxG motif of PlnE comes close to the GxxxG motif of PlnF enabling the polar amino acids in the center of the two peptides to interact. Model B: the N-terminal GxxxG motif of PlnE interacts this time with the GxxxG motif of PlnF, allowing the polar amino acids in the center to interact in a lesser degree. Yellow boxes denote the hypothesized GxxxG motifs. Proposed Hydrogen bonds are indicated with gray lines. Red: acidic residues; Blue: basic residues; Green: hydrophobic residues. The initial conceptual design of these models was performed by our collaborator P. E. Kristiansen.

In order to generate initial dimer structures, e.g. possible conformations of the two peptides relative to each other, we used the online ZDOCK docking server [118]. ZDOCK performs docking simulations and searches for local energy minima of the system, employing fast Fourier transformation, while treating each peptide as a rigid body and exploring only its six-dimensional (rotational and translational) space. Two

different conformations were selected that would resemble as close as possible the suggested dimer models presented in Figure 2-3. In the first, the peptides are positioned parallel to each other, while in the second they are positioned in an antiparallel manner. Initially the z-dock server produced 2000 predictions of possible dimer structures. Those predictions were used as input to an in-house Matlab script that screened out the best dimers based on the GxxxG motifs complementarity. Three such GxxxG motifs are present in Plantaricin EF. We chose as the initial parallel conformation the dimer structure that brought closer the $G_{20}xxxG_{24}$ motif of PlnE with the $G_{30}xxxG_{34}$ motif of PlnF. We chose as the antiparallel one the structure that brought closer the $G_{5}xxxG_{9}$ motif of PlnE with the $G_{30}xxxG_{34}$ motif of PlnF.

The DPC micelle models were created using the online CHARMM-GUI server [119], that performs short molecular dynamics simulation using the CHARMM engine [120]. Next, we combined the micelles with the peptides using VMD, resulting in the initial peptide-micelle structures.

The simulation parameters were kept the same for all the systems. Initially each system was minimized using the conjugate gradient algorithm provided in NAMD. This was followed by gradual heating to 303.15 K while the peptides and lipid atoms were subjected to positional harmonic restrains. Then numerous equilibration steps were performed while the restrains were gradually removed. Equilibration and production runs were carried out in the NPT ensemble at atmospheric pressure. A timestep of 2 fs was employed. Van der Waals potential was truncated at 10 Å introducing a switching function at 9 Å, while the real space cutoff distance of the PME electrostatics calculation was also set at 10 Å. Coordinate snapshots were recorded every 2 picoseconds.

2.3. Results and Discussion

2.3.1. Simulation of individual peptides in water

Each of the two peptides was introduced in a separate box, which was created by surrounding the protein with a 30 Å water layer. This corresponds to ~25,000 molecules of water. Sodium and chloride ions were added to counter the charge of each peptide and to add 0.15M NaCl, which resembles the ion concentration of biological fluids. Production simulations (that are called E_w for PlnE and F_w for PlnF) were conducted for 85 ns. The stability of the peptide structures was accessed by calculating the dihedral

angles formed (Figure 2-4a) as well as their potential energy (Figure 2-4b).

In contrast to the CD studies, Plantaricin E is very stable in a water box. One contiguous helix is observed through the simulations. In the model, there is no discernible curvature along the long axis of the peptide, indicating that the curvature observed in experiments may be the result of the interaction with the spherical micelle. The phi dihedral angle for aminoacids 10 to 32 is on average equal to -65.3±3.9 and their psi angle -38.02 ± 4.1 degrees. The values for dihedral angles that define an α-helix are -64±7 degrees for phi and -41±7 degrees for psi.

Figure 2-4: Dihedral angles and Energy analysis for the individual peptides in aqueous solution

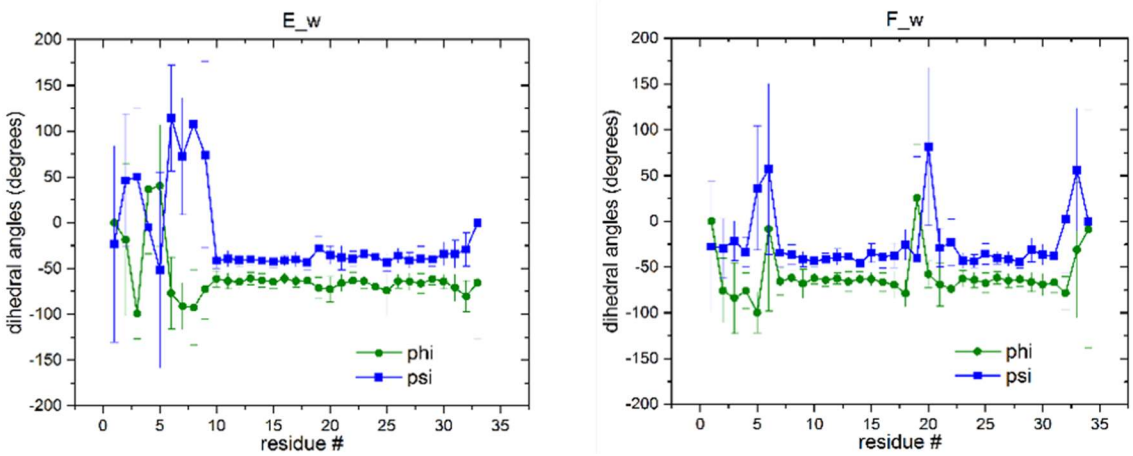

a. Mean dihedral angles for each residue of Plantaricin E (E_w) and Plantaricin F (F_w) in a water box. The values for dihedral angles that define an α-helix are -64±7 degrees for phi and -41±7 degrees for psi.

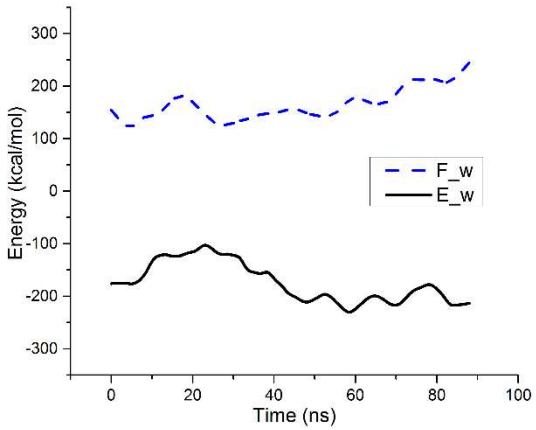

b. Energy of the peptides Plantaricin E (E_w) and Plantaricin F (F_w) in a water box

On the other hand, the helix of PlnF seems to be divided into two distinct helical substructures around the proline residue (aminoacids 7 to 17 and 23 to 31). Energetically PlnE seems to reach a minimum and to be stabilized, however PlnF is continuously increasing. The last snapshot of the simulations can be found in Figure 2-5.

Figure 2-5: Final snapshots of the simulation of individual peptides in water

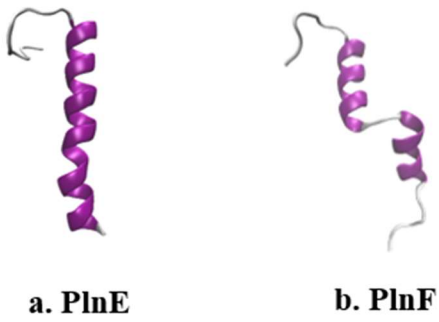

a. PlnE **b. PlnF**

Final snapshot of the simulation of individual peptides in water. Cartoon representation based on the STRIDE algorithm [121]. (magenta: α-helix, blue: 3-10-helix, cyan: turn, white: coil)

2.3.2. Simulation of proposed dimers in water

The two proposed models of the dimer were solvated as described before. Production runs of 80 ns were performed. The energy and dihedral angles of each peptide were analyzed to evaluate their stability. Furthermore, we quantified the formation of hydrogen bonds, in order to identify peptide domains or residues involved in interactions

Dihedral angle analysis revealed that the structure of both peptides deviates substantially from their NMR structure, apparently due to the peptide-peptide interaction. In both cases, short α-helical like domains are formed for each peptide (Figure 2-6a o Figure 2-6b).

Interestingly, in both models Plantaricin F is the one that is most structured, in contrast to the case of single peptides in water. Moreover, the energies of the peptides fluctuate significantly in the second half of the simulation (Figure 2-6c); there is an increase of the energies of both complexes, followed by a sharp decrease. Although we cannot yet conclude to a possible structure of the dimer in water, analysis of the hydrogen bond propensity of each residue in the peptide can provide some useful first information.

Figure 2-6: Dihedral angles and energy analysis for the proposed complexes in aqueous solution

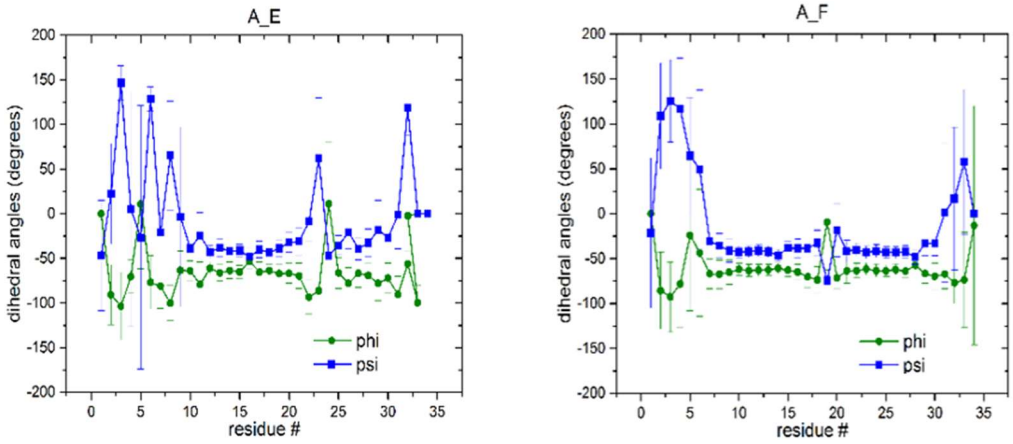

a. Mean dihedral angles for each residue of Plantaricin E (E_w) and Plantaricin F (F_w) in Model A. The values for dihedral angles that define an α-helix are -64±7 degrees for phi and -41±7 degrees for psi.

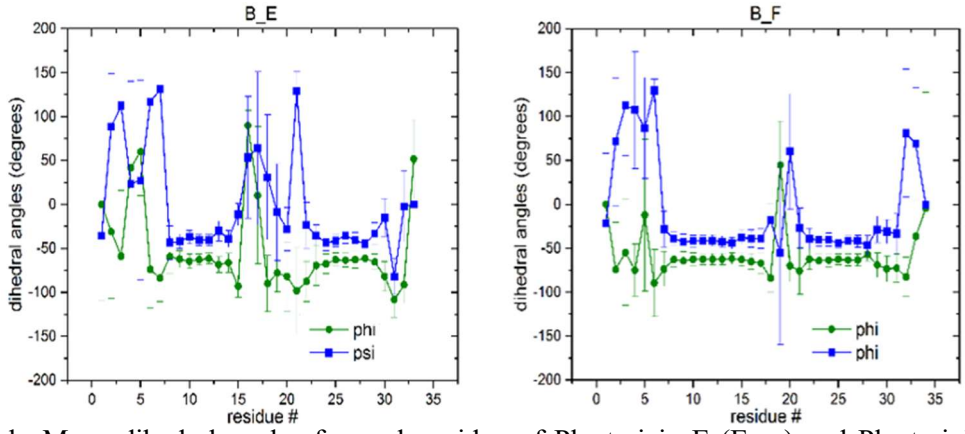

b. Mean dihedral angles for each residue of Plantaricin E (E_w) and Plantaricin F (F_w) in Model B. The values for dihedral angles that define an α-helix are -64±7 degrees for phi and -41±7 degrees for psi.

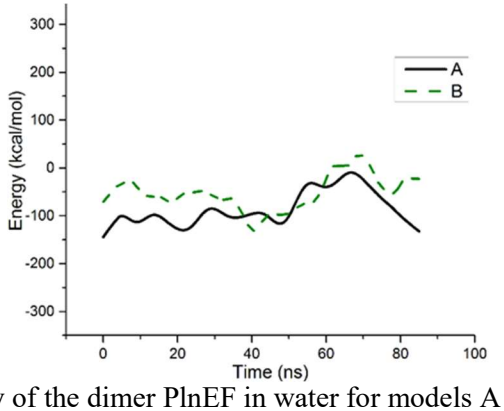

c. Potential energy of the dimer PlnEF in water for models A and B

The hydrogen bonds (Hbonds) that were created between the two peptides were calculated in each simulation. Only those that are present in more than 10% of the snapshots taken are considered significant. In the case of model A, hydrogen bonds were present between the side chains of Arg13 of PlnE and Asp22 od PlnF, as well as Asp17 of PlnE and Arg29 of PlnF with an occurrence (occ.) of 82.76% and 70.38% respectively though the course of the simulation.

These results agree with the proposed model. However, another hydrogen bond between the backbone atoms of Tyr6 of PlnE and Ala17 of PlnF is present with occ.=17.01%. This may be the reason of the disruption of the structure of the peptides around these residues. It is very interesting, that the Tyr residue lies inside the GxxxG domain on PlnE and this might be a first indication of how these motifs affect the interaction between the peptides. Focusing on the last 40 ns of the simulation we find that the hydrogens bonds between R13-D22 and D17-R29 prevail, with occ. 84.35% and 65.15%, however the Y6-A17 hbond in no longer important. Conversely, an Hbond between Ser21 of PlnE and His33 of PlnF is beginning to have a strong presence with occurrence equal to 9.4%.

During the simulation of model B, the hbond Arg13-Asp22 was present again, with an occurrence of 64.61%. Arg29 of PlnF interacts now with the side chain of Ser11 of PlnE (occ.=29.14%), in contrast with the proposed model that implies they should be in the outer surface of the dimer (Figure 2-3) and not interacting. Furthermore, a hydrogen bond is formed between the side chains of His14 of PlnE and Ser26 of PlnF (occ.=19.20%). However, what could be considered problematic is the connection with an internal hydrogen bond between the side chains of Arg13 and Asp17 of Plantaricin E that creates a bend on its structure and thus attenuates the interaction between the two peptides. The same hydrogen bonds are observed during the last half of the simulation, with only the occurrence of R13-D22 having increased slightly.

2.3.3. Simulation of the individual peptides in the presence of DPC micelles

Pre-equilibrated DPC micelle structures were obtained from the online server CHARMM-GUI. Each peptide was placed in different orientations with respect to the micelle surface in order to better examine the helical domains observed by the NMR experiments. Each orientation was chosen, so that a different surface of a helix, with similar hydrophobic character, faces the micelle (Figure 2-7).

In total, seven systems were created, four for PlnE and three for PlnF. In models Es3, Es1, and Fs1 mostly hydrophobic aminoacids face the micelle, so the peptides were expected to be inserted into the micelle leaving the polar aminoacids to interact with its surface. The production simulations have run for 20. Dihedral angle analysis, as well as energy calculations were performed to monitor the stability of the peptides and their interaction with the micelle. Snapshots of two of the systems can be found in Figure 2-8.

Figure 2-7: Definition of the different Peptide-micelle systems

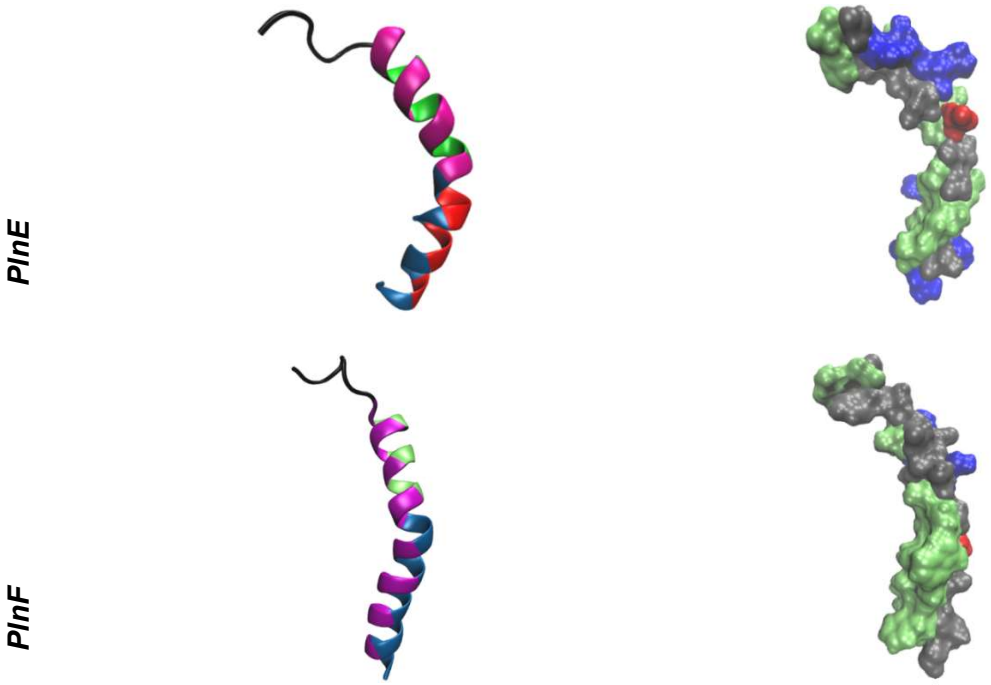

a) Definition of the residue groups that face the micelle: Es1:green, Es2:magenta, Es3:blue, Es4:red, Fs1:magevta, Fs2:green, Fs3:blue

b) Accessible surface area. Red: acidic residues; Blue: basic residues; Green: hydrophobic residues; Gray: polar uncharged residues

The distance of the center of the mass of the Plantaricin E with respect to the micelle is reported in Figure 2-9. Only in the case of simulation Es1, does Plantaricin E enter the hydrophobic core of the micelle, while it keeps its initial orientation. The more it was inserted inside the micelle the more favorable the interaction became, as the energy of interaction between the peptide and the micelle was decreasing. Nonetheless, we see that the energy of the peptide increases during the last 5 ns. In simulations Es2 and Es3

the initial polar aminoacid placement near the polar heads of the lipid, forced the peptides to stay on the surface. There is a measurable increase of energy in ES3, because even though there are favorable interactions with the micelle, the peptide bends around Ser21 probably creating strains. In Es4 the peptide quickly departs and appears to not interact with the micelle. This could be because there were no polar residues facing the micelle originally, to initialize the interaction between them. In most simulations, the dihedral angles were considerably stable and agreed with the NMR measurements.

Figure 2-8: Snapshots of systems Es1 and Es2

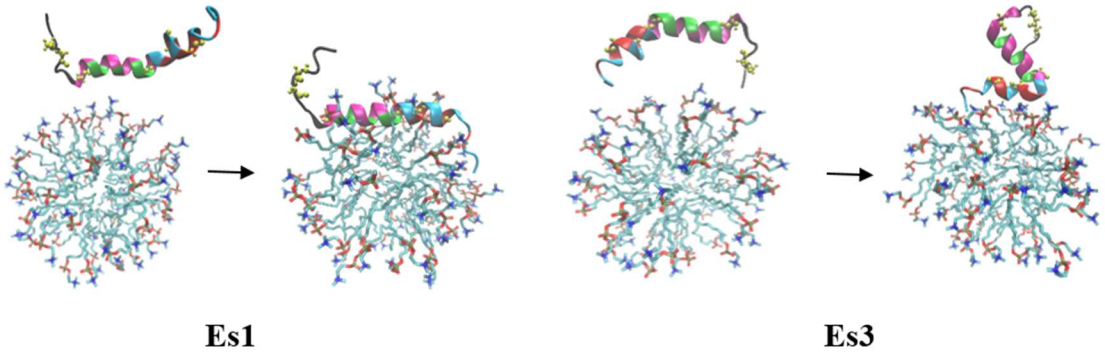

Initial and final snapshots of systems Es1 and Es2. The peptides are colored based on the scheme in Figure 2-7. The hydrophobic core of the micelles is colored cyan, while its polar heads red and blue.

Figure 2-9: Center of mass the peptides with respect to the micelle

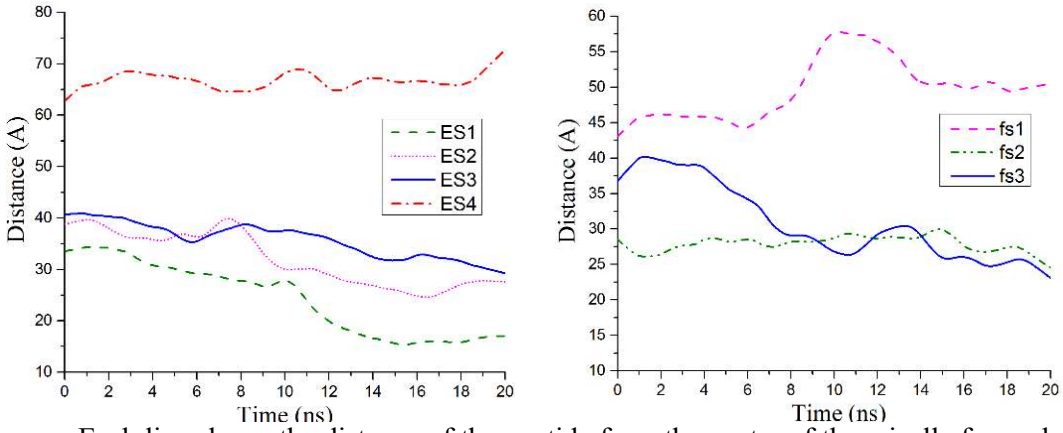

Each line shows the distance of the peptide from the center of the micelle for each simulation. The hydrophobic core of each micelle extends from 0 to ~19Å.

Regarding Plantaricin F, simulation of model Fs1 was the most prominent to result in insertion of the peptide in the micelle, however this event was not observed. The reasons are probably similar to the non-insertion of PlnE in ES4. On the other hand, in both Fs2 and Fs3 the peptide remained on the surface of the micelle, surrounded by the polar head groups of the DPC molecules, and exhibited similar behavior as PlnE in Es2 and Es3.

2.4. Conclusions

The simulations we describe in this chapter indicate that the peptides interact strongly with each other, as well as with DPC micelles – a simple model of membrane environment. Based on experiments that have been conducted previously, it would be expected that they would not demonstrate structural elements in an aqueous environment. However, this is not the case. Plantaricin E seems to be quite stable in water in contrast to Plantaricin F. Nonetheless, one cannot come to conclusion with only 85ns of simulation, since there would not be enough time for the peptides to unfold properly. However, the investigation of folding and unfolding dynamics of these peptides is not of primary interest for our research. When they are introduced together, it is observed that a lot of their initial structure is lost in favor of interaction between them.

The simulations of the peptides in presence of a DPC micelle provided an insight on which parts of each peptide are more potent to interact with either the polar head groups or the hydrophobic core of a membrane mimicking system. It seems that the helix, formed by residues 8-24 of Plantaricin E has an amphiphilic character. The one side of the helix, which is consisted of hydrophobic residues, can interact strongly with a membrane core as shown in simulation Es1. Simultaneously, this enables the free polar residues on the other side of the helix (including Arg13 and Asp17) to interact potentially with PlnF. On the other hand, Plantaricin F forms two helical domains, which could interact with a membrane, as shown in simulations Fs2 and Fs3. The other side of the C-terminal helix (where Asp22 and Arg29 are located) could form Hbonds with PlnE. Nonetheless, the insertion of PlnF reached only the polar surface and the outer level of the hydrophobic core of the micelle, suggesting that this peptide cannot serve as a transmembrane protein individually. However, interaction with Plantaricin E or a transmembrane protein may stabilize and facilitate the insertion of Plantaricin F in the membrane as well.

Chapter 3

Behavior of a class IIb bacteriocin and its mutants on the surface of a model lipid bilayer

3.1. Introduction

The details of the mechanism of action of bacteriocins are unclear. As discussed in paragraph 1.2.1 the bactericidal activity of AMPs is linked to permeabilization of the cell membrane or disruption of a vital process of the target organism. In both cases, AMPs are hypothesized to interact with the bacterial membrane surface of their target host, mainly by electrostatic forces [34,122–124]. In many cases, AMPs are thought to form aggregates and pores, which induces an ion efflux that leads to cell death [124,125]. It has been shown that the activity of class II bacteriocins is similarly connected with the disruption of the membrane of the targeted bacteria [82]. However, there is no direct evidence that they form aggregates or pores on their own. On the other hand, experiments have revealed that their activity is often associated with the presence of specific transmembrane proteins that act as receptors [53]. Diep *et al.* reported that a class IIa bacteriocin, Lactococcin A, binds to the cytoplasmic component IIAB of man-PTS. Upon binding, man-PTS likely undergoes a conformational change that results in unregulated flux of ions and eventual cell death [68]. Similarly, another transmembrane protein, UppP/BacA, has been identified as a potential receptor for Lactococcin G, a class IIb bacteriocin [78]. However, the detailed interaction of the class II bacteriocins with their transmembrane receptor is unknown.

The receptor mediated mode-of-action apparently involves the so-called "*membrane catalysis*" [44]. First the bacteriocins interact with the bacterial membrane and then diffuse laterally until they encounter their receptor, rather than diffuse in the aqueous solution. In this manner, the rate of interacting with the target transmembrane protein is increased. The reduction of dimensionality has been dubbed "the nature's trick" to

overcome the diffusion control barrier [126]. Nisin and other class I bacteriocins are thought to follow a dual mechanism of action. At micromolar concentrations, nisin peptides interact directly with the membrane and form target-independent pores, while at nanomolar concentrations they bind to lipid A, a component of Gram-negative bacterial membranes, and form target-mediated pores [42]. It could be speculated that class II bacteriocins have a dual MOA as well and the interaction of the peptides with the membrane could be presumed a key step underlying their mechanism of action.

We are interested in class IIb bacteriocins, and particularly in Plantaricin EF (PlnEF). In paragraph 2.1 we summarized the experimental studies conducted previously about the behavior and MOA of PlnEF. We know that PlnEF kills the target organism by causing membrane disruption and uncontrollable leakage of the cell content. For the bactericidal activity, both peptides are needed at a 1:1 ratio, indicating that they form a dimer complex. It is not clear when the peptides interact with each other; however, structural studies and our results presented in 0 suggest that the peptides reach the membrane first as they are mostly unstructured in water.

Based on the above results we imagine the mechanism of action of PlnEF as depicted in Figure 3-1. The two peptides interact first with the membrane and are adsorpted on the surface where they adopt α-helical structures (A). Then they either associate and form a surface dimer (D) or are inserted in the bilayer (B) and form a transmembrane dimer (C). In an unknown fashion the dimer then causes membrane permeabilization, possibly by disrupting the continuum of the membrane or by interacting with a membrane protein receptor (E).

In the work described in this chapter, we employed atomistic molecular dynamics simulations to investigate the behavior of the class IIb bacteriocin PlnEF on the surface of lipid bilayer. We are interested in the specific amino acids or structural motifs that are responsible for the interaction between the peptides and the interaction of the peptides with a model membrane of Gram-positive bacteria. Additionally, we simulated peptides that contain a single amino acid substitution, and compare the results from simulations to the bactericidal activity. The work described in this chapter has been presented in a peer-reviewed publication [102].

Figure 3-1: Possible steps of the MOA of PlnEF

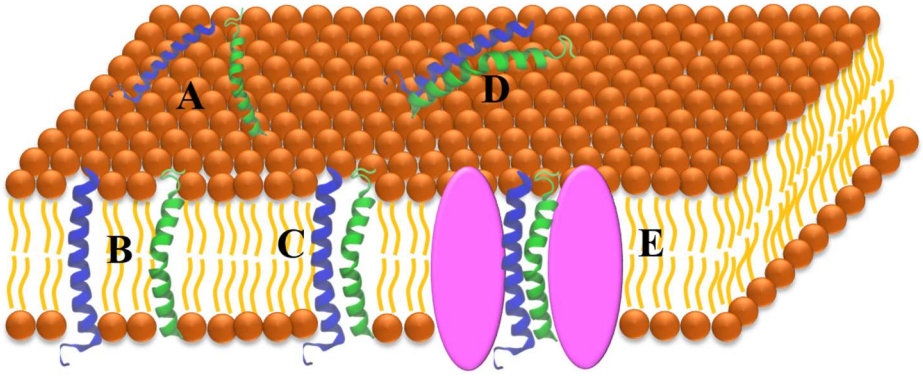

Previous experimental studies as well as our simulation (presented in 0) suggest that the peptides first interact with the membrane and adopt a α-helical structure. Therefore, we can assume that the first step of the mechanism of action of PlnEF is the adsorption of each peptide (PlnE in blue, PlnF in green) individually on the surface of the bilayer (A). Then the peptides could insert in the membrane (B) and upon interaction, form a transmembrane dimer (C). The dimer could cause membrane disruption or interact with a receptor (in pink) in a pore forming fashion (E). Alternatively, the peptides interact first on the surface (D) and enter the membrane as a dimer (C) or interact with a receptor (E) to cause cell death.

3.2. Materials and methods

Eigth different systems were studied with atomistic molecular dynamics (MD) simulations. Each system contains models of the two peptides (PlnE and PlnF), a lipid bilayer that mimics the bacterial membrane, water molecules, and ions. The first system contains the wild type peptides. In addition, we chose to simulate seven dimers that contain single amino acid mutations at key positions (simulations E(G20A), E(R13D), E(I32R), F(S26T), F(D22R), F(P20A), F(R29I)), in combination with the cognate wild type peptide, and compare the results to measured differences in activity.

3.2.1. Simulation Methods and Parameters

Molecular dynamics simulations were carried out using the NAMD 2.9 simulation engine [115] with the CHARMM param36 force field [116] under constant pressure and temperature (NPT ensemble). The simulation parameters were kept constant in all the simulations. Initially each system was minimized using the conjugate gradient algorithm provided in NAMD. This was followed by gradual heating to 310 K while the peptides and lipid atoms were subjected to positional harmonic restraints. Then numerous

equilibration steps were performed while the restraints were gradually removed. Equilibration and production runs were carried out at atmospheric pressure. A timestep of 2 fs was employed. Van der Waals potential was truncated at 12 Å, introducing a switching function at 10 Å, while the real space cutoff distance of the PME electrostatics calculation was also set at 12 Å. Coordinate snapshots were recorded every 10 picoseconds. Both wild type configurations were simulated for 400 ns in total, while the simulations of the systems with the mutated peptides were run for 200 ns.

3.2.2. Atomistic model of PlnEF, and a membrane

The 3D structures of the two peptides that constitute the bacteriocin PlnEF, PlnE and PlnF were obtained from the PDB database (PDBID 2jui and 2rlw respectively) [112]. The structure of the mutated peptides was created using the VMD mutator plugin, employing the structure of the wild type peptides as a scaffold [117].

A model lipid bilayer containing POPG (1-palmitoyl-2-oleoyl-sn-glycero-3-phosphoglycerol) and POPE (1-palmitoyl-2-oleoyl-sn-glycero-3-phosphoethanolamine) lipids at 3:1 ratio was used to simulate the membrane of Gram-positive bacteria. Analysis of the bacterial membranes of many Gram-positive bacteria reveals that PE and PG heads prevail at the ratio mentioned above [127]. It would be ideal to be able to simulate model bilayers as complex as real cell membranes, however due to computational cost we have to use a more simplistic model. The model used is a symmetric model since in an atomistic bilayer system one cannot differentiate between the inner and outer environment of a cell, that gives rise to the asymmetry of real cell membranes [128]. POPG and POPE lipids at a 3:1 ratio were used before to simulate a similar system as well [100]. The structure of the model bilayer was obtained from the online server CHARMM-GUI and was simulated for 50 ns before the insertion of the peptides to ensure the equilibration of the membrane features [119].

In total, each system contains the two peptides, 160 lipid molecules, more than 8,000 molecules of water and enough NaCl ions to make the system electroneutral and to create an additional 0.15 M physiological salt solution.

3.2.3. Positioning of the peptides on the surface of the membrane

We used the methodology described at paragraph 2.2 to generate initial dimer structures. Then the dimer structures were positioned parallel to the surface of the

membrane, guided by our peptide-micelle simulation results presented in 0 and optimizing for the most polar surface of the dimers to face the polar surface of the membrane. The two different conformations were simulated only in the case of the wild type peptides. All the systems containing mutations were simulated only in the parallel conformation since it was found to be more energetically favorable for the case of the wild type peptides.

3.2.4. Bacteriocin activity assay

The experimental activity measurements described in this chapter were provided by B. Ekblad and P. E. Kristiansen at the Department of Biosciences, in the University of Oslo, Norway. The experimental methodology is described in the appendix A. We contributed to the choice of mutants to be tested and interpretation of the results, guided by our previous simulations as well as results of the simulation of the wild type peptides.

3.3. Results and Discussion

We focus on simulations of the wild type peptides adopting two conformations, a parallel one, and an antiparallel one. We are interested in the interactions between the peptides that comprise the dimer, as well as the interactions of the dimer with the membrane. In addition, we chose to simulate seven more dimers that contain mutations at key positions (simulations E(G20A), E(R13D), E(I32R), F(S26T), F(D22R), F(P20A), F(R29I)). The objective of these simulations is to investigate how different amino acids affect the nature and the strength of the interactions observed in simulations containing the wild type peptides and compare the results to the antimicrobial activity of the peptides. Our ultimate goal is to explore any possible connection between the experimental activity of the various mutants and the biophysical image observed during the simulations. We first report the experimentally observed activities of the wild type and mutant variants of PlnE and PlnF. The results of the molecular dynamics simulations follow.

3.3.1. Experimental antimicrobial activity

Antimicrobial activity of the wild type and mutant variants of the two peptides that constitute the bacteriocin PlnEF, were determined against three indicator strains in a microtiter plate assay system, essentially as described by Nissen-Meyer *et al.* [129] The relative activity of the different peptide combinations against the indicator strains is

shown in Table 3-1.

Table 3-1: Antimicrobial activity of PlnEF

Peptide combination	LTH1174	NCDO 990	NCDO 521
E + F	1	1	1
E(R13D) + F	>512	>64	>256
E(D17R) + F	>512	≥ 32	≥ 64
E (G20A) + F	≤ 0.5	0.5 ± 0	0.3 ± 0.1
E(I28R) + F	24 ± 9	-	-
E(I32R) + F	10 ± 4	-	-
E + F(P20A)	2 ± 1	9 ± 1	5 ± 2
E + F(D22R)	40 ± 16	32 ± 0	16 ± 0
E + F(S26T)	8 ± 6	7 ± 2	5 ± 2
E + F(R29D)	20 ± 8	16 ± 0	21 ± 9
E + F(R29I)	8 ± 3	-	-
E(R13D) + F(D22R)	>256	>64	≥ 128
E(R13D) + F(R29D)	>256	>64	>256
E(D17R) + F(D22R)	>256	>64	≥ 64
E(D17R) + F(R29D)	>256	>64	>256
E(I28R)+ F(R29I)	49 ± 19	-	-
E(I32R)+ F(R29I)	25 ± 11	-	-
E(R13D)	>2560	>320	>1280
E(D17R)	>2560	>320	>1280
F(D22R)	>2560	≥ 160	90 ± 60
F(S26T)	>2560	>320	≥ 320
F(R29D)	>2560	>320	>1280

Relative mean MIC values and standard error of the mean of various wild type and mutant peptide combinations against three different indicator strains. The strains used were: *Lactobacillus curvatus* LTH1174, *Pediococcus pentosaceus* NCDO 990 and *Pediococcus acidilactici* NCDO 521. The MIC values were determined from three or more independent measurements.

Several mutations have been tested. Most of the mutated peptides exhibited worst

or similar activity when compared to the wild type peptides (Table 3-1). Only the mutation of Gly 20 of PlnE to an Ala (G20A) contributed to an increase in activity. Substituting the Arg residue at position 13 in PlnE with an Asp (R13D) was very detrimental. The same trend was seen when substituting the Asp residue with an Arg at position 17 (D17R) in PlnE. Decreasing the hydrophobicity of the C-terminus of PlnE, by substituting Ile at positions 28 or 32 to an Arg (I28R and I32R), resulted in a significant reduction of activity.

Figure 3-2: Snapshots from simulations of the wild type peptides

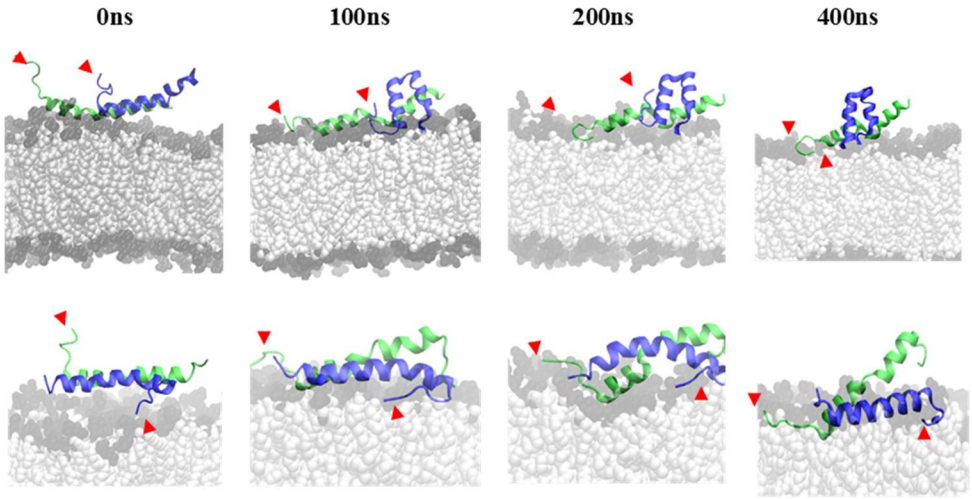

Snapshots from simulations of the wild type peptides in a parallel conformation (top row) and in an antiparallel conformation (bottom row) at 0 ns, 100ns, 200ns and finally 400ns. In the first snapshot, the structure of the peptides is similar to their NMR structure. PlnE is shown in blue and PlnF in green. Both peptides are shown in cartoon format. The lipids are shown as a sequence of spheres, using their van der Waals radius. The hydrophobic tails are colored light grey while the hydrophilic heads are colored dark grey. Red triangles point to the N-terminal of each peptide.)

Substituting the Pro residue in PlnF with an Ala (P20A) did not have any marked effect on the activity. The Ser residue at position 26 in PlnF was substituted with a Thr residue (S26T), which resulted in approximately 8-fold reduction in activity. The activity is hence decreased compared to the wild type combination. Similar behavior was observed during the mutation of Arg at position 29 of PlnF to an Ile (R29I). The mutations R29D and D22R of PlnF reduced the activity approximately 20 to 40 times, respectively.

Combinations of different mutants with opposite charge, such as the E(R13D) with

F(D22R) or E(D17R) with F(R29D), were also tested, to investigate if some of the wild type activity was retained (Table 3-1**).** All combinations were detrimental for the indicator strains tested. In all cases the mutated variants of the peptides tested without their complementary peptide, did not result in any activity against the indicator strains tested.

3.3.2. Simulation of the wild type bacteriocin PlnEF

The simulations were run for 400 ns each. In both the parallel and antiparallel conformations, the peptides adopted a stable structure after the first 50 ns (snapshots of the simulation can be found in Figure 3-2).

Figure 3-3: RMSD analysis

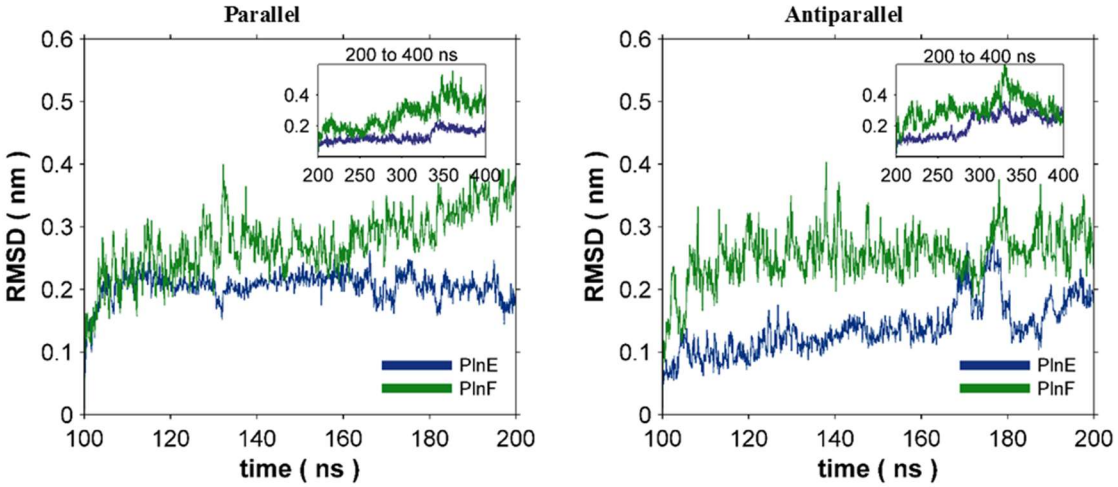

RMSD analysis of wild PlnE (blue) and wild PlnF (green) in the parallel and antiparallel conformations. Main figure: the analysis was performed from the 100th to the 200th ns, with respect to the structure of the peptides at 100th ns. Both the peptides in both simulations are stable for 100 ns. They have backbone RMSD values 0.1-0.3 nm, which is comparable to the NMR analysis. Inlet figures: RMSD values are shown from the 200th to the 400ns, with respect to the structure of the peptides at the 200th ns. Further evolution of the simulations revealed that the structure do not deviate significantly over 200 extra ns.

The peptide structures changed very little between 100 and 200 ns, with the root mean square deviation (RMSD) of the backbone atoms of the individual peptides only varying between 0.2-0.3 nm (Figure 3-3), which is comparable to the optimal rmsd values originated from NMR studies [112,130]. We continued the simulations, until reaching 400 ns, to ensure that the structure of the peptides did not change. The RMSD of PlnE was only 0.1-0.2 nm for the final 200 ns (Figure 3-3a insert). PlnF exhibited a

temporal increase in its RMSD value (picked at 0.5 nm) at the end of the simulations (Figure 3-3b insert). Further analysis was performed over a span of 100 ns (from the 100th to the 200th ns).

Figure 3-4: Structural analysis of wild type PlnEF

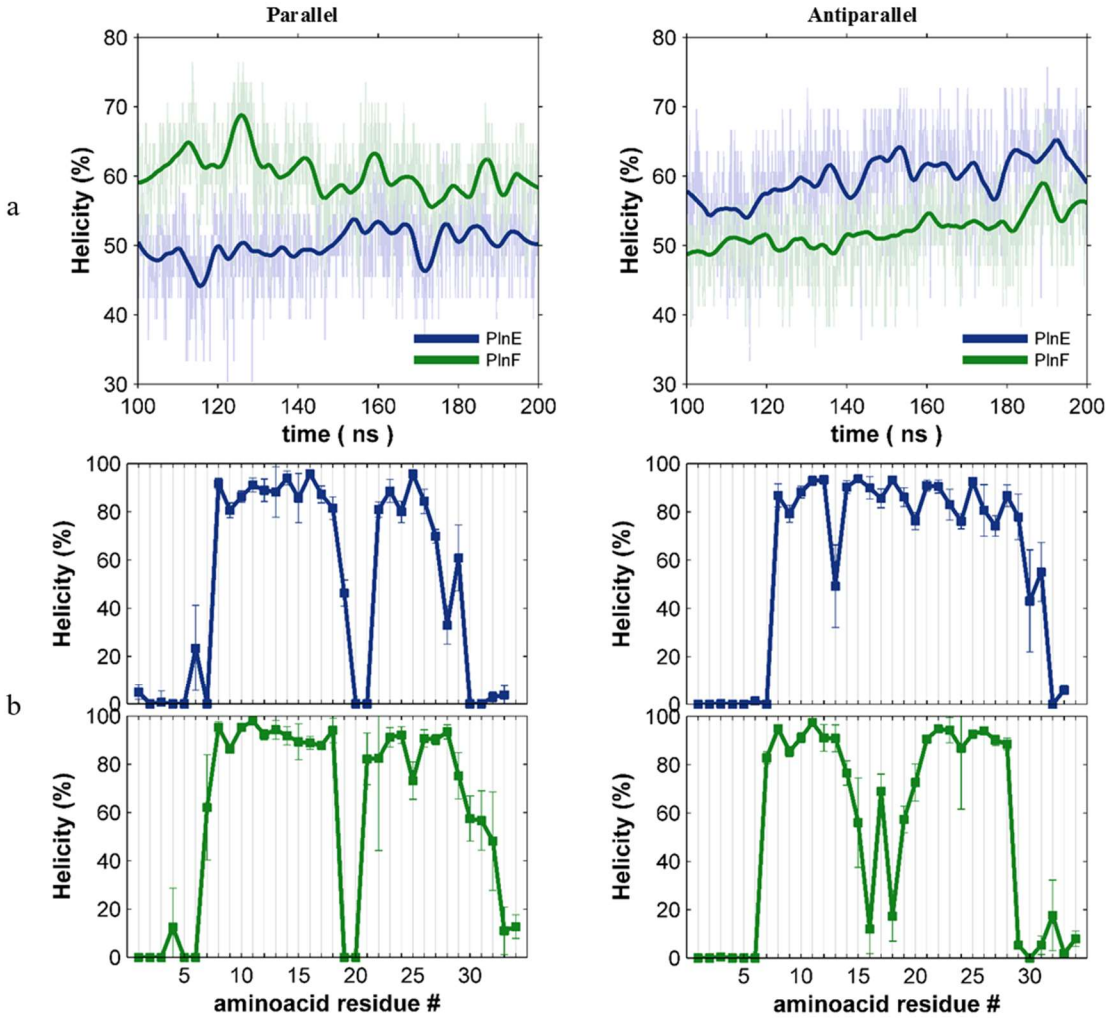

Structural analysis of wild PlnE (blue) and wild PlnF (green) in the parallel and antiparallel conformations. The overall helicity (a) and helicity per residue (b) are shown for each peptide in the parallel and antiparallel conformation. In figure a, row data are plotted with light color, while the darker colored lines represent running averages over 10 frames.

Secondary structure of the peptides

NMR studies revealed that PlnE forms two α-helical regions (residues 10 to 21 and 25 to 31) separated by the flexible $G_{20}xxxG_{24}$ motif, having a total of 51-57% helical

content, while PlnF forms one helix (residues 7 to 32) with a kink around P20 and has 76% helical content [112]. During the simulation of the parallel dimer conformation, the helical contents, and distributions of both peptides are in great agreement with the NMR results (Figure 3-4). However, we notice a more distinct bending of PlnE around G20 and a discontinuity of the α-helix of PlnF, which could explain the significant decrease of the helical content of PlnF (Figure 3-4). The flexibility of the peptides around these regions may be associated with the presence of amino acids that are known to disrupt helices, such as Glycine (G20 of PlnE) and Proline (P20 of PlnF) [131,132]. Moreover, hydrogen bonds are formed between polar amino acids and particularly the hydroxyl group of Serine (such as S26 and S16 of PlnF, Figure 3-5) with neighboring backbone amides. These hydrogen bonds could presumably enhance the flexibility of the α-helical domains and their bending angle, as suggested by various studies [133–135].

Figure 3-5: Serine contribution to multiple hydrogen bonds

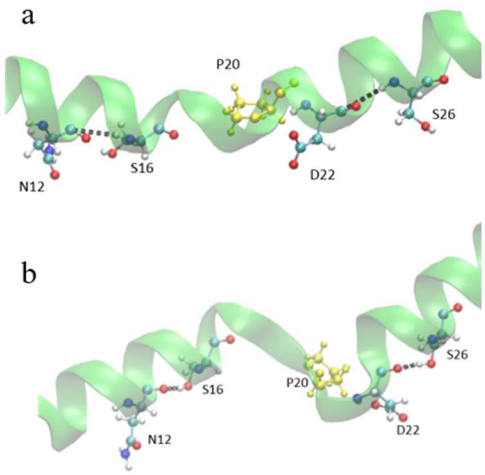

Example of the diverse role of Serine aminoacids that is suggested to modulate a Proline kink. Top: Serine residues form α-helical backbone hydrogen bonds with residues four positions earlier. Bottom: The hydroxyl of the functional group of Serine residues attacks the backbone amide four positions earlier. PlnF is shown as green cartoon. The Proline residue is colored yellow, while all the other residues are colored per atom. Carbon atoms are colored cyan, hydrogen atoms blue, oxygen atoms red and nitrogen atoms blue

In the simulation of the antiparallel dimer conformation, we observed a different behavior (Figure 3-4). The helical content of PlnE is increased, as it now forms one continuous helix from residue 8 to 31. On the other hand, the helical content of PlnF is

markedly decreased and it forms two short α-helices.

The difference between the NMR structures and the structures resulting from the simulations could be attributed to the following: i) the peptides were studied individually during the NMR studies, ii) the cell membrane model used for the NMR studies was DPC micelles while a lipid bilayer was used in the simulations. Thus, the presence of the complementary peptide, as well as the different membrane models could effectively alter the environment and may result in a different structure.

Interaction of the peptides with the membrane

In the simulation of the parallel dimer conformation, two regions of PlnE interact strongly with the membrane (Figure 3-6). The first region includes residues 4 to 10, with the interaction being mediated by salt bridges and hydrogen bonds between primarily residue K10 with the membrane and, to a lesser extent, between R8, Y6 and N7 with the membrane (Figure 3-6 and Figure 3-7). The second region includes amino acids 31 to 33, where hydrogen bonds and a prevalent salt bridge are formed between R33 and the membrane. The first region inserts measurably into the lipid surface.

Figure 3-6: Distance of the wild-type peptides from the membrane center

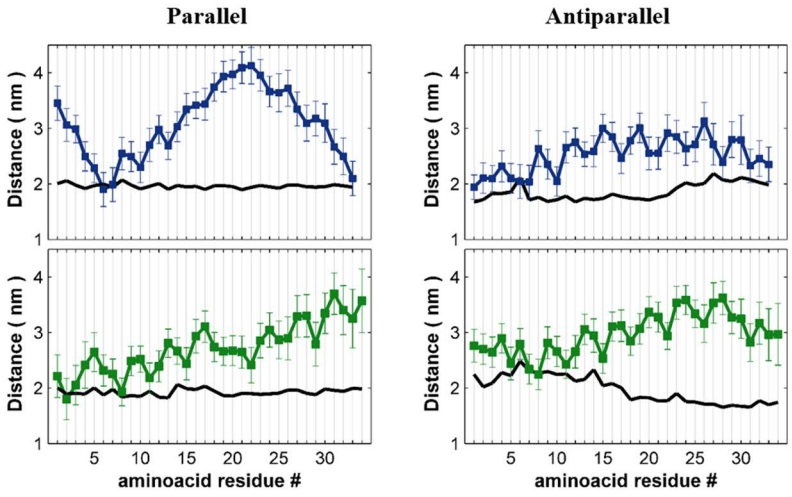

The distance per residue of each peptide from the membrane center is shown, along the z-direction; the black line represents the local distance of the Phosphate groups of the leaflet containing the peptide from the center of the membrane

PlnF interacts with the membrane only through its N-terminus, (residues 1 to 15). Three salt bridges are formed throughout the simulation between R8, R11 and K15 with the membrane, as well as multiple hydrogen bonds. Notably, bidentate hydrogen bonds

are formed between the side chains R8 and R11 with the membrane phosphate groups. These type of interactions have been reported previously in literature and are believed to increase the penetration of Arginine rich peptides in the membrane [136,137]. The total potential energy contribution of the interaction between the peptides and the membrane is approximately -1360 kcal/mol. However, these local interactions do not seem to disrupt the integrity of the membrane, as revealed by the homogeneity of the lipid density of the leaflet containing the peptides (Figure 3-8).

Figure 3-7: Membrane – peptide interactions

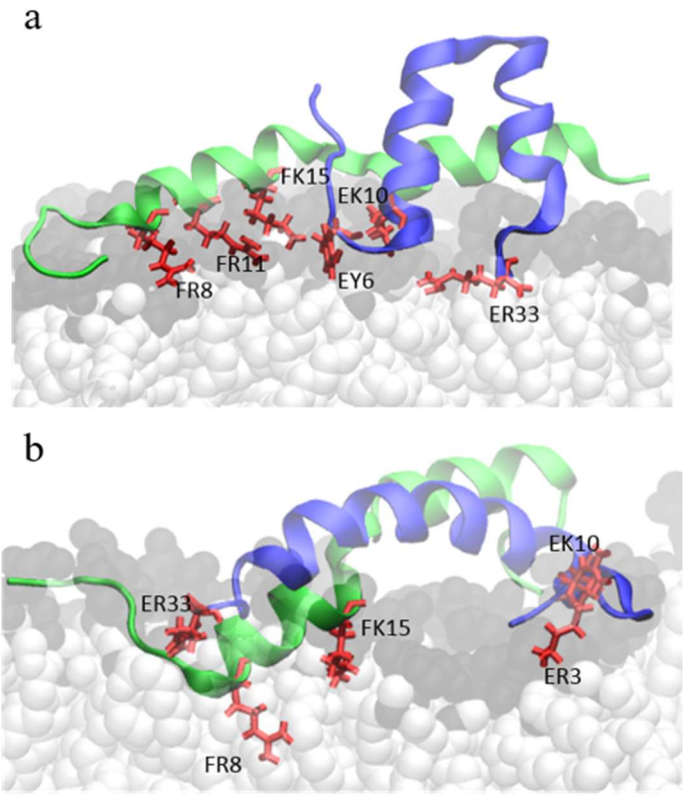

Snapshot of the simulations of the parallel conformation (top) and antiparallel (bottom) showing the most representative interactions between the dimer and the membrane. Individual residues that take part in these interactions are colored red and named in black. PlnE is shown in blue and PlnF in green. Both peptides are shown in cartoon format. The lipids are shown as a sequence of spheres, using their van der Waals radius. The hydrophobic tails are colored light grey while the hydrophilic heads are colored dark grey.

In the case of the antiparallel dimer conformation, on the other hand, there is a significant deformation of the leaflet containing the peptides (Figure 3-8). Indeed, the

potential energy of interaction between the peptides and the membrane is approximately -1800 kcal/mol. A closer look reveals that PlnE interacts with the membrane more strongly than in the parallel model (Figure 3-6 and Figure 3-7). Two regions of interaction between PlnE and the membrane can be distinguished. The first includes the N-terminal residues 1 to 10, forming various hydrogen bonds and salt bridges with the membrane, most importantly R3 and K10, and a second region that includes residues 28 to 33. PlnF exhibits similar behavior as in the parallel model.

Figure 3-8: Membrane deformation

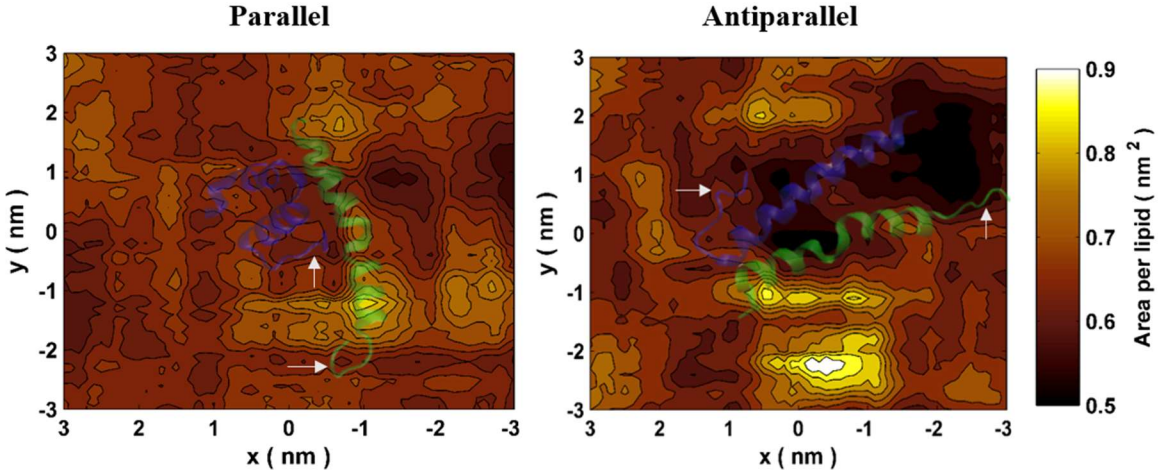

The average area per lipid for the layer containing the peptides is shown. A transparent snapshot of an average structure of the dimer indicates where the peptides are positioned on the layer from a top view. The wild PlnE is colored blue, while the wild PlnF green. White arrows point to the N-terminal of each peptide.

Peptide-peptide interactions

The two peptides interact with each other around their middle section throughout the simulation of the parallel dimer conformation, forming various hydrogen bonds and salt bridges. Mainly, a salt bridge is formed between K10 of PlnE and D22 of PlnF initially, which is replaced later by a salt bridge between R13 of PlnE and D22 of PlnF. A hydrogen bond is formed strongly between R3 of PlnE and the backbone of V18 of PlnF. Interestingly, intramolecular hydrogen bonds are formed in PlnE, between amino acids F1, R3 and D17, which connect the N-terminal coil region of PlnE with its N-terminal α-helix. Moreover, hydrophobic residues, located at the C-terminus of PlnF and the N-terminus of PlnE, are buried in the area between the two peptides, presumably making the interaction between the two peptides more entropically favorable.

In contrast, the two peptides interact only weakly in the simulation of the antiparallel dimer conformation. The only salt bridge formed in this case, is the one between R13 of PlnE and D22 of PlnF. The potential energy of interaction between the peptides is positive (15.3 kcal/mol while in the case of the parallel this is -39.4 kcal/mol).

In neither simulation do the GxxxG motifs bring the helices in close contact (Figure 3-9). This behavior shows that the GxxxG motifs do not bring helical domains in proximity at the membrane surface. This observation is in agreement with the findings of recent computational and spectroscopic studies which revealed that the GxxxG motifs not always provide a dimerization surface [138,139].

Figure 3-9: The behavior of possible GxxxG motifs

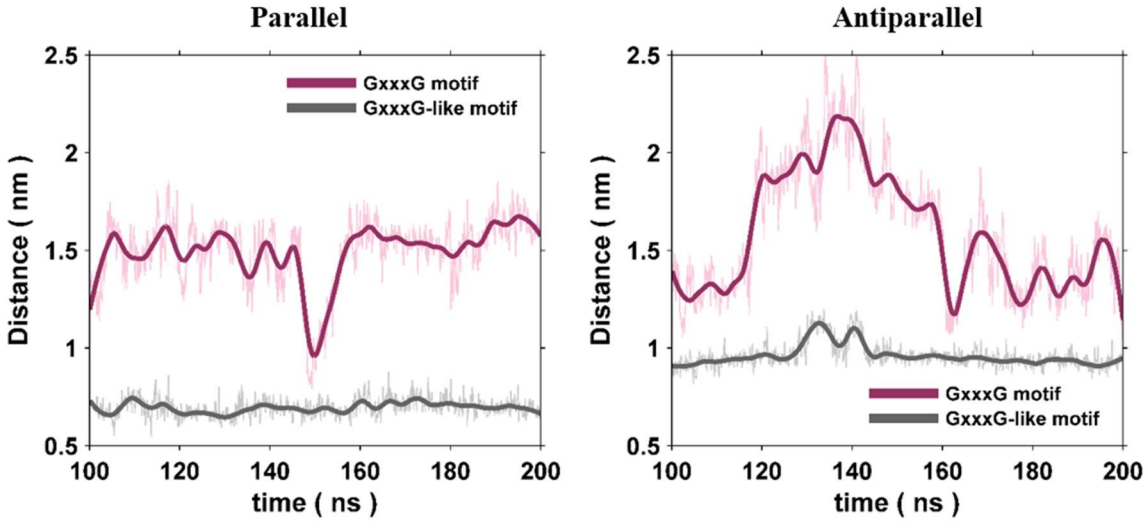

Evolution of important GxxxG and GxxxG like motifs through the simulations of the parallel and antiparallel conformations. In both models, the GxxxG motifs (parallel: G20xxxG24 of PlnE - G30xxxG34 of PlnF ; antiparallel:G5xxxG9 of PlnE - G30xxxG34 of PlnF) are located more than 1nm away, indicating that they do not contribute to the interaction between the peptides. On the other hand, we observed other GxxxG-like motifs that aid the interaction of helical domains of the peptides. In the parallel model: the distance between the V12xxxV16 motif and the A23xxxG27 (both belonging in PlnE) is ~0.7nm. While in the antiparallel model, the distance between the V12xxxV16 motif of PlnE and the V24xxxV28 of PlnF is ~0.9nm. Row data are plotted with light color, while the darker lines represent running averages over 10 frames.

On the other hand, in the parallel conformation, the $V_{12}xxxV_{16}$ motif and the $A_{23}xxxG_{27}$ (both in PlnE) let the two helical domains of PlnE approach each other and intensify the bending around G20. In contrast, in the antiparallel conformation the

$V_{12}xxxV_{16}$ of PlnE motif and the $V_{24}xxxV_{28}$ of PlnF allow the proximal contact of the N-terminus of PlnE and the C-terminus of PlnF (Figure 3-9).

3.3.3. Simulation of dimers of PlnE and PlnF that contain single amino acid substitutions

The interaction of an antimicrobial peptide with a membrane model indicates which residues may be important for its activity. However, it is not obvious how a modification of these residues will affect the activity. We simulated various mutant dimers in order to examine how the biophysical key observations, originated from the simulations of the wild type peptides, might be connected with the bactericidal activity. The dimers were simulated only in the parallel conformation since we determined that under these conditions the peptides would be more likely to interact favorably with each other.

All simulations were run for 200 ns. In only five of these systems (mutants E(G20A), E(R13D), E(I32R), F(S26T), F(D22R)), the structure of the peptides was stabilized after the first 50 ns and their rmsd value was 0.2-0.3 nm. Further analysis was performed between the 100^{th} and 200^{th} ns. During simulations on F(P20A) and F(R29I) the structure of the peptides continued to evolve throughout the simulation and the helices slowly unraveled (data not shown). Therefore, no further analysis is shown for systems F(P20A) and F(R29I).

Simulation of the mutant E(G20A)

The first system contains a mutation on Glycine 20 (G20) of PlnE to an Alanine. This residue was chosen as it plays an important role in the structure of PlnE. It is located in the middle of the peptide, dividing its structure into two α-helical regions. Glycine is a residue known to disrupt α-helices, while Alanine is an amino acid with high α-helical propensity [131]. Experimentally, this mutation increased the activity of the peptides slightly (Table 3-1).

In the simulation of the E(G20A) mutant (Figure 3-10a and Figure 3-11a), PlnE forms one continuous α-helix as expected. The mutation of G20 to an Alanine enhanced the helical content of PlnE, prompting the creation of a stiff helix. This hinders the flexibility of the peptide and thus only one terminus of PlnE is able to interact with the membrane. Specifically, the residues K30 and R33 that are positioned in the C-terminus of PlnE, form salt bridges with the membrane phosphate oxygens. The mutation has no

effect on the structure of PlnF or its interactions with the membrane. Interestingly, the two peptides interact more strongly in the PlnE-G20A mutant. Mainly two stable salt bridges are formed between the peptides. The first is the one present in simulations of the wild type peptides as well, e.g. a salt bridge between R13 of PlnE and D22 of PlnF. The second salt bridge formed is between D17 of PlnE and R29 of PlnF. The release of the N-terminus of PlnE from the membrane (Figure 3-12a), which was presumably caused by the mutation, likely enabled the two latter residues to approach each other and interact.

Figure 3-10: Snapshot of the systems with mutant peptides

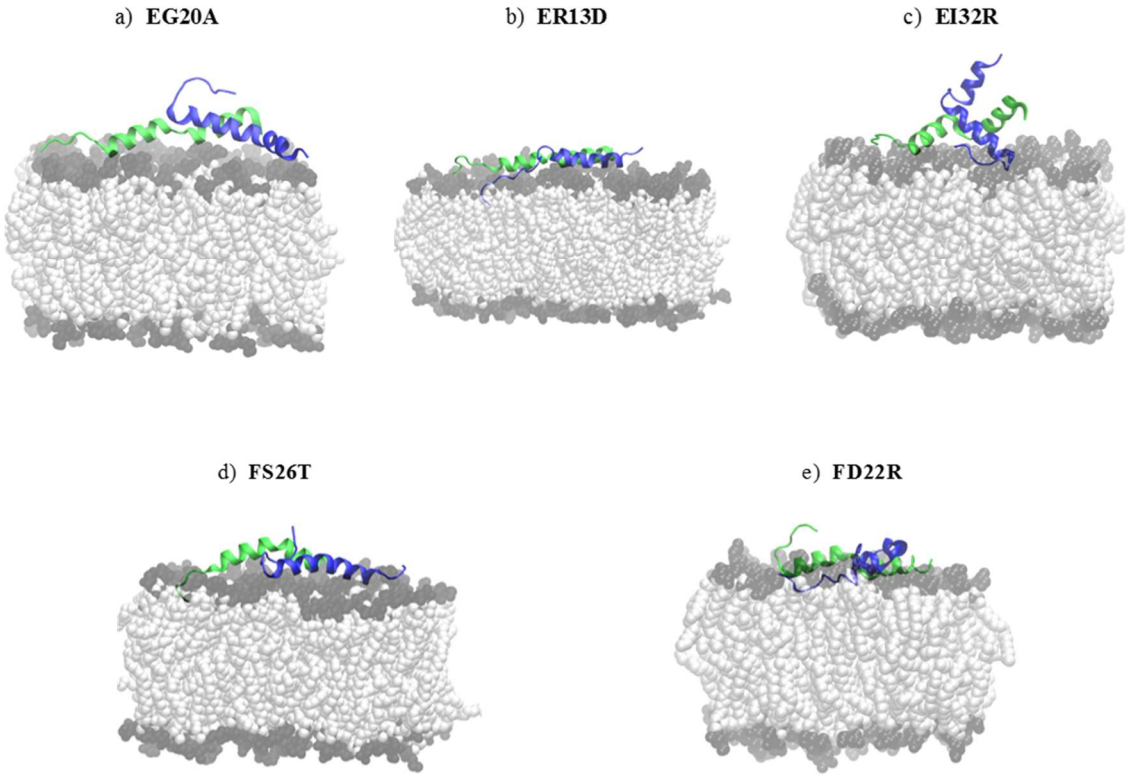

Final snapshots (at 200ns) from the simulations of the systems that contain a mutation. PlnE is shown in blue and PlnF in green. Both peptides are shown in cartoon format. The lipids are shown as a sequence of spheres, using their van der Waals radius. The hydrophobic tails are colored light grey while the hydrophilic heads are colored dark grey.

Simulation of the mutant E(R13D)

The next system we simulated includes a mutation from an Arginine to an Aspartic acid in position 13 of PlnE. R13 of PlnE was the primary source of electrostatic

interaction between the two wild type peptides forming a salt bridge with D22 of PlnF. We were interested in examining how this mutation affects the overall behavior of the peptides. We expected it to have significant effect on their interaction, since this mutation was detrimental to the antimicrobial activity.

Figure 3-11: Structural analysis of the systems containing mutated peptides

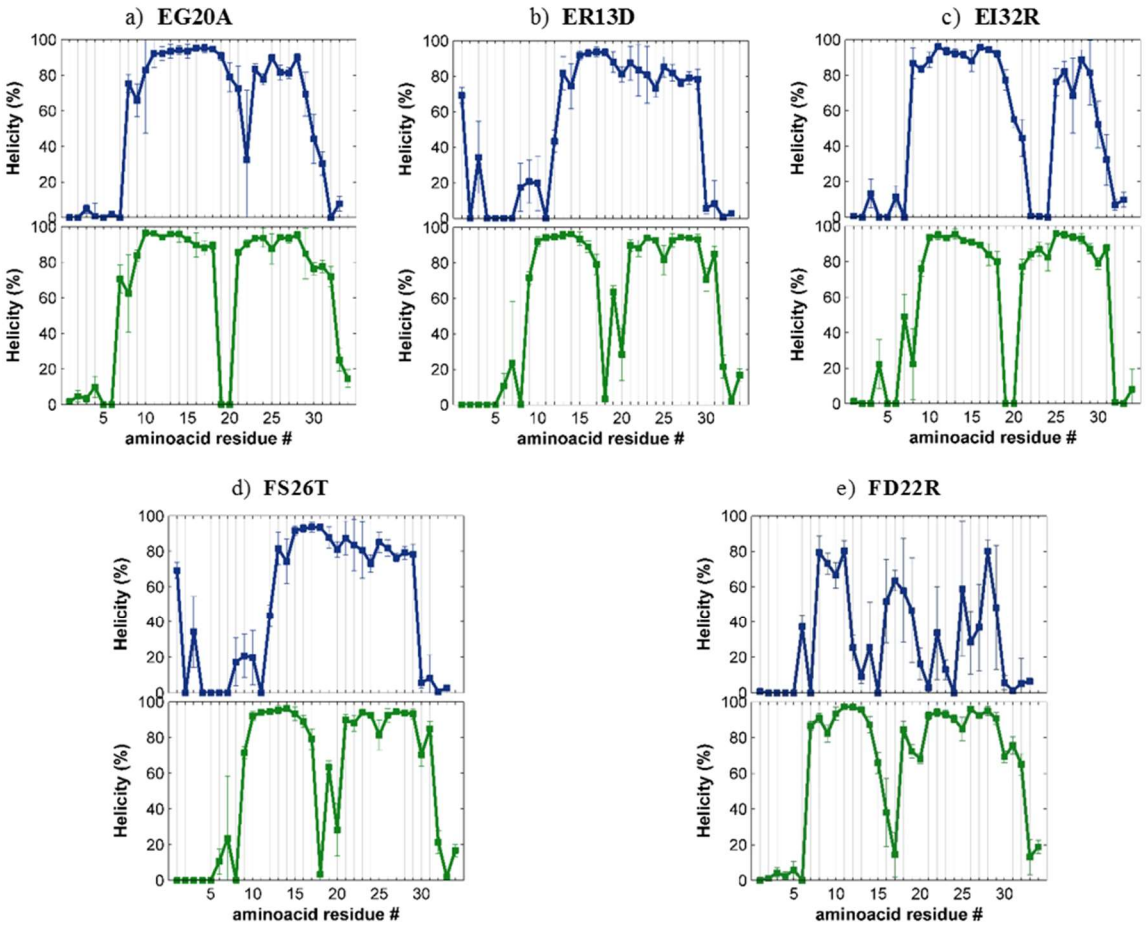

Structural analysis of the systems containing mutated peptides. The percent of the helicity per residue in each simulation is shown. PlnE is colored blue, while the PlnF green.

As expected, the mutation caused a marked decrease in the strength of the interactions between the two peptides. The E(R13D) mutation (Figure 3-10b and Figure 3-11b) caused a loss of secondary structure to the N-terminus of PlnE. Consequently, there is one helical region formed from amino acids 13 to 29. Initially, the unstructured region interacts with the membrane, luring the rest of the peptide towards the membrane (Figure 3-12b). The amount of salt bridges and hydrogen bonds between PlnE and the

membrane is significantly increased with respect to the wild type simulations. PlnF forms two helical regions divided around P20. In contrast to all the previous simulations, both termini of PlnF interact with the membrane. This could be attributed to the absence of interactions with PlnE, rendering PlnF more flexible.

Simulation of the mutant E(I32R)

A mutation of the hydrophobic amino acid I32 to R32 of PlnE believed to increase the interaction of PlnE with the membrane, based on the simulations of the wild type PlnEF bacteriocin. We were thus interested in exploring how such a mutation would modify the activity, the structure, dynamics, and interactions. Activity tests showed that this mutation decreases the bacteriocin activity.

Contrary to the expectations, the C terminal of PlnE(I32R) moves away from the membrane allowing only the N terminal to approach the membrane (Figure 3-12c). The two opposite trends could be the reason that there is a loss of structure of PlnE around residues 20 to 24 (Figure 3-11c). Regarding PlnF, there are not significant deviations from its structure and interactions with the membrane comparing to the simulation of wild type peptides.

There are some interactions between the two peptides (i.e. R13 of PlnE and D22 of PlnF) initially, that disappear later. Interestingly, hydrophobic residues at the C terminal of PlnF (V28, F31, I32) are buried among hydrophobic residues of both the helical regions of PlnE (V12, V15, I19 and I25, I28, L29) (Figure 3-10c).

Simulation of the mutant F(S26T)

The oxygen of the side chain of both Serine and Threonine form hydrogen bonds with the backbone amides of neighboring residues [133]. It has been suggested that when such hydrogen bonds are located close to Proline kinks, they can modulate the angle of the kink. Experimentally, this mutation resulted in a decrease in activity, revealing that Serine and Threonine are not interchangeable.

In the simulation, the mutation of S26 to a Threonine affects the structure of PlnF (Figure 3-10d and Figure 3-11d). Despite the two helical regions, the curvature is smoother compared to the wild type simulations. This allows both termini of PlnF to interact with the membrane (Figure 3-12d). Moreover, T26 does not form a hydrogen bond with N22 of PlnF, but rather interacts with the membrane, likely driving the C-

terminus onto the membrane. The two peptides interact with each other occasionally. However, the salt bridge between R13 of PlnE and D22 of PlnF is not present. As a probable consequence, PlnE, which adopts one continuous helix, is free to interact with the membrane through both its termini.

Figure 3-12: Distance of the wild-type peptides from the membrane center

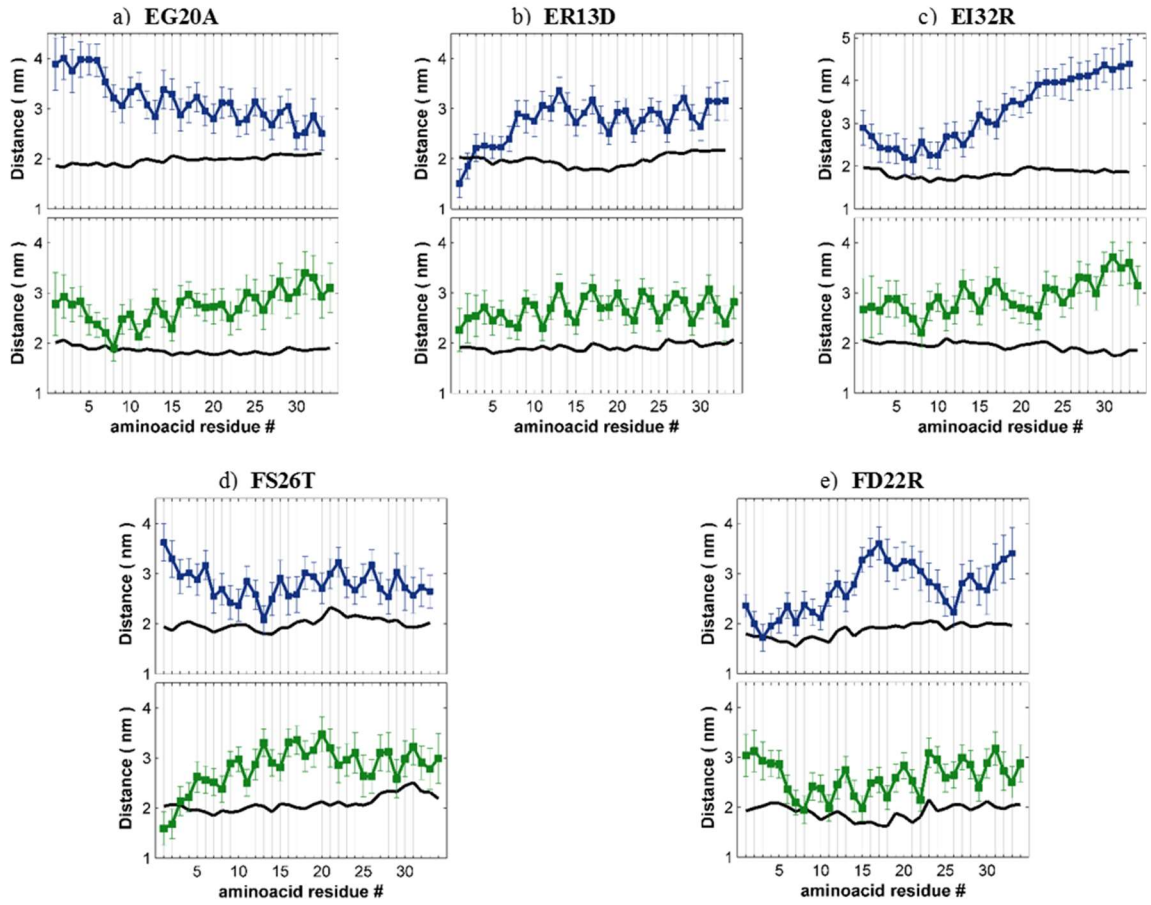

The distance per residue of each peptide from the membrane center is shown, along the z-direction for the systems containing mutated peptides. The black line represents the local distance of the Phosphate groups of the leaflet containing the peptide from the center of the membrane. PlnE is colored blue, while the PlnF green.

Simulation of the mutant F(D22R)

The mutation on PlnF(D22R) (similarly to the PlnE(R13D)) was expected to affect the interaction between the peptides making up the bacteriocin PlnEF. In simulations, the mutation caused a termination of interactions between the two peptides. Thus, leading to increased interactions of each peptide with the membrane. Both the two distinct helical regions of PlnF approach the membrane (Figure 3-10e,Figure 3-11e and

Figure 3-12e). Remarkably, the effects of the mutation are more apparent on PlnE. Since the polar residues of PlnE do not longer interact with PlnF, they are free to approach the membrane (Figure 3-12e). We believe that this leads to the reduction of the helical content of PlnE, as there is a strong drive for its polar residues to face the surface of the membrane. Interestingly, the distance between the two peptides is decreased and various hydrophobic amino acids come close increasing non-favorable interactions and the potential energy of the system.

3.3.4. Connection of simulated biophysical interactions with the experimental activity

The few mutations that were simulated had a significant effect on the peptide-peptide interactions as well as the interactions of the dimer with the membrane. We calculated the energy of these interactions by adding the contribution of the van der Waals and electrostatic forces between each participant. These values were calculated as the averages over the last 100ns of each simulation. We note that, of course, the internal energy is only one of two components dictating the relevant free energy of the system, the other being the entropic contribution. It is very challenging to accurately compute entropic contributions to free energies using molecular simulations, especially for the multiple systems studied herein. Nevertheless, we believe that it is useful to discuss the changes of internal energy upon mutation.

We find that in antithesis to the canonical model of the antimicrobial peptide activity, which suggests that the peptides interact primarily with the membrane, increased such interactions are not favorable to the activity of PlnEF (Figure 3-13a). It is also notable that there are interactions that are consistently present, i.e. the C-terminus of PlnE and the N-terminus of PlnF interact with the membrane in all but one mutant.

Interestingly, the peptides interact with each other stronger in systems that exhibit higher activity (Figure 3-13b). These two observations presumably are not independent. We noticed that there is a competitive nature between the two types of interactions. In other words, when a mutation prevented the interaction between the peptides, they interacted more with the membrane and vice versa.

Figure 3-13: Correlation between experimental activity and interactions in simulations

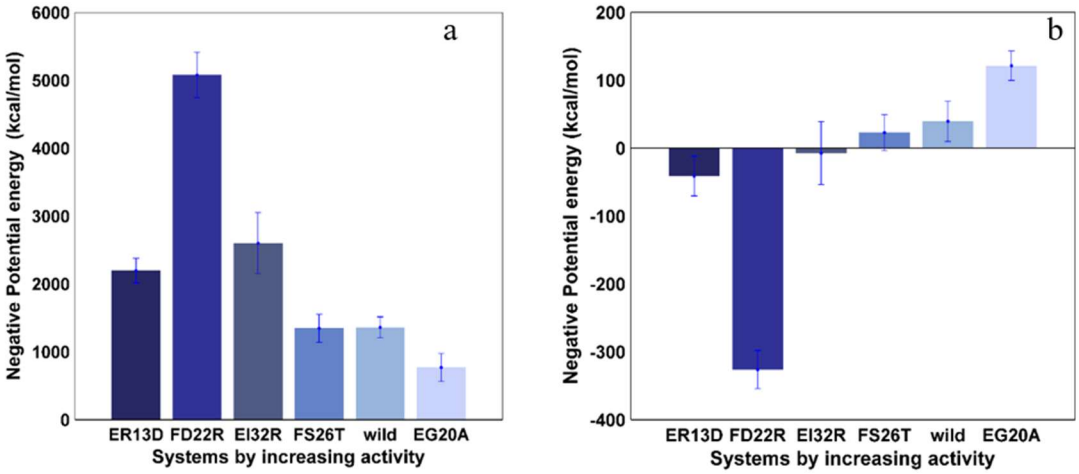

Correlation between the experimentally observed activities of Plantaricin EF and its mutants with the energy of interactions calculated from the simulations. a. Negative potential energy of peptide-membrane interactions for each system. b. Negative potential energy of peptide-peptide interactions for each system. The bars are colored based on the activity of each system, ranging from high (dark blue) to low (light cyan) activity.

3.4. Conclusions

Little is known about how class II bacteriocins attack their targets. It has been suggested that they employ a receptor-mediated mode-of-action. Nevertheless, there are indications that they interact with the membrane initially. Therefore, we simulated the two-peptide bacteriocin PlnEF on the surface of a model lipid bilayer. The structure of each peptide was previously determined. However, their relative positioning on the membrane was unknown. Previous experiments, has shown that the presence of both peptides is required and it is assumed that the interaction between them is essential to function [140].

The simulations reveal that there are persistent structural regions and interactions with the membrane both in a parallel and antiparallel model of the bacteriocin. PlnE interacts with the membrane primarily through its N-terminal amino acids while there are few salt bridges formed between the last few residues of its C-terminus and the membrane. On the other hand, PlnF interacts with the membrane solely with its N-terminus, while its C-terminus is mainly dissolved in the aqueous subphase. The

interesting difference between the parallel and antiparallel model of the bacteriocins is the reduction in peptide-peptide interactions observed in the simulation of the antiparallel dimer conformation compared to the parallel conformation. Based on our simulations and the activity measurements done here it is assumed that the interaction between the peptides is essential to function. Our findings indicate that the parallel model of the bacteriocin have stronger peptide-peptide interactions on the surface of the membrane than the antiparallel model, however an opposite trend could be possible in a transmembrane dimer.

To explore two types of interactions: peptide-peptide and peptide-membrane interactions and connect them with the experimentally observed activity, we simulated the wild type peptides and seven mutants and tested their activity. The N-terminus of PlnF and C-terminus of PlnE interacted with the membrane in all but one systems. We observed an evident trend of decreasing interactions in models with higher activity. The middle section of the peptides is mainly responsible for the peptide-peptide interactions. Interestingly, when these interactions are diminished or even missing, the system exhibits a lower activity. This strengthens the argument that the interaction between complimentary peptides is vital for the bactericidal activity of class IIb bacteriocins. Additionally, we noticed that when the reduced interactions between the peptides led to lose of structure, a behavior observed in CD experiments before. This would make the dimer insertion to the membrane less probable, since α-helical structures have high prevalence in transmembrane proteins. Therefore, we could conclude that the peptides form a dimer on the surface of the membrane instead of being inserted individually.

In this study, we simulated only a first step of the mechanism of action of PlnEF. Ideally, we would focus on the interaction of peptides with potential transmembrane protein receptors, but currently there is not sufficient information to build a reliable model for molecular dynamics simulations. In the next chapters, we explore the dynamics of a possible transmembrane dimer of the bacteriocin.

Chapter 4

Designing the structure of a Transmembrane Class IIb Dimer

4.1. Introduction

Plantaricin EF is a two-peptide bacteriocin that depends on the complementary action of two different peptides (PlnE and PlnF) to function. The two peptides are assumed to form a dimer. The structures of the individual peptides have previously been solved by Nuclear Magnetic Resonance (NMR), but the dimer structure and how the two peptides interact have not been determined [112]. In 0, we examined the behavior of the peptides in water and in the presence of DPC micelles, a membrane mimic similar to what was used in the NMR experiments. Thus, we were able to have a first look at the behavior of the peptides through molecular dynamics simulations. In Chapter 3, we simulated possible dimers of PlnEF on the surface of a lipid bilayer as well as peptides that carried a single point mutation. We identified residues that engage in key interactions between the peptides and the membrane and we demonstrated that there is a correlation between such interactions and the experimentally-observed activity. In this chapter, we aim to further our understanding of the important residues of PlnEF through an extensive mutational analysis. We then use these results in addition to our conclusions from the previous chapters, to build a possible transmembrane dimer model for PlnEF that we evaluate with MD simulations.

So far, all two-peptide bacteriocins identified contain GxxxG motifs. These motifs, together with GxxxG-like motifs, are known to mediate helix−helix interactions in membrane proteins [80]. Here we have analyzed the effect of substituting the various small amino acids (Gly, Ala and Ser) to assess whether any of these motifs are important for the interactions between PlnE and PlnF and, by extension, their antimicrobial activity. As described in Chapter 3, the GxxxG motifs do not seem to facilitate peptide-peptide interactions on the surface of the membrane, however this does not imply that they will not mediate the peptide association in a transmembrane conformation.

Additionally, we substituted the Tyrosine and Tryptophan residues of PlnE and PlnF, and constructed four fusion polypeptides to investigate the relative orientation of a transmembrane PlnEF dimer in target cell membranes. Through atomistic MD simulations, we further investigated the behavior of the dimer at different positions across the z-axis of a lipid bilayer in order to study the behavior of such a possible dimer.

The results described in this chapter have been presented in a peer-reviewed publication which we coauthored [103]. Our contributions to that publication were the designing of the transmembrane dimer-membrane complex, performing and analyzing the MD simulations, interpreting the results, and connecting them to the experimental observations. The methods we employed are detailed in the next paragraphs, while we direct the reader to section Appendix A for a description of the experimental procedures used by our collaborators. Similarly, in this chapter we include the results from our work while the detailed result of the experiments can be found in section C.

4.2. Materials and methods

4.2.1. Experimental methods

A detailed description of the bacterial strains chosen, their growth conditions, DNA isolation and bacteriocin expression can be found in paragraphs B.1 to B.3. The mutagenesis analysis protocols are described in paragraphs B.5 and B.4. The fusion peptide construction methods and analysis can be found at B.6 and finally the activity measurement protocol is described in B.7.

4.2.2. Building the Dimer Model

In our previous simulations, we constructed possible dimer models through docking of the two peptides PlnE and PlnF. Our criteria for picking the final models was the proximity of the suggested GxxxG motifs and the docking score. However, the GxxxG motifs did not enhance the peptide-peptide interactions as anticipated. The explanation for this could be that the motifs were not active under the conditions of the previous simulations, or because the two peptides were not close enough in the initial dimer model due to the rigid body nature of the docking calculations. Therefore, this time we decided to take a different approach - instead of using the final pdb structures, we used the NMR restrains (that the pdb structures were derived from) and added restrictions

that would reflect the GxxxG motifs.

The structure of an antiparallel dimer was calculated using CYANA (operated by Per Eugen Kristiansen) [141] and the structural restraints for PlnE (PDB ID Code: 2jui) and PlnF (PDB ID Code: 2rlw) were downloaded from the protein data bank. Additional restraints were inserted between residues in the G_5xxxG_9 motif of PlnE and the $S_{26}xxxG_{30}$ motif of PlnF (that was suggested from the mutational results to assist in the dimerization of the peptides) and between Arginine 13 of PlnE and Aspartic acid 22 of PlnF as well as between Aspartic acid 17 of PlnE and Lysine 15 of PlnF, to have them face towards each other. 100 structures were calculated and the lowest energy structure was used as a dimer model in the molecular dynamics simulations.

4.2.3. Molecular Dynamics (MD) Simulation Methods and Parameters

The dimer was placed into the model membrane using the online server CHARMM-GUI [119]. Two distinct models were built by positioning the dimer at different distances from the center of the membrane along the z-axis. In model one, the dimer was placed with the aromatic residues on the surface of the lower leaflet and the peptides penetrating through both the upper and lower surface of the model membrane. In model two, the residues W23 of PlnF and Y6 of PlnE lie inside the membrane core.

The lipid bilayer was built to mimic the membrane of Gram-positive bacteria, using 1-palmitoyl-2-oleoyl-sn-glycero-3-phosphoglycerol (POPG) and 1-palmitoyl-2-oleoyl-sn-glycero-3-phosphoethanolamine (POPE) lipids in a 3:1 ratio. The dimer-membrane systems were solvated in a 0.15 M NaCl aqueous solution with the VMD software [117]. Counterions were added as necessary to electroneutralize each system.

NAMD 2.10 [115] was used for molecular dynamics simulations, with the CHARMM param36 force field [142]. Systems were first minimized with a conjugate gradient algorithm, and then gradually heated to 310 K. Equilibration and production runs were carried out at constant temperature and atmospheric pressure, using the Nose-Hover algorithm provided in NAMD.

Simulations were conducted for 200 ns using a 2 fs timestep. The van der Waals potential was turned off at 12 Å, introducing a switching function at 10 Å. Electrostatic interactions were calculated with the particle mess Ewald summation, with a real space cutoff truncated at 12 Å.

4.3. Results and Discussion

4.3.1. Model of Plantaricin EF inserted into membrane bilayer based on mutational assays and the known NMR structures of the individual peptides

The results of the experimental study indicate that PlnE and PlnF interact in an antiparallel manner and that the G_5xxxG_9 motif in PlnE and the $S_{26}xxxG_{30}$ or $G_{30}xxxG_{34}$ motifs PlnF are involved in helix-helix interactions. However, due to Gly34 being the last residue in PlnF, the $G_{30}xxxG_{34}$ motif is an unlikely candidate for helix-helix-stabilization. More importantly, an antiparallel interaction between $G_{30}xxxG_{34}$ in PlnF and G_5xxxG_9 in PlnE results in strong charge repulsion between the peptides. The positively charged residues Arg13 in PlnE and Arg29 in PlnF come close in space when the peptides are arranged using these GxxxG motifs. This is also the case for the negatively charged Asp17 in PlnE and Asp22 in PlnF. Moreover, previous MD simulation of the two Pln-peptides presented at Chapter 3 Moreover, previous MD simulation of the two Pln-peptides presented at Chapter 3 revealed that the G_5xxxG_9 motif in PlnE and the $G_{30}xxxG_{34}$ motif PlnF did not bring the two peptides in close contact: the peptides interacted only weakly (only one salt bridge, between Arg13 in PlnE and Asp22 in PlnF, was formed), and the potential energy of interaction between the peptides was positive.

The other possibility, that G_5xxxG_9 in PlnE and $S_{26}xxxG_{30}$ in PlnF interact in an antiparallel manner, results in a dimer that may be stabilized by two salt bridges between Arg13 in PlnE and Asp22 in PlnF and between Asp17 in PlnE and Lys15 in PlnF. This conformation is consistent with the observation that changing the charges of these residues was detrimental to the antimicrobial activity, shown in Chapter 3. Figure 4-1 represents a structural model of Plantaricin EF in which the two peptides interact through the G_5xxxG_9 motif in PlnE and the $S_{26}xxxG_{30}$ motif in PlnF in an antiparallel transmembrane orientation in a model lipid bilayer.

In this structural model, the N-terminus of PlnE and C-terminus of PlnF form a blunt end. In contrast, there is a one amino acid overhang on PlnF on the other end, formed by the C-terminus of PlnE and N-terminus of PlnF, both of which (according to the results obtained with the fusion polypeptides) face towards the cell's outside (Figure 4-1). The preference for an aromatic residue at position 6 in PlnE, Tyr6, suggests that this end positions itself in or near the membrane interface on the cytosolic side of the membrane. Residues Arg8, Arg11 and Lys15 in PlnF are brought close to PlnE Gly20

and Gly24 and may explain the detrimental effect of substituting the latter two residues with the positively charged Lys, while being able to accommodate all other substitutions (Figure 4-1).

Figure 4-1: Proposed model of the Plantaricin EF dimer

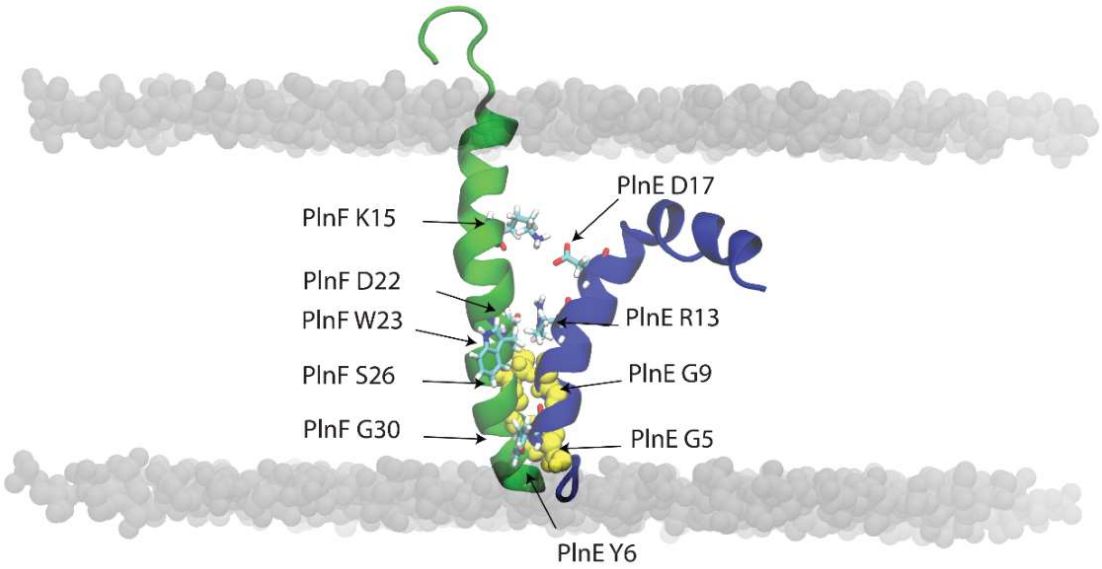

The model of the Plantaricin EF dimer resulting from combining the structural restraints from the NMR studies of the individual, the results from activity assays on mutants of PlnE and PlnF, and the conclusions from the simulation of the peptides on a model membrane surface. PlnF is shown in green, while PlnE is shown in blue. The head group atoms of the lipids are shown as grey spheres. Glycine and serine residues thought to be important for the interaction between the two peptides are drawn as yellow spheres. Other important residues are drawn in stick representation.

4.3.2. Molecular dynamics (MD) simulation and evaluation of the membrane-inserted model of Plantaricin EF

The proposed model was inserted in a lipid bilayer and analyzed using MD simulation. In this simulation, only very small changes were observed in the structure and orientation during the 200 ns of MD simulation (Figure 4-2). Both peptides are mostly helical during the last 150 ns of simulation (Figure 4-3a).

The distance between the G_5xxxG_9 motif in PlnE and $S_{26}xxxG_{30}$ motif in PlnF seems to be fairly stable, and it even decreases toward the end of the MD simulation (Figure 4-3b) indicating that the overall interaction around the suggested interaction motifs improves during the simulation.

Figure 4-2: Evolution of the simulation of the Plantaricin EF dimer model

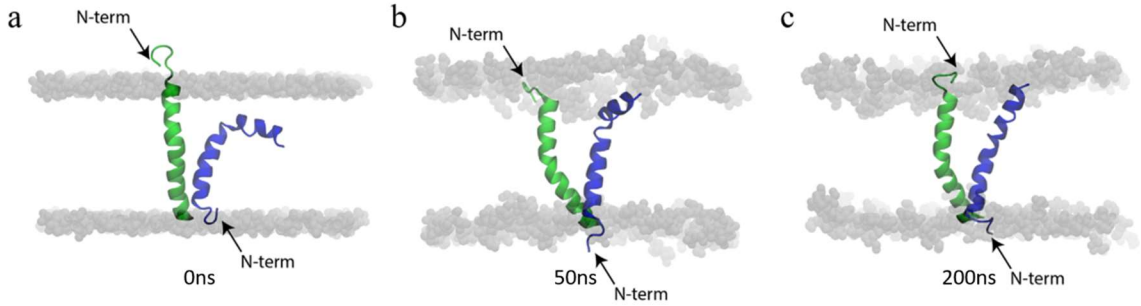

The plantaricin EF dimer model at different time steps during the molecular dynamics simulation. The figures at 0 ns, 50 ns and 200 ns are shown in Figure a, b, and c, respectively. PlnF is shown in green cartoon drawing in all the pictures, while PlnE is shown in blue. The head group atoms of the lipids are shown as grey spheres

Figure 4-3: Molecular dynamics simulation trajectories between 50 ns and 200 ns

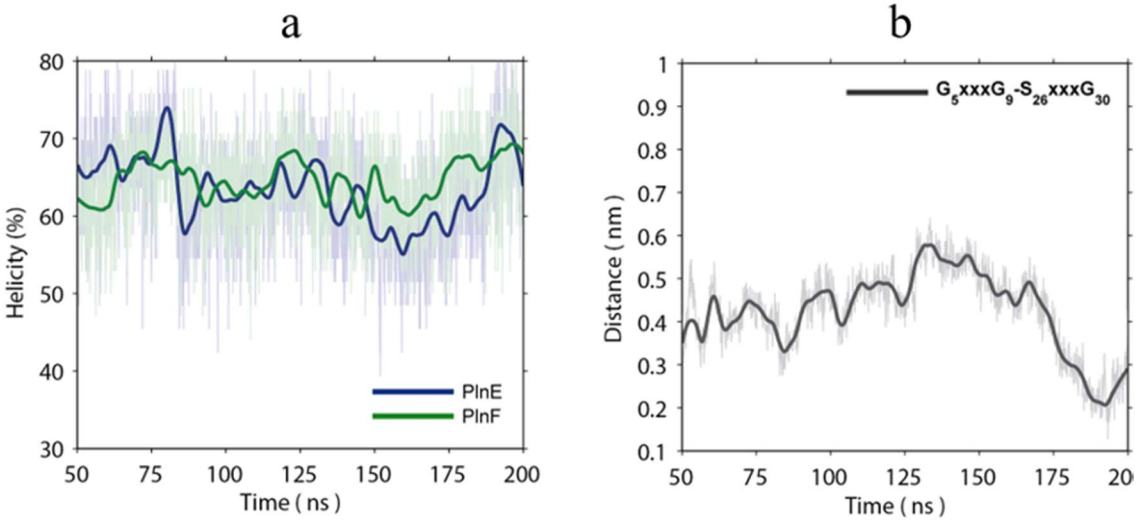

In a, the % α-helicity of PlnE is shown in blue, and of the PlnF in green. Distance between the center of mass of PlnE G5xxxG9 and center of mass of PlnF S26xxxG30 motifs are shown in b. Thin lines illustrate the measured distances in each frame, while the thick lines illustrate the sliding average.

Several interactions between the peptides seem to be of importance during the simulation. Importantly, we observe the same intermolecular hydrogen bonds/salt bridges as hypothesized, that is, between PlnE R13 and PlnF D22 and (to a lesser extent) between PlnE D17 and PlnF K15, as illustrated in Figure 4-4. Interestingly, K15 seems to switch interaction partners, between PlnE D17 and PlnF N12, back and forth throughout the simulation, the latter residue being closer to the outer lipid head groups.

In addition, apart from the strong electrostatic interaction, there is also an intramolecular hydrogen bond between PlnE D17 and PlnE R13, further stabilizing the “polar center” of the dimer. The combination of hydrogen bonds between PlnE D17, PlnE R13, and PlnF D22 that are present throughout the simulation may in fact be a variation of a cluster of interhelical hydrogen bonds/salt bridges called “polar clamps”, which is a common motif found in transmembrane regions of membrane proteins [143]. There is also a hydrogen bond between PlnE R3 and the terminal oxygen at the C-terminal of PlnF on G34 during most of the simulation.

Figure 4-4: Interactions between the peptides.

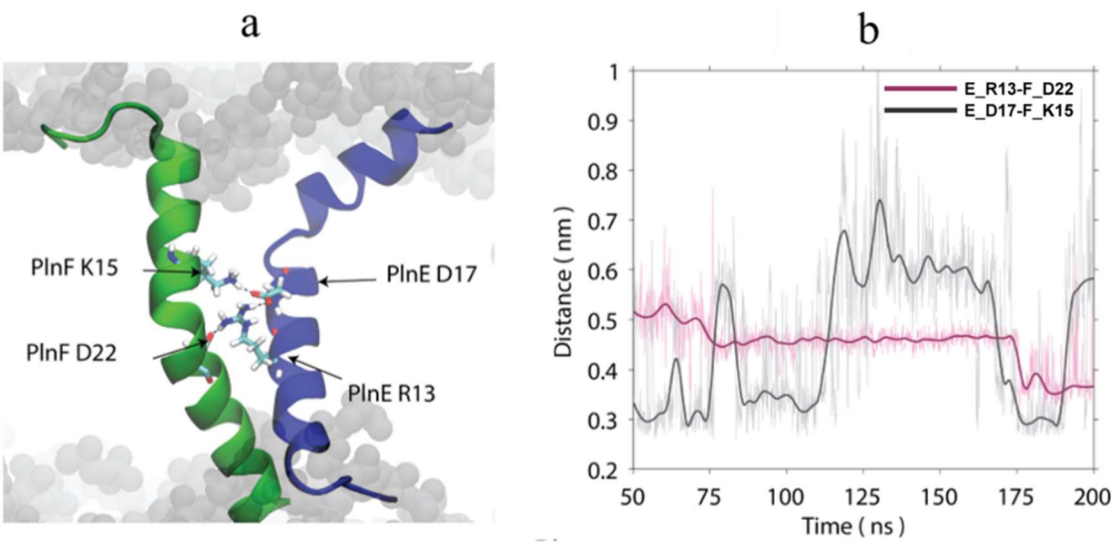

Stabilizing electrostatic interactions are shown in a. The structures are in cartoon drawing, PlnE is in blue and PlnF is in green, and the lipid head groups are shown as grey spheres. Atoms of the residues of importance are colored according to atom type: carbon is in light green, hydrogen is white, oxygen is red and nitrogen is blue. In b, we calculated the distance between the center of mass of the carboxyl, guanidinium, or ammonium groups of the respective residues: the red curve is between PlnE R13 and PlnF D22, while the black one is between PlnE D17 and PlnF K15, respectively. Thin lines illustrate the measured distances in each frame, while the thick lines illustrate the sliding average.

The MD analysis also reveals that the dimer is further stabilized by aromatic interactions and cation-π interactions. Consistent with the results from the mutation studies, the aromatic amino acid Tyr at position 6 in PlnE seems to be stably inserted into the bottom leaflet of the lipid bilayer (possibly the inner membrane interface based on the fusion peptide results) (**Figure 4-5**). Furthermore, this residue interacts via a

staggered (parallel) cation-π interaction with the aromatic residue F31 in PlnF. A T-shaped cation-π interaction is observed for PlnF W23 and H14 in PlnE as well. In fact, W23 seems to coordinate with both PlnE H14 and PlnE K10 in such a way that if one of these residues changed slightly in position, the others moved as well, keeping a stable internal distance throughout the simulation - the only exception being the distance between W23 in PlnF and H14 in PlnE in the timeframe between 115 -150 ns (Figure 7C and 7D). The W23-K10 cation-π interaction may help stabilize the dimerization in a similar manner as reported by Peter, B. *et al.* for the chloride intracellular channel protein 1 transmembrane domain [144].

Figure 4-5: Cation-π interactions stabilize the dimer's position in the membrane.

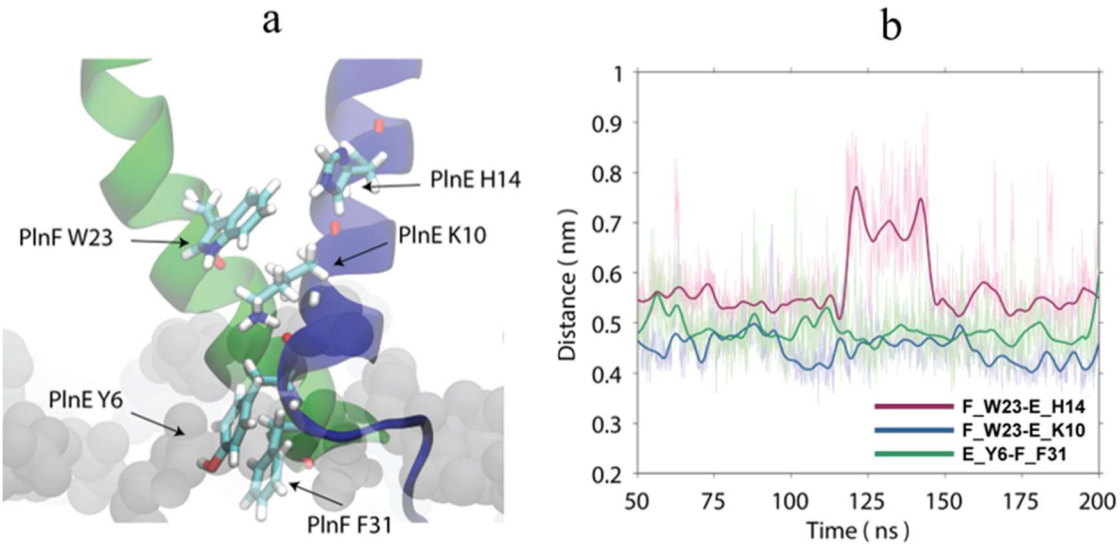

The important aromatic cation-π interactions that anchor the dimer in the bilayer are shown in a, while trajectories showing the variation in distances in the MD simulations between 50 ns and 200 ns are shown in b. The structures in a are cartoon drawings of PlnE in blue and of PlnF in green, while the lipid head groups are shown as grey spheres. Atoms of the residues of importance are colored according to atom type: carbon is light green, hydrogen is white, oxygen is red and nitrogen is blue. The curves in b are between the center of mass of the aromatic rings, carboxyl, or ammonium groups. The red, blue, and green curves show the distance between PlnE H14 and PlnF W23, PlnE K10 and PlnF W23, and between PlnE Y6 and PlnF F31, respectively. Thin lines in B) and D) illustrate the measured distances in each frame, while thick lines illustrate the sliding average.

S26 in PlnF is initially hydrogen-bonded with the backbone carbonyl oxygen of G9 in PlnE for the first 100 ns of simulation, before it switches to an intramolecular hydrogen bond with D22 during the final 100 ns. This is, however, not the only serine in the

peptides that is hydrogen-bonded. In both PlnE and PlnF there is a pattern of three Ser residues separated by 9 other residues. In PlnE, all of these serine hydroxyl groups are hydrogen-bonded at least part of the time to the carboxyl group of residues i-4 (Figure 4-6). Similar hydrogen bonds are also observed for PlnF between S16 and N12, and S26 and D22. These serine interactions may be of importance in internal stabilization of the helices, and might explain why Ser instead of Gly is in the $S_{26}xxxG_{30}$ motif in PlnF.

Figure 4-6: Serine residues contribution to the hydrogen bond network

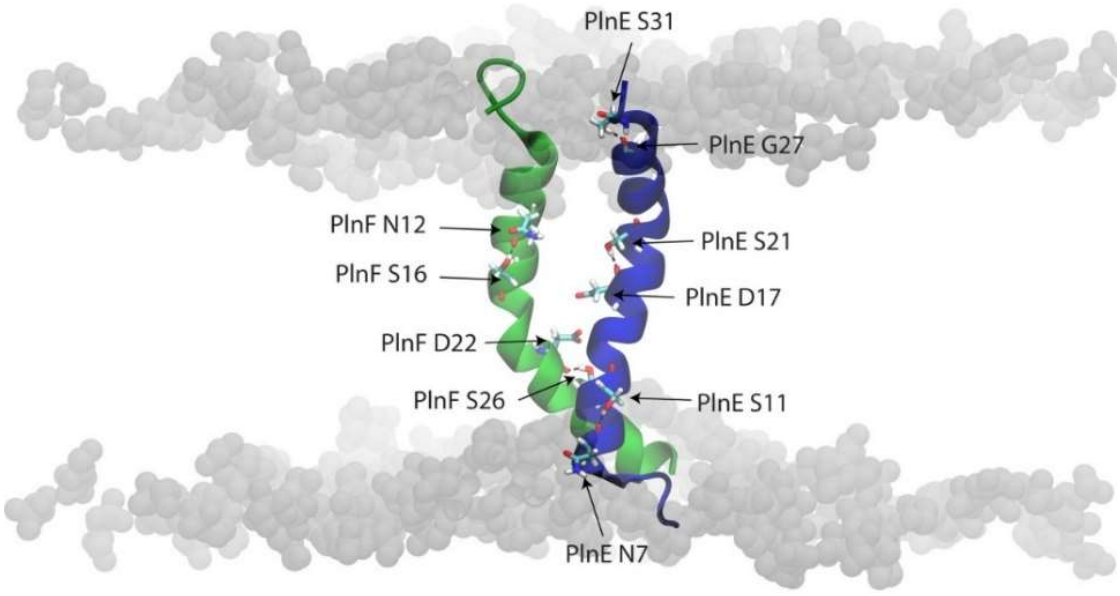

Interactions between the sidechain hydroxyl groups of serine residues in PlnE (blue) and PlnF (green) observed during the molecular dynamics simulation. The structures are in cartoon drawing, PlnE is in blue and PlnF is in green, and the lipid head groups are shown as grey spheres. Atoms of the residues of importance are colored according to atom type: carbon is in light green, hydrogen is white, oxygen is red and nitrogen is blue

The transmembrane bacteriocin dimer interacts with the lipid phosphate groups through a number of hydrogen bonds Figure 4-7. In PlnE, residues R26, K30, and K33 in the C-terminal region interact with the top lipid phosphate groups and F1, R3, Y6, N7, and K10 in the N-terminal region interact with the top lipid phosphate groups. PlnF anchors to the bottom lipid phosphate groups through its C-terminal residues R29, H33, and G34, and it anchors to the top lipid phosphate groups through its N-terminal residues V1, F2, H3, Y5, S6, A7, R8, R11, N12, N13, Y14, and K15 (Figure S5). The

hydrogen bonds formed between hydroxyl groups of PlnF Y5 and PlnF Y14 with the lipid phosphate groups may, to some extent, explain why substituting with hydrophobic, positively charged, or aromatic amino acids were detrimental to activity.

Figure 4-7: Number of hydrogen bonds between each residue and the membrane

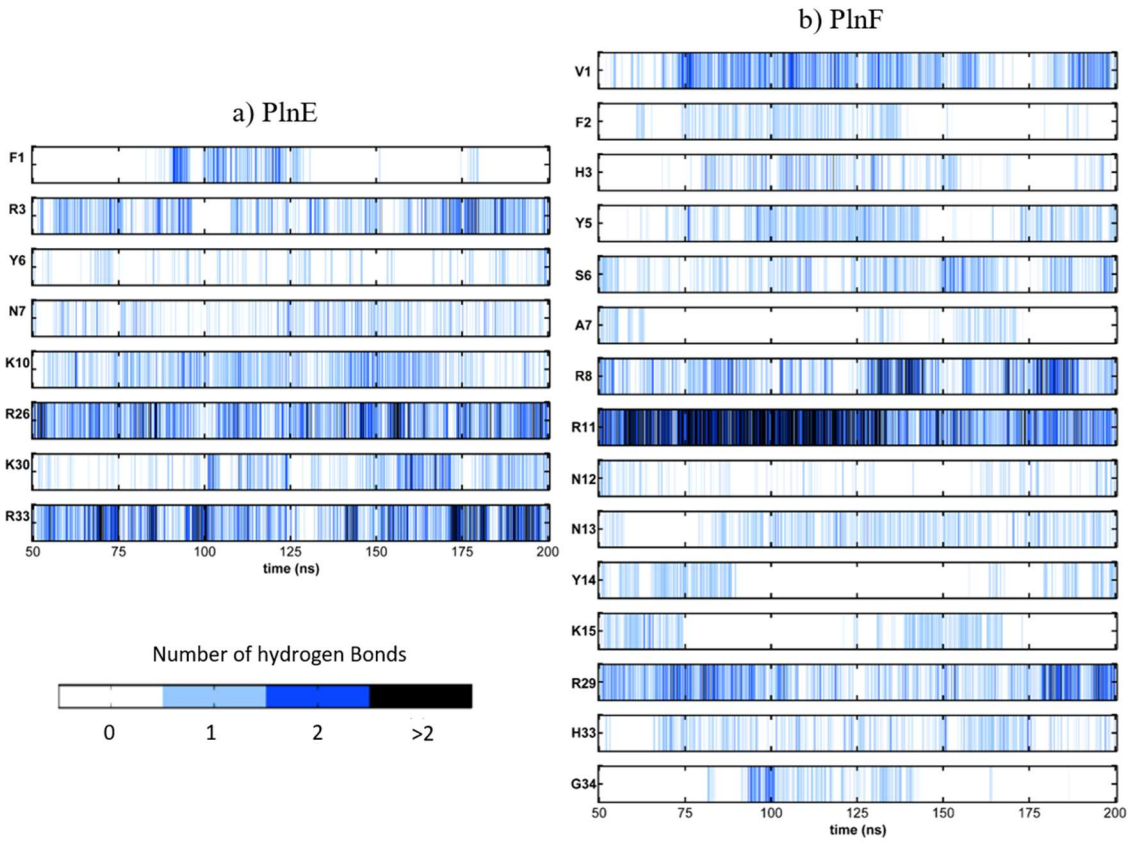

Hydrogen bonds between a) PlnE and b) PlnF and the membrane lipid head groups are shown. The colorbar illustrates how the different colors indicate different numbers of hydrogen bonds; the darker the color the more hydrogen bonds there are.

To determine whether the stability of the Plantaricin EF structure (shown in Figure 4 3) depends on it being in a transmembrane position and in a predominantly hydrophobic environment, we also performed a simulation in which the structure was partly inserted into the membrane (instead of as a transmembrane entity - Figure 4 10). In this latter simulation, the structure is also in agreement with the results above except that Tyr6 in PlnE is no longer in the membrane interface, but rather in the hydrophobic core of the membrane. After approximately 50 ns, the peptides moved toward the membrane surface and ended up positioned on the surface of the bilayer, a result that was perhaps

not unexpected, since substituting Tyr6 with a hydrophobic amino acid was detrimental to the bacteriocin activity. Furthermore, the bacteriocin structure lost much of its α-helical character during the MD simulation and therefore becomes inconsistent with the NMR structures.

Figure 4-8: Snapshot of the MD simulations of an alternative model

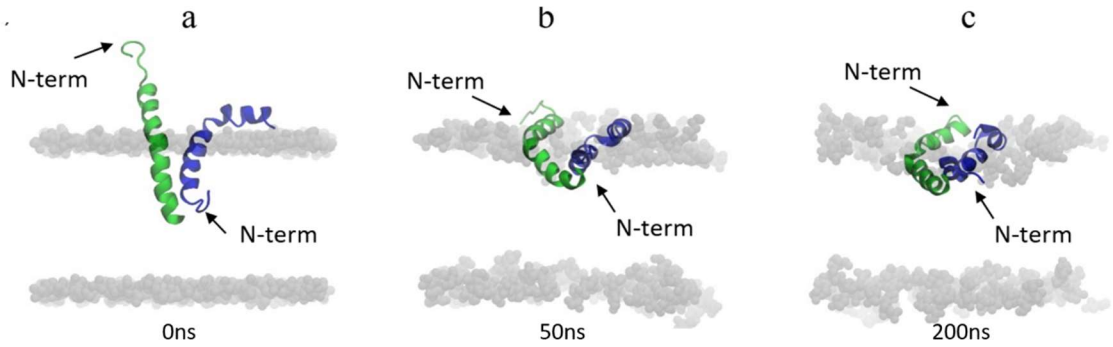

The dimer model positioned perpendicularly to the membrane through the upper leaflet of the membrane bilayer at a) 0 ns (the design structure), b) at 50 ns in, and c) at 200 ns. PlnF is shown in green, while PlnE is shown in blue. The head group atoms of the lipids are shown as grey spheres.

4.4. Conclusions

PlnEF is a potent two-peptide bacteriocin whose mechanism of action depends on the association between PlnE and PlnF. In this chapter, we discussed the effect of different mutations on the activity of the peptides and we designed a transmembrane model of this that we further investigated with molecular dynamics simulations.

To begin with, all the GxxxG and GxxxG-like motifs in both PlnE and PlnF were mutated to evaluate if any of these motifs is vital for the antimicrobial activity of the bacteriocin. These motifs are hypothesized to function as dimerization surfaces, therefore, we suggest that if they are important for the activity, then they should be in close contact and induce interactions between PlnE and PlnF. We found that in the systems where the residues in the G5xxxG9 motif in PlnE and the S26xxxG30 motif in PlnF were mutated, there was a significant loss of activity. Therefore, we conjectured that the two peptides come in contact around those motifs.

Four fusion polypeptides were constructed in order to examine what is the possible orientation of the dimer. Results from that experiment suggest that the peptides lie

antiparallel to each other when they are in a transmembrane conformation. Additional mutations of aromatic amino acids guided us into positioning the antiparallel dimer in a model lipid bilayer.

Atomistic molecular dynamics simulation of the dimer model in the bilayer confirmed its stability and approved that the two peptides come in close contact through the GxxxG motifs. Moreover, it revealed that the peptides interact strongly through a “polar clamp” at their middle section, and specific cation-π interactions, which also assist the dimer’s anchoring in the membrane. The MD simulations facilitated the visualization of the dimer and provided an explanation for most of the detrimental mutations, such as PlnE G20K and G24K.

In this chapter, we discussed how we constructed a transmembrane dimer model of the peptides. In the next chapter, we investigate the dimer though a 1μs long atomistic simulation and examine the impact of the dimer’s presence to the rest of the system (membrane, water, ions). We then pose the question of whether or not the transmembrane insertion of the dimer could lead to the membrane permeabilization by itself, i.e. by forming a small pore and not through a receptor-mediated mechanism of action.

Chapter 5

Could class IIb bacteriocins induce pore formation?

Bacteriocins are antimicrobial peptides (AMPs) produced by bacteria, and they show great potential as novel antibiotic agents [45]. They are typically active at lower concentrations and exhibit higher specificity against their targets when compared to other AMPs [25]. To exploit the full potential of bacteriocins and use them as a platform to develop new antibacterial agents, an understanding of their mechanism of action (MOA) is necessary.

Molecular dynamics simulation is a powerful tool that has shed light into the MOA of various AMPs in atomistic or near-atomistic detail [92,93,125,145–148]. These studies show that the majority of AMPs kill target cells by forming different types and sizes of pores in the cell membrane. In the case of bacteriocins, in most (experimental and computational) studies of the last decade, it is assumed that the peptides exert their antimicrobial activity by a receptor-mediated mode-of-action, particularly those peptides that exhibit high selectivity [68,78,149,150]. Apart from Nisin and class IIc bacteriocin AS-48, both of which are broad spectrum bacteriocins, direct interaction of a bacteriocin with its receptor and pore-forming evidence have not been demonstrated thus far [97,151].

The activity of PlnEF, like most LAB bacteriocins, was shown experimentally to be related to membrane permeabilization, as we summarized in paragraph 2.1. In the previous chapters, we explored the behavior of the peptides on the surface of membrane models through molecular dynamics simulations and compared it to experimental studies. With this information and additional experimental guidance, we detailed the design of a transmembrane dimer structure and its positioning on a lipid bilayer.

In this chapter, we present the 1 μs long atomistic molecular dynamics simulation study that we performed on the transmembrane dimer. We analyze the peptide structure and important amino acids that are responsible for the anchoring of the peptide in the membrane. We further investigate the impact of the dimer's presence on the rest of the

system (the membrane, water, and ions). Most importantly, we show that the transmembrane PlnEF dimer can form a small toroidal pore that allows water permeation and suggests possible ion conduction. This is the first time (to our knowledge) that a LAB bacteriocin has been shown to form pores on its own. We believe this finding could be of importance to the design of new bacteriocins, as it would steer the search for better bacteriocins toward peptides that form more stable pores, interact more strongly with the membrane in specific regions, and increase water or ion permeability.

5.1. Materials and methods

We studied the antimicrobial peptides PlnE and PlnF inside a bacterial cell membrane-mimicking model with 1 μs-long atomistic molecular dynamics simulation. The system contains lipid molecules, water, ions, and the peptides that are believed to form a dimer. We characterized the structure and behavior of the peptides, as well as the interactions that took place between them. We also focused on the response of the membrane to the presence of the dimer. Finally, we studied how the water and ions act with respect to the dimer-membrane morphology.

5.1.1. System components

PlnE and PlnF are medium-size bacteriocins with 33 and 34 residues, respectively. Their sequences can be found in Table 2-1. The two peptides were structured individually and deposited earlier in the pdb database with accession codes 2jui for PlnE and 2rlw for PlnF [152]. A detailed description of the dimer structure we created can be found in section 4.2.2. The structure of this dimer and its positioning in the membrane are described in **Figure 4-1**.

In order to create the dimer-membrane complex, the dimer was inserted into the membrane using the CHARMM-Gui server [119]. A bilayer consisting of POPG (1-palmitoyl-2-oleoyl-sn-glycero-3-phosphoglycerol) and POPE (1-palmitoyl-2-oleoyl-sn-glycero-3-phosphoethanolamine) lipids in a 3:1 ratio was used as a bacterial cell membrane-mimicking model of Gram positive bacteria. Each leaflet contains 120 lipids that were placed randomly at the 3:1 POPG:POPE ratio.

To ensure proper hydration of the system, the dimer-membrane complex was solvated by adding 3 nm of TIP3P water at the negative and positive direction of the z-axis, using the VMD solvator plugin [115]. The ion concentration of the system was set

to 0.15M NaCl to mimic a physiological salt solution. Additional sodium ions were introduced to make the system electroneutral. The ionization was achieved by randomly adding Na^+ and Cl^- ions with the VMD autoionize plugin [115]. In total, the system contains the two dimers (1,035 atoms), 240 lipid molecules (30,360 atoms), 17,269 water molecules (51,807 atoms), 221 sodium ions, and 49 chloride ions. The total system size was approximately 10 nm x 10 nm x 12 nm before the beginning of the simulation, and it was reduced to 8.7 nm x 8.7 nm x 10.8 nm after equilibration.

5.1.2. Molecular dynamics

The atomistic molecular dynamics simulation was conducted with the NAMD 2.10 simulation engine [115], using the CHARMM 36 force field [142] under constant pressure and temperature (NPT ensemble). All the parts of the simulation were carried out on the Stampede supercomputer through the XSEDE portal.

The system was minimized for 1 ns using the conjugate gradient algorithm provided in NAMD. Then the temperature was increased gradually to 310 K while the peptides and lipid atoms were subjected to positional harmonic constraints. This was followed by four 1 ns equilibration simulations, while the constraints were progressively removed. After all the constraints were removed, a final 10 ns equilibration step was performed to allow all the components of the system to relax from the previous constraints and improve their interactions before the production runs. At this stage, we ensured that there was no drastic change in the size and morphology of the system through visual inspection. Finally, we ran for a total of 1μs of atomistic molecular dynamics simulation.

Equilibration and production runs were carried out at atmospheric pressure, using the Nosé-Hoover Langevin piston pressure control method as implemented in NAMD. After the heating stage, the temperature was kept constant at 310K with a Langevin thermostat. Periodic boundary conditions were applied in each simulation. Van der Waals potential was truncated at 1.2 nm, introducing a switching function at 1 nm, while the real space cutoff distance of the PME electrostatics calculation was also set at 1.2 nm. A timestep of 2 fs was employed, while coordinate snapshots were recorded every 10 ps.

The different types of analysis performed were realized using the VMD software through its TCL scripting interface, other VMD plugins, and various in-house Matlab scripts [117]. For the Cartesian PCA-based cluster analysis, we used the CARMA

software [153]. All the simulation snapshots were recorded using the VMD software [117]. Most of the analysis was performed on a 0.1 ns resolution, except for the analysis of the water and ion permeation that ware performed at a 0.01 ns resolution.

5.2. Results

. Initially we performed structure stability analysis of the peptides to access their dynamics. We investigated the different intramolecular interactions between the two peptides. We finally examined the dynamics of the membrane, as well as water and ion permeation through the bilayer. Snapshots of the simulation are shown in Figure 5-1.

Figure 5-1: Snapshots of the 1 μs long simulation

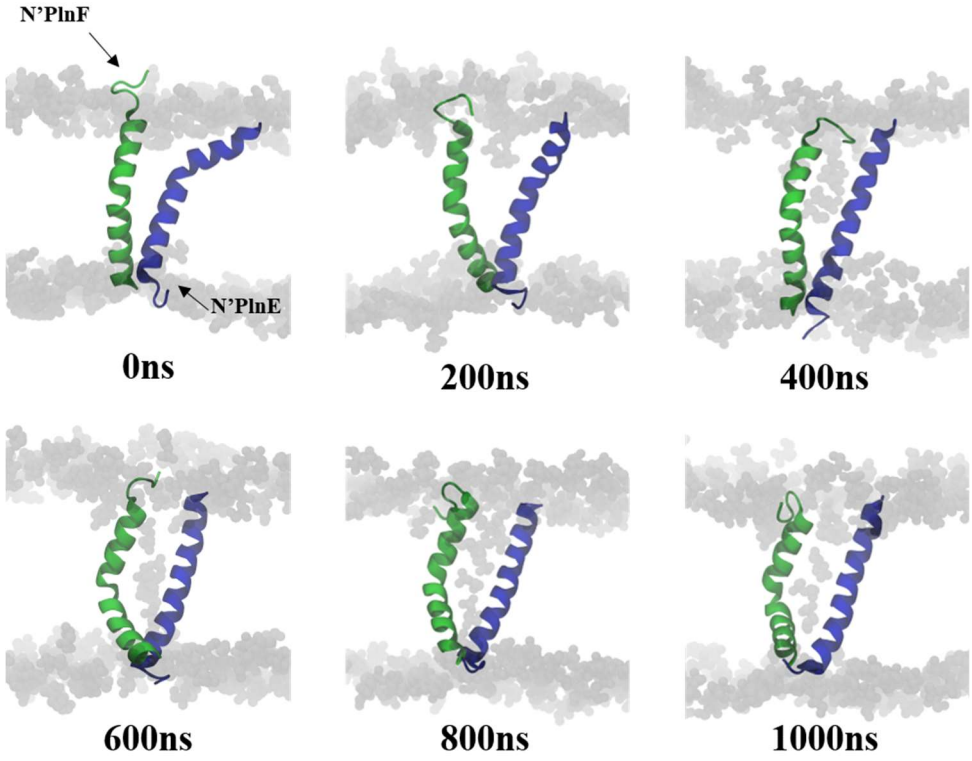

Snapshots at different points in time are shown in the pictures above. PlnF is shown in green cartoon drawing in all the pictures, while PlnE is shown in blue. The head group atoms of the lipids are shown as grey spheres. The N' and C' terminai are indicated in the 0 ns figure and orientation remains unchanged through the simulation. It is important to note that the pictures were taken from different viewpoints that would better demonstrate the evolution of the peptides and of the membrane.

5.2.1. Structural analysis of the peptides

The stabilities of the structures of each peptide individually and of the dimer were analyzed using root mean square deviation (RMSD) and radius of gyration (Rg) calculations. For the first 100 ns there is an increase of the backbone RMSD of the peptides with respect to the design structure of the dimer (Figure 4-1). However, after the 100th ns, and particularly after the 200th ns, the structure of both the peptides stabilizes. The average backbone RMSD of PlnE with respect to its structure at 200 ns is 0.27 ± 0.06 nm, while for PlnF the same RMSD is 0.31 ± 0.06 nm. These values can be accepted as low, because they are comparable to RMSD values of structures originated from NMR studies [112,130]. The radius of gyration is a more meaningful measure that indicates the space that the dimer occupies and how this space varies in time (Figure 5-2a). PlnE has a constant Rg after the 200 ns mark, while PlnF goes through changes until up to about 300 ns. The Rg of the dimer as a whole fluctuates for the first 300 ns, probably due to fluctuations of the individual Rg of the peptides. It reaches a minimum at ~500 ns and increases again later.

We performed Cartesian principal component analysis (PCA) analysis on the dimer to clarify the above observation. Two clusters were identified (cluster I and II) as shown in (Figure 5-2b,c,d,e). The first cluster includes most of the frames from ~350 ns to ~650 ns, while the second cluster includes frames from ~700 ns to 950 ns. The transition in the Cartesian space of the peptides that occurred from 650 ns to 700 ns is not directly visible and we try to explain it better in the rest of our analysis. The average structure of cluster 1 is located at the 554th ns (Figure 5-2d) while for cluster 2 at the 825th ns (Figure 5-2e).

The structure of the peptides is α-helical for most of their length. PlnE has an increasing α-helical content after the first 200 ns of the simulation. The helicity of PlnF increases after the 200th ns as well, however it drops after the 700th nanosecond. PlnE has high helicity from the 6th to the 30th residues. PlnF forms two short α-helices, with a flexible center around residues 18 and 19. The loss of the helicity of PlnF during the last 300 ns of the simulation is due to significant loss of structure at the last few residues in its N-terminal. Despite this small loss of structure, the peptides remain anchored to the bilayer throughout the simulation (Figure 5-3).

Figure 5-2: Structure analysis of PlnE, PlnF and the dimer PlnEF.

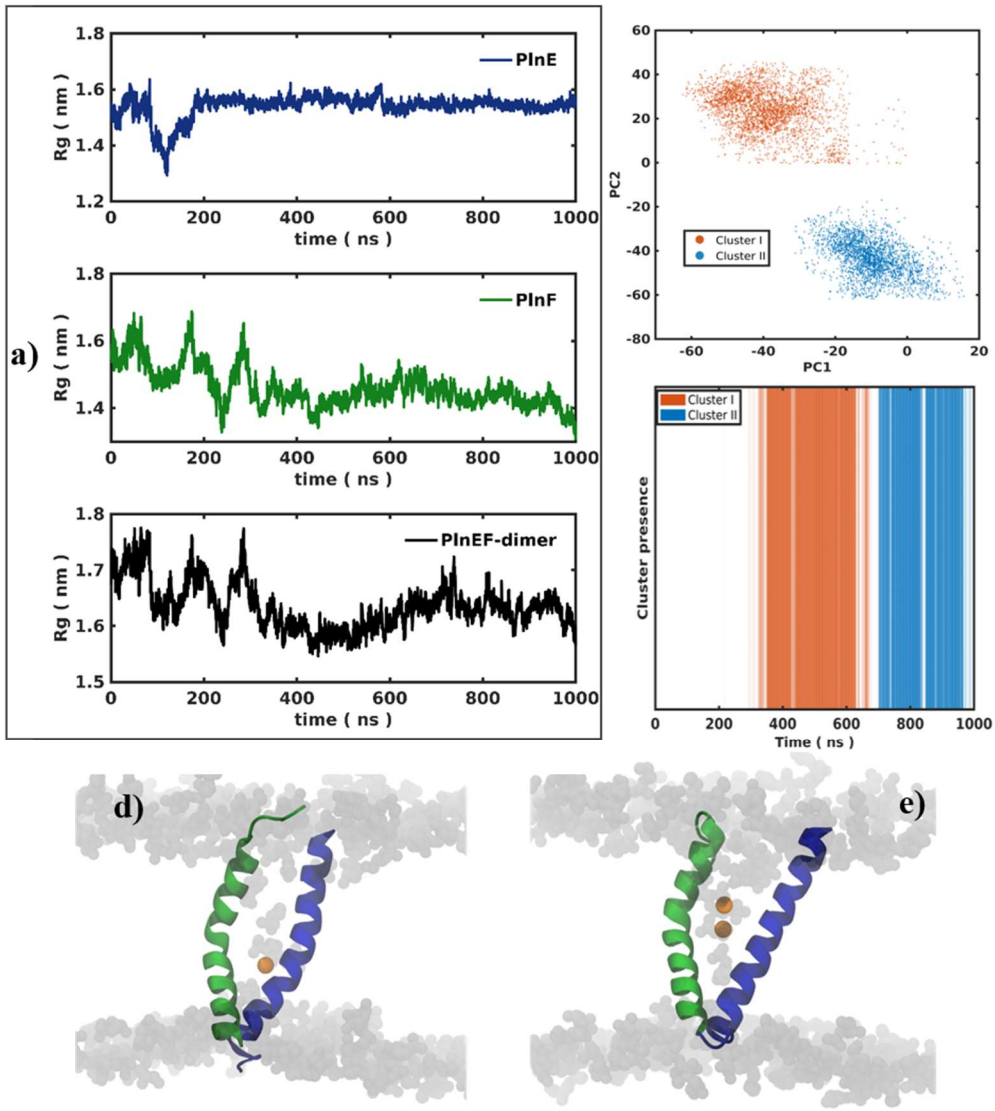

The timeline of the radius of gyration of the peptides is shown in a, individually (PlnF in green and PlnE in blue), and of the dimers (black). In b and c we show the results of the Cartesian PCA analysis of the dimer. In b, each point that belongs to either cluster is plotted against the first two principle components (PC1 and PC2). In c, we indicate at which times the cluster was more present. Orange indicates the frames that can be grouped as "Cluster I", while blue indicates the frames that can be grouped as "Cluster II". One can find snapshots in d and e of the average structure of Cluster I at 554 ns and of Cluster II at 825 ns, respectively. PlnF is shown in green cartoon drawing in all the pictures, while PlnE is shown in blue. The head group atoms of the lipids and sodium ions are shown as grey and orange spheres, respectively.

Figure 5-3: Distance of each peptide residue from the center of the membrane

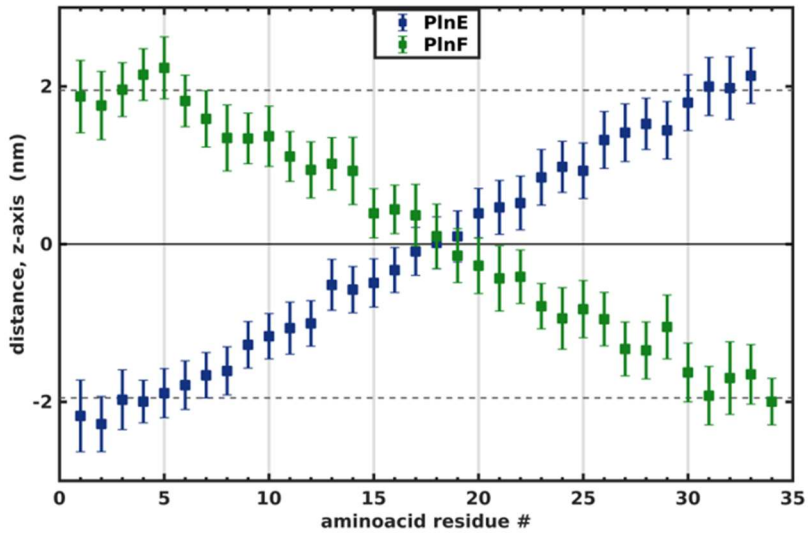

Average distance per residue of each peptide from the membrane center is shown along the z-direction. Blue symbols represent PlnE residues, while green symbols represent PlnF residues. The error bars represent the standard deviation of the per residue distance. The dashed grey lines indicate the upper and lower limits of the membrane.

5.2.2. Intramolecular interactions

In Chapter 4, three different types of interactions were identified as possibly playing an important role in the dimerization of PlnEF: the GxxxG motif, polar and electrostatic interactions and cation-π interactions. We performed similar analysis on the 1 μs simulation and we examined whatever differences, if any, were present in the two clusters.

The distance between the two GxxxG motifs increases around the time Cluster I appears, and it fluctuates later around the time Cluster II appears. When this behavior was inspected visually, there was not a significant difference in the structure of the peptides or in the way they interacted through the GxxxG motifs (Figure 5-4b). The only small difference was observed in the angle between the two helical parts where the GxxxG motifs were located - i.e. at 800 ns, the helices were better-aligned with a smaller angle between them, while at ~500 ns the angle was somewhat wider. Throughout the simulation, the peptides are close enough that they do not allow water or ion molecules to go through, which creates a hydrophobic block at the lower part of the dimer.

During the 1 μs long trajectory, we detected three pairs of electrostatic interactions.

Those are the salt bridges that are formed: i) between Aspartic acid 17 of PlnE (E-D17) and Lysine 15 of PlnF (F-K15); ii) between Arginine 13 of PlnE (E-R13) and Aspartic acid 22 of PlnF (F-D22); and iii) between Arginine 13 of PlnE (E-R13) and Aspartic acid 17 of PlnE (E-D17).

Figure 5-4: Intramolecular Interactions

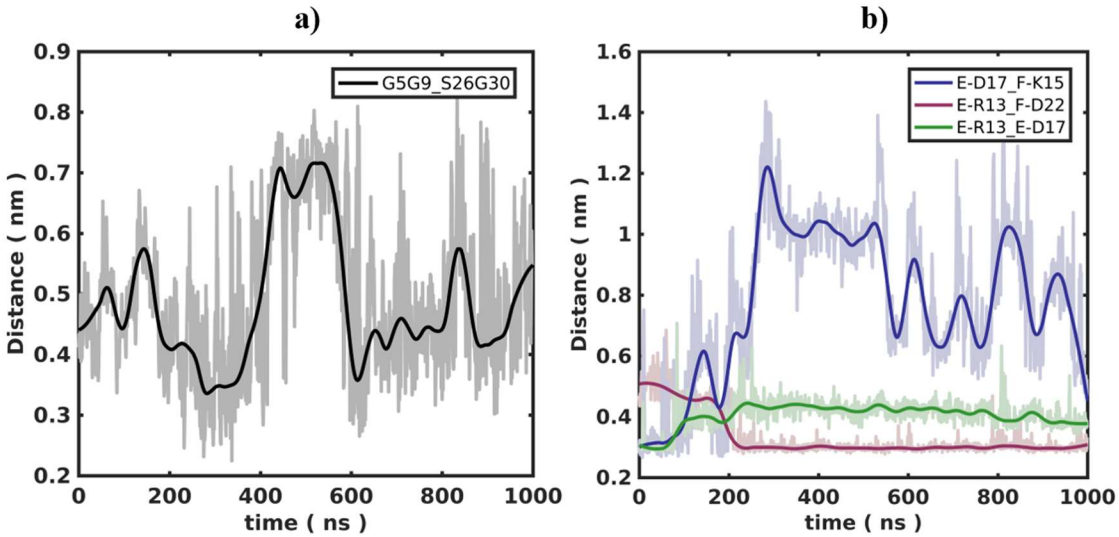

The intramolecular interactions that bring the two peptides in close proximity are shown in the figures above. a) The GxxxG motif present in PlnEF: the distance between the center of mass of PlnE G5xxxG9 and center of mass of PlnF S26xxxG30 motifs is shown in grey. b) The important electrostatic interactions between PlnE and PlnF: the distances between the center of mass of the carboxyl, guanidinium, or ammonium groups of the respective residues are plotted in figure b. In both graphs the darker lines illustrate the sliding average over 10 frames.

Initially, E-D17 interacts with both F-K15 and E-R13, forming a hydrogen bond with each of these residues and thus bringing the middle section of the two peptides closer (Figure 5-4b). After about 200 ns, E-D17 ceases to interact with F-K15 and is left to only interact with E-R13. The place of F-K15 was taken by other charged entities, such as lipid heads and sodium ions, which were increasing inserted from the top of the dimer (top is defined as the N-terminal of PlnF and C-terminal of PlnE). As the distance between F-K15 and E-D17 was increasing, the distance between E-R13 and F-D22 was decreasing, thus bringing the two peptides closer together at the bottom of the dimer. The above three-way interactions between E-R13, E-D17, and F-K15 and between E-R13, E-D17, and F-D22 are a common motif found in transmembrane proteins, called

the “Polar Clamp” [143]. In this motif, the side chains of polar amino acids such as Arg, Asp, Ser, and Thr, that can form at least two hydrogen bonds, are “clamped” by hydrogen bonds formed between them.

In the simulation, we identified three pairs of cation-π interactions, pictured in (**Figure 5-5**). Tryptophan 23 of PlnF (F-W23) is located on the inside of the bottom bilayer, and it interacts with both Lysine 10 of PlnE (E-K10) and Histidine 14 of PlnE (E-H14). When they are close, the aromatic rings of F-W23 and E-H14 are perpendicular to each other, forming a T-like shape. Interestingly, around Cluster I, the distance between F-W23 and E-H14 is increased. On the other hand, the consistent cation-π interaction between Phenylalanyl 31 of PlnF (F-F31) and Tyrosine 6 of PlnE (E-Y6) ceases to exist after the 700th ns, as the aromatic rings of these two residues move further apart and face different directions (while before they were facing each other - Figure 5-5b and c).

Figure 5-5: Network of cation π interactions

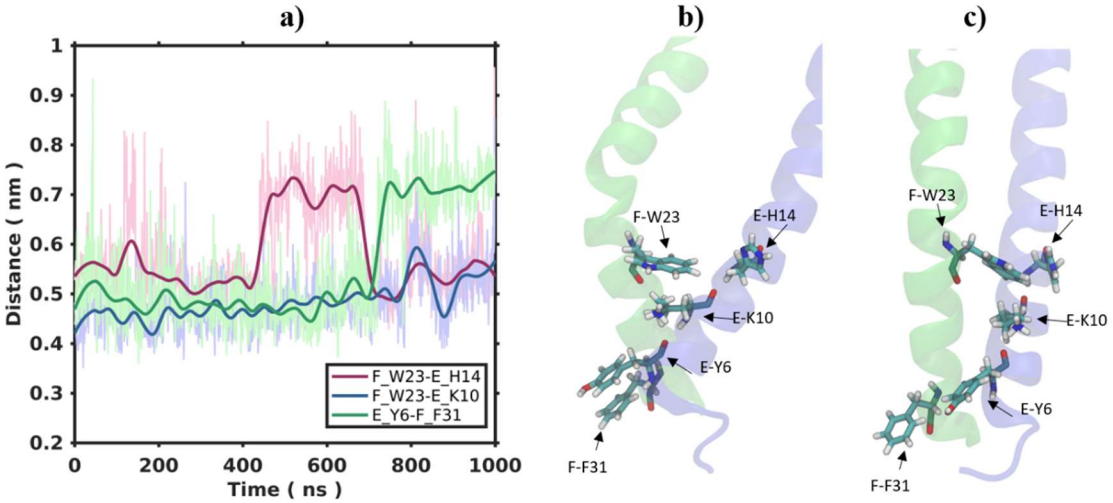

In figure a, we plotted the distances between residues that maintained a network of cation-π interactions during the simulation. The distances are calculated between the center of mass of the aromatic rings or ammonium groups. Darker lines illustrate the sliding average over 10 frames. Two snapshots that show the indicative behavior of the cation-π interactions are shown in b and c, at 610 ns for Cluster I and at 872ns for Cluster II, respectively. PlnE is illustrated in blue cartoon representation, and PlnF in green. Atoms of the residues of importance are colored according to atom type: carbon is light green, hydrogen is white, oxygen is red, and nitrogen is blue.

5.2.3. Membrane behavior around PlnEF

It was expected that the insertion of the peptides in the bilayer will alter its structure

and behavior as a response. Therefore, we analyzed various aspects of the membrane morphology to determine to what extent the presence of the dimer alters it.

We first examined the membrane visually to ensure that there was not any significant distortion or micelle formation. Indeed, at no point during the 1000 ns was the curvature of the membrane altered substantially. Moreover, we used the MEMBPLUGIN package to examine different features of the bilayer, such as order parameters, area per lipid, and membrane thickness [154]. We compared the results with a simulation of a pure POPG:POPE bilayer (in the same 3:1 ratio) and we found that the average values (over all lipid molecules) did not deviate considerably. However, there was substantial differences in the lipid molecules in the proximity of the dimer.

Figure 5-6: Membrane thinning around the peptides

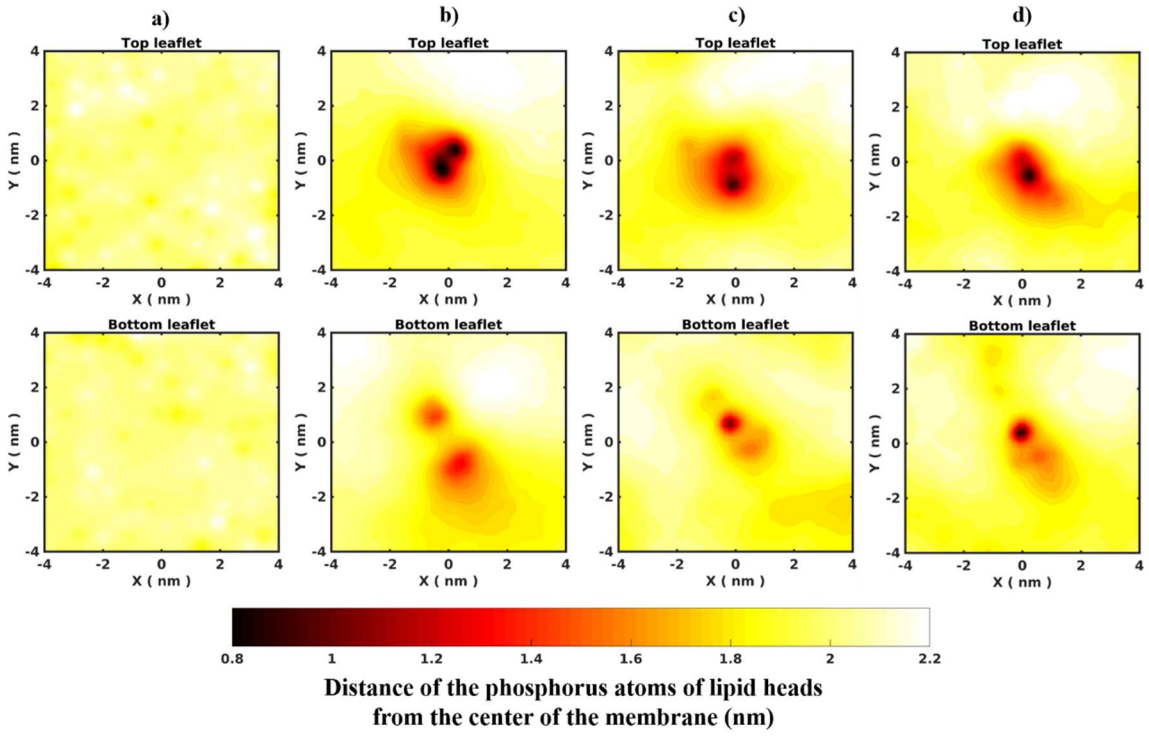

The distance of the phosphate atoms of the lipid heads from the center of mass of the membrane is shown. At the red colored areas, the lipid headgroups are inserted deeper into the bilayer core and they interact more with the peptides. The calculations were averaged over 100 ns windows to avoid temporal artifacts. From left to right: a) initial design structure – before any simulation, b) average from 450 ns to 550 ns (Cluster I), c) average from 750 ns to 850 ns (Cluster II), and d) average from 900-1000 ns (final structure). In all figures, the membrane is centered around the dimer.

In order to better visualize the local deformation of the membrane around the peptides, we calculated the distance from the center of the mass of the phosphate atoms (P) of each lipid molecule on both leaflets of the bilayer, and plotted it as a colored surface (Figure 5-6). In Figure 5-6a, one can see that the phosphate atoms (and thus the lipid heads) were distributed at equal distance from the center of the mass. As the simulation proceeded, water, ions, and lipid headgroups started being attracted to the dimer. In the top bilayer, the lipid headgroups interacted with the numerous polar residues located in the N-half of PlnF and the C-half of PlnE, toward the middle section of the peptides. The headgroups (from the top bilayer that were next to the peptides) were steered toward the area between the two dimers, progressively decreasing their distance from the center of the bilayer (Figure 5-6b).

At the bottom leaflet, the lipids interact with aromatic and charged amino acids at the end of the C' of PlnF and N' of PlnE, and therefore are not inserted significantly into the membrane. Interestingly, there are two regions of deformation at the bottom leaflet where the phosphate atoms move upward. This happened because the phosphate atoms interacted with the side of PlnF and the side of PlnE, but did enter the area between the two peptides. At a later time (Figure 5-6c and Figure 5-6d), the area affected at the bottom leaflet shrinks, however, the phosphate atoms get closer to the center of the bilayer. It is evident that the progressive thinning of the membrane became better defined and resembled a pore hole with diameter 0.5-2 nm.

We follow the definition for the presence of a transmembrane pore proposed by Sengupta et al.[155], in that the onset of a toroidal pore is defined when the phosphate atoms can no longer be considered as two distinct groups - i.e. a top and a bottom leaflet. Two phosphates are in the same group when they are closer than a cutoff distance of 1.2nm. In Figure 5-7a, we calculated the minimum distance between phosphates, starting at the top and bottom bilayers. When this distance is below 1.2 nm, then according to the above definition, the phosphates are clustered in one group. It is apparent that there is an insertion of some lipid headgroups into the membrane even from the 0 ns mark (which is after the minimization and equilibrations runs). The poration of the lipid bilayer started after 200 ns, and for the next 300 ns the minimum distance between the two bilayers is about the cutoff distance of 1.2nm. For the remainder of the simulation the minimum distance was below the cutoff value, and we can therefore

argue that a toroidal pore was formed.

Figure 5-7: Individual phosphate behavior near the pore

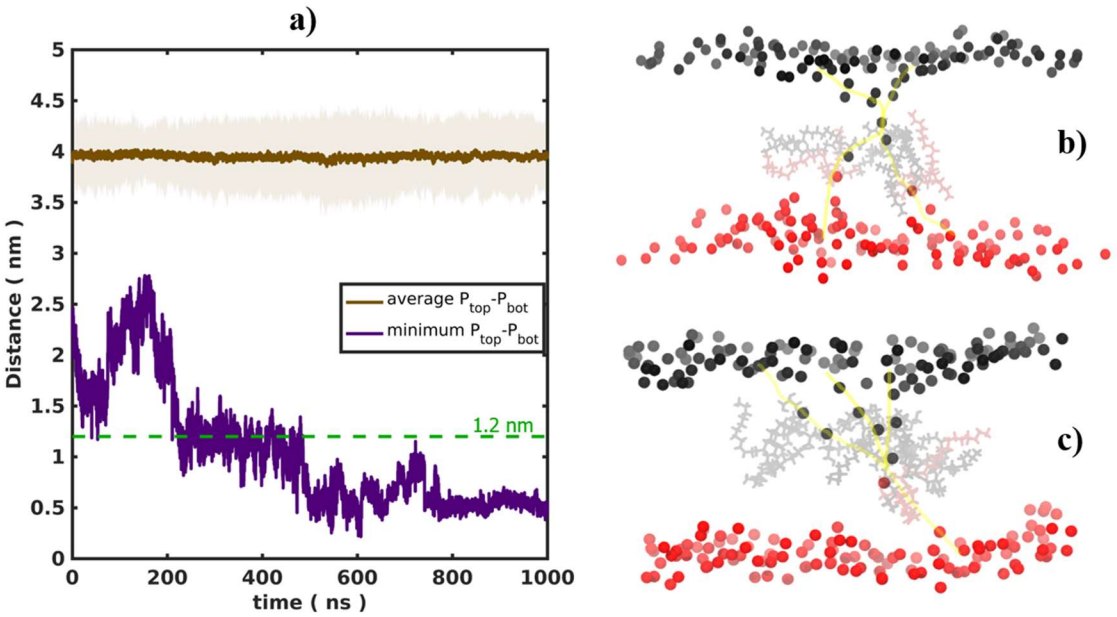

The distance between the phosphate atoms of the lipid heads of the top and bottom bilayers are plotted in figure a. The distance between the average position of the phosphates in the top and bottom bilayers is colored brown (with the standard deviation windows shown in lighter brown). The minimum distance between the phosphates in the top and bottom bilayers is shown in purple. The cutoff distance where we consider the two bilayers as separate is 1.2 nm (green line). In picture b, there is a snapshot of the membrane at 509 ns (Cluster I) while in picture c there is a snapshot at 863 ns (Cluster II). The phosphates that initially belonged to the top bilayer are colored black, while the ones that belonged to the bottom bilayer are colored red. We show the tails of the lipids that insert deeper in the hydrophobic region in grey. Finally, the different poration pathways, based on the network of the phosphate atoms, are drawn in yellow.

During the Cluster I frames (350-650 ns), two poration pathways appeared (Figure 5-7b), with the lipids accumulating inside the top half and outside the bottom half of the dimer, while the minimum distance between the leaflets fluctuated. Interestingly, there was a short-term increase of the minimum distance at ~700 ns, and then it was stabilized at 0.5 nm for the remainder of the time (**Figure 5-7c** - Cluster II). During this latter part of the simulation, the lipid heads form a single poration pathway that is wider in the top and narrower near the bottom leaflet. Finally, we visually examined the tails of the lipids that are inserted into the membrane (Figure 5-7b and c). In both snapshots, the tails of these lipids have an almost perpendicular orientation to the z-axis, indeed

resembling a toroidal pore.

It is important to note, that the number of phosphates that come close is significantly smaller than the total 240 phosphates in the system. This is apparent, as the distance between the average position of phosphates in the top and bottom bilayers (which is the membrane thickness) remains at 3.96 nm ± 0.4 nm for the entire simulation (Figure 5-7a, brown line). Thus, the membrane as a whole is not disturbed significantly by the presence of the peptides in the time scale we examine, but there is only a local disruption surrounding the dimers.

5.2.4. Behavior of ions near the dimer

The thinning of the bilayer and the insertion of lipid heads in the hydrophobic core describe only the structure of a pore. To examine the dynamics of the pore, we studied the permeation of water and ions through it. We monitored the trajectories of all the ions (both sodium and chloride ions) and the oxygen (from each water molecule). We characterized a permeation event as successful if an atom crossed the whole 4 nm long membrane area, in contrast to Adelman et al., where they set the cutoff distance at 3 nm, covering only the hydrophobic core area [156]. Then we considered an insertion in the top leaflet to be successful if an atom entered through the top of the bilayer and reached at least halfway through the upper quarter of its hydrophobic core (at 0.75 nm above the center of the membrane). In an analogous manner, we defined the successful insertion through the bottom bilayer.

As expected, chloride ions did not enter the membrane. Due to their negative charge, they are not attracted to the negatively-charged lipid heads present on the surface of the bilayer or in the pore. 34 unique sodium ions entered the top bilayer in 49 successful insertion events (some ions entered multiple times), while only 22 unique sodium ions were inserted in the bottom bilayer in 27 successful insertion events. The average uninterrupted time an ion spent in the inner hydrophobic core of the membrane when entering from the top bilayer was 25 ns, with a maximum of 712 ns. The trajectory of the chloride that spent 712 ns in the hydrophobic core is shown in Figure 5-8e. In contrast the average time a chloride spent when entering from the bottom was only 5 ns with a maximum of 27 ns..

Moreover, we calculated the time the ions needed to go from the polar surface of the membrane (at 1.5 nm from the center of the membrane) to the cutoff distance of 0.75

nm (from the center of the membrane). The ions entering through the top bilayer, traversed this space in 1.89 ns on average, while in the case of the ions entering through the bottom, the trip was 27% longer, averaging at 2.40 ns.

Figure 5-8: Transmembrane path of cations traversing the membrane

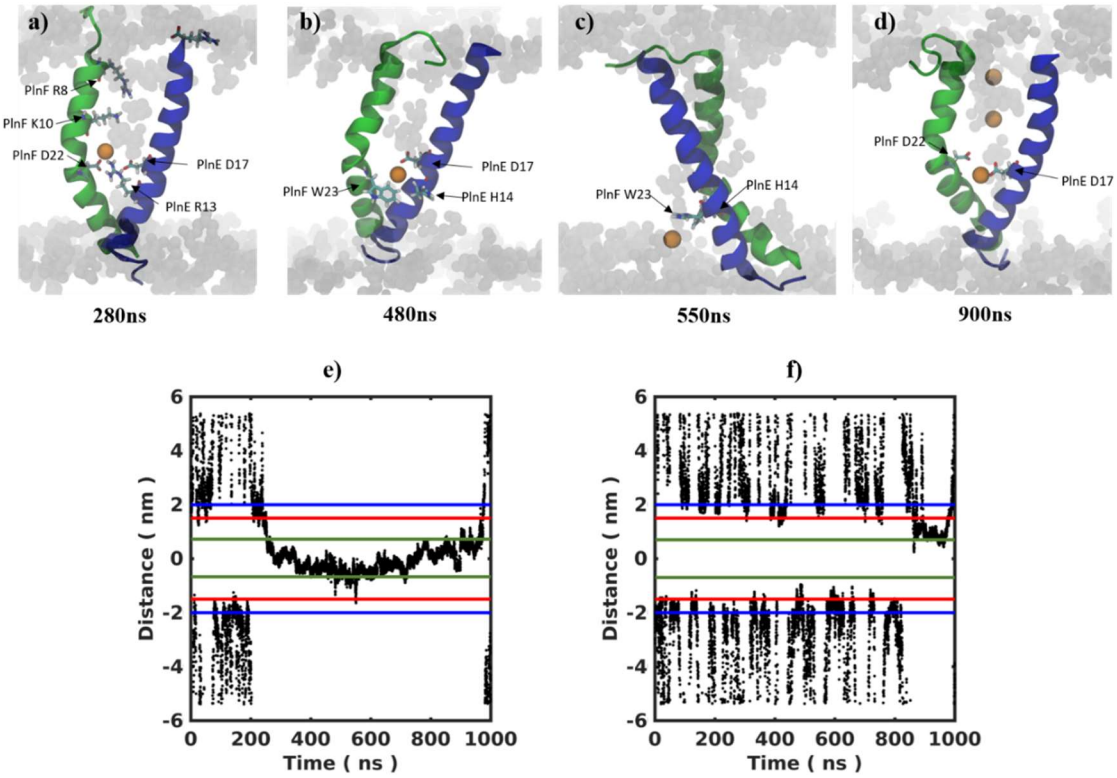

The path that the cation follows through the membrane is described in figures a, b, c, and d, alongside the important interactions that drive this behavior. PlnE is illustrated in blue cartoon representation and PlnF in green. Atoms of the residues of importance are colored according to atom type: carbon is light green, hydrogen is white, oxygen is red and nitrogen is blue. The headgroup atoms of the lipids and sodium ions are shown as grey and orange spheres, respectively. In figures e and f, the evolution of the trajectories of two cations is shown: e) one ion that reached the bottom bilayer starting from the top, and f) an ion that successfully inserted in the hydrophobic core of the membrane though the top bilayer. The blue, red and green lines indicate a distance of 2, 1.5, and 0.75 nm from the center of the membrane, respectively.

No ions successfully permeated the 4 nm long membrane. If we had used the Adelman cutoff, we would have had one ion passing through the 3 nm of the membrane hydrophobic core (Figure 5-8e), however, this would have been a false positive permeation event since the ion ends up being trapped at the surface of the bottom bilayer and never exits to the solvent.

Initially, a sodium ion enters through the top bilayer as it gets attracted to the polar clamp between E-D17, E-R13, and F-D22 (Figure 5-8a). It then moves further down as it interacts with F-W23 through cation-π interactions (Figure 5-8b). When it reaches the bottom layer it interacts strongly with the lipid heads there, however, the cation-π interaction with F-W23 is still present (Figure 5-8c), which leads to the ions re-entrance in the hydrophobic core (Figure 5-8d). In the meantime, more ions entered into the pore that interacted mostly with the surrounding lipid heads rather than the peptides (Figure 5-8d,e,f). Through this journey, PlnF shows flexibility around its middle section to accommodate for the different interaction networks around the dimer.

5.2.5. Water permeability through the pore

Similar analysis was performed on the trajectories of the water molecules. 750 molecules of water successfully traversed though the 4 nm pore in the bilayer. Surprisingly, 374 of them entered through the top bilayer while the rest 376 entered through the bottom. Additionally, there were 7,070 successful insertion events through the top layer and only 2,920 successful attempts from the bottom leaflet. The path that the water molecules followed through the pore was guided from the network of polar interactions set up by the inserted lipid heads and polar amino acids. During the frames of Cluster I, water would go through the pore via two pathways (Figure 5-9a), avoiding the area between the C' of PlnF and the N' of PlnE. Later, only a single pathway continued (Figure 5-9b) and the flow of water was better defined into one column.

The average time the water molecules spent travelling through the pore was 14.7 ns. We noticed that some water molecules resided in the hydrophobic core longer than others, interacting with other molecules around them, such as sodium ions lipids headgroups and polar residues. To analyze this behavior further, we divided the bilayer into 40 0.1 nm bins along its z-axis and performed k-means clustering on the time each water molecule spent in the bin. We identified three water types (Figure 5-9c). We also calculated the average time that molecules of each water type needed to traverse through the membrane (Figure 5-9d).

291 water molecules were grouped into type A. The average time they needed to cross the membrane was 12.5 ns. They spent most of that time near the middle of the bilayer, at a distance ~0.1nm from the center. There they interacted strongly with the lipids heads that had fallen from the top bilayer, the ion shown in Figure 5-8c and

residues Serine 21 and Aspartic acid 17 of PlnE, as well as Glycine 19 of PlnF.

Figure 5-9: Behavior of water as it traverses the pore

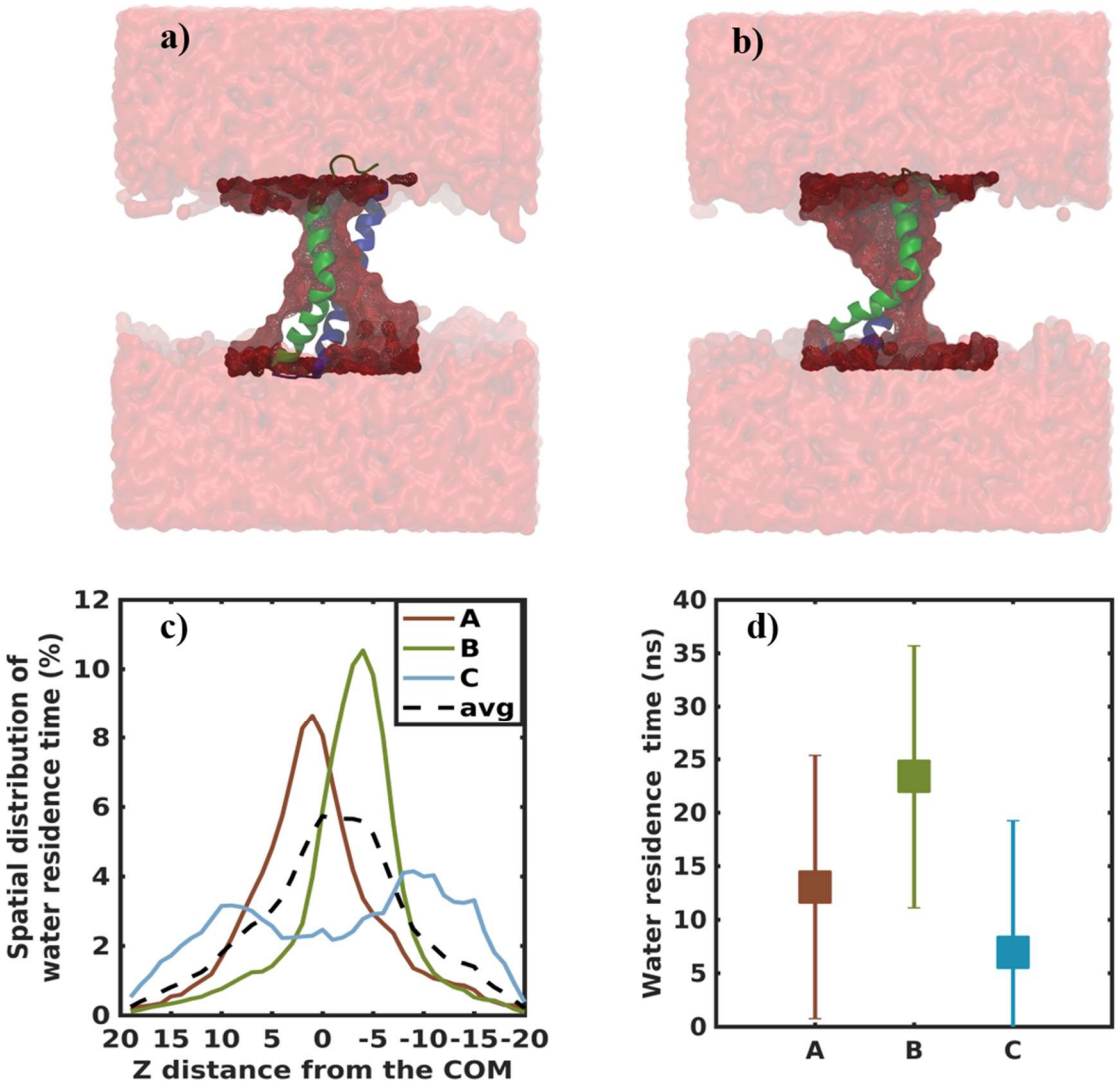

Two different snapshots of the simulation are pictured at a) 580 ns (Cluster I), and b) 892 ns (Cluster II), showing the double and single water networks present at each cluster. PlnE is illustrated in blue cartoon representation and PlnF in green. Water is represented as a red surface, and water molecules located further than 2 nm from the center of the mass of the membrane are represented as a lighter red surface. In figure c, we calculated the distribution along the z-axis of the water residence time as they move through the pore (the average is shown in black dotted line). We used this information to cluster the molecules into three groups: A in red, B in green, C in blue. The residence time in the membrane of each of these water groups is reported in d.

258 molecules belong to water type B. They are different than type A, in that they spent 55% more time, ~24 ns, in the hydrophobic core, lingering at 0.4 nm below the center of the membrane. They interacted similarly with the ions and lipid heads, however this time they were strongly coordinated between Tryptophan 23 and Aspartic acid 22 of PlnF, and Arginine 13 and Histidine 14 of PlnE. Finally, there are 201 molecules in group C. These water molecules cross the membrane faster, with an average time of 6.6 ns. They spent most of their time at both ends of the pore interacting with the polar headgroups.

5.3. Discussion

In this chapter, we have presented the results of a 1μs long atomistic MD study of a class IIb dimer. We have demonstrated for the first time that this two-peptide bacteriocin is able to form a small toroidal pore in a model bilayer that allows water permeation and, possibly, ion conduction.

First, we analyzed the evolution of the dimer structure and the space it occupies. The transmembrane dimer was stable and did not translocate along the z-axis of the bilayer during the simulation. We identified two clusters of dimer structure similarity, one around the middle of the trajectory (Cluster I) and one toward its end (Cluster II). Through the rest of the analysis we looked for differentiation of the behavior of the system components (dimer, lipids, water, and ions) between the two clusters. The only perceptible variance in the structure of the dimer was the interchange of two pairs of cation-π interactions (Figure 5-5). On the other hand, there was a clear change in the behavior of the non-protein molecules around Cluster I versus Cluster II. At Cluster I, the pore was divided into two paths below the middle of the dimer, in which the lipid heads, ions, and water participated in two distinct interaction networks with polar residues of the dimer, while at Cluster II there was only a single path.

We then further analyzed the motifs that support the interaction between the two peptides. GxxxG or GxxxG-like sequences are conserved structural motifs present in many transmembrane proteins. It has been suggested that these motifs provide a relatively flat dimerization surface, allowing the peptides to come into proximity to them. The mutational analysis of PlnEF, described in Chapter 4, revealed which residues,

belonging in a few such possible motifs on PlnEF, are vital to the antimicrobial activity of the dimer. Based on the dimer structure we designed (shown in Figure 4-1), we allowed the G5xxxG9 motif in PlnE and the S26xxxG30 motif in PlnF to come close together. As seen in Figure 5-4a, the distance between these two motifs fluctuated from 0.3 to 0.7 nm. Kleiger et al. calculated the interhelical distance of the GxxxG motifs of various transmembrane dimers and found that it varies from 0.57 to 0.7 nm [157]. Therefore, the suggested GxxxG motifs in PlnEF (G5xxxG9 motif in PlnE and the S26xxxG30 motif in PlnF) can be assumed to successfully contribute to the dimerization of PlnEF.

Next, we examined how the association of the two peptides around the G5xxxG9 motif in PlnE and the S26xxxG30 motif in PlnF differed between the two clusters. In both cases the motifs were close enough to be considered as dimerization surfaces, yet their relative orientation changed slightly. GxxxG motifs are often linked to the formation of dimers with negative crossing angles between the peptides (such as −40° in the case of the parallel Glycophorin A dimer) [158]. It was shown that the more splayed the crossing angle is, the more extended the contact surface between the two peptides appears to be [159]. In the case of the epidermal growth factor receptor (EGFR), the change in the angle of the transmembrane helices that associate through a GxxxG motif is believed to play a key role in the activation of EGFR [159]. Therefore, we assume that even a small change on the crossing angle of the peptides could be important. In PlnEF, the exact calculation of the crossing angle has significant noise because the helical parts - that the motifs are located in - are short, i.e. i) PlnF bends around Proline 20 allowing only a short 10 amino acid long helix, that contains the S26xxxG30 motif to approach PlnE, and ii) the motifs are close to the terminai of both peptides (in contrast to Glycophorin A and other dimers, where the motifs are located closer to the middle of the peptides [80]). Nevertheless, we observed that in Cluster II the angle between the peptides was smaller and the two helices were better aligned, while in Cluster I the center of mass of the motifs were further apart, suggesting a possible two-state mechanism.

It is important to note, that there is a considerable number of studies utilizing MD in order to investigate the behavior of GxxxG motifs and analyze the dimerization process of different peptides [160–165]. Yet none of them has investigated the pore-forming capacity of dimers associating through the GxxxG motif, and no study has examined whether GxxxG motifs facilitate ion or water penetration. Moreover, previous work has

been based on coarse-grained MD simulations, in which each particle of the system corresponds to more than one atom. Even though coarse-grained MD is a more computationally-affordable method, it results in information loss - e.g. distinct hydrogen bonds cannot be calculated.

We also performed a 40 μs long coarse-grained MD simulation of the system using the Martini force field (results not shown). We observed that, like in the atomistic MD, the dimer structure was stabilized through persistent electrostatic interactions. However, the polar interactions we observed in the atomistic model were missing (such as Serine residues forming different hydrogen bonds). Moreover, the structure of both peptides resembled straighter helices. Most importantly, neither water nor ions could enter the area between the peptides, possibly because the Martini water model replaces four atomistic water molecules and it may be too bulky to fit efficiently in the pore opening [166].

Nishizawa et al. recently compared the accuracy of the description of the dimerization of transmembrane helices between coarse-grained MD and atomistic MD simulations [164]. Their analysis revealed that the Potential of Mean force (PMF) of dimerization of the peptides was an order of magnitude steeper in coarse-grained MD simulations than in atomistic ones, indicating that the peptides have a higher tendency to dimerize when modeled with coarse-grained force fields. Interestingly, the atomistic simulations agreed very well with the experiments. This discrepancy (i.e. the strong dimerization of the peptides) might additionally explain why in our coarse-grained simulation the peptides do not allow water to penetrate inside the dimer.

In many cases the GxxxG motifs might offer a dimerization surface; however other interactions possibly provide the sufficient contacts for the peptides association [158]. In the previous chapters, charged and polar residues around the upper middle section of PlnEF were shown to create important hydrogen bonds and a characteristic “polar clamp” between the two peptides and bring them close to each other. Interestingly, the interaction between Aspartic acid 17 of PlnE and Lysine 22 of PlnF seized to exist after the first 200 ns of the simulation of the transmembrane dimer, as the two residues moved further apart and interacted with other components (water and ions) (Figure 5-4b; a salt bridge is considered important if the charged side chains are closer than 0.4 nm). This interaction might only be important for the initial association of the two peptides and

their insertion in the bilayer.

The rest of the polar and charged residues that are in the hydrophobic core of the bilayer create a network of interactions that attract lipid headgroups, water, and ions. It has been established that the center of many transmembrane proteins, which induce protein permeabilization or are proton channels, include regions rich in hydrogen bond donors and acceptors that create a water or proton accessible path [167–169]. Additionally, appropriately-spaced basic and acidic residues create high-affinity transmembrane domains that are called “charge zippers”. These motifs, which do not typically tolerate mutations, are located in the center of transmembrane oligomers and create a hollow cavity with “eyelets” that allows ion conduction [169]. An example of such a “charge zipper” are the salt bridges formed in the center of PlnEF (Figure 4-4a and Figure 5-4b).

In Chapter 4, we demonstrated that the position of aromatic residues in PlnEF was vital to the anchoring of the dimer in the bilayer. Aromatic residues are well known to stabilize the placement of transmembrane peptides and proteins in membranes, forming cation-π interactions with the positively charged atoms in the lipid heads [170,171]. Aromatics can participate in cation-π interactions with other types of molecular groups as well, such as positively charged amino acids and cations.

Moreover, the role of aromatic amino acids in gating ion channels or being near ion binding centers has been well-documented [172–174]. For example, aromatic residues play a key role in the ion transport mechanism of different potassium and sodium channels: Tryptophan residues are placed near the ion binding site, while Tyrosine and Tryptophan pairs are located near the pore rim, gating the channel [172].

A similar conclusion could be drawn for PlnEF. Tryptophan 23 of PlnF (F-W23) is a significant attractor of water and ions, while Tyrosine 6 of PlnE could act as a gate. When the distance between Tyrosine 6 of PlnE (E-Y6) and Phenylalanine 31 of PlnF (F-F31) is small, their interaction locks together the very ends of the C-terminus of PlnF and the N-terminus of PlnE, and the angle between the GxxxG motifs is wider (Cluster I, Figure 5-5b); but when these residues do not interact, they allow the helices to come closer (Cluster II, Figure 5-5c). Interestingly, substitutions of E-Y6 and F-W2 with other aromatics were well-tolerated in experiments, indicating that all that is needed in these positions are amino acids with aromatic rings (Figure C-2).

The polar cavity between the peptides attracted lipid heads near the dimer that in turn started bending and progressively getting inserted more into the bilayer, forming a toroidal pore. The activity of many AMPs has been associated with pore formation [175]. In most well-documented cases, the peptides form well-defined, wider pores, the walls of which are lined only by AMPs (barrel stave pore) or by AMPs and lipid headgroups (toroidal pore). In both cases, usually more than two AMPs are needed. A different case is that of the AMPs Melittin and Magainin-2 [155,176,177]. They both were shown to form water-filled, disordered toroidal pores with a diameter of about 1.5-3 nm, which are concentration dependent. It was recognized that one or two peptides are needed to line the pore, while more are required to aggregate on the surface of the membrane [155]. Similarly, we observed a nanometer toroidal pore which is less well-defined than the typical wide pores of other AMPs, and is lined with only a few lipid-headgroups and the peptides.

The poration of a cell membrane leads to the passive transport of water and, to a lesser extent, ions, while failure of controlling this process results in cell death [177]. Leontiadou et al. performed MD simulation of Magainin MG-H2 on a model bilayer: they observed that 3 water molecules per ns permeated the membrane unidirectionally (J-3 waters/ns), and they calculated the single-pore permeability coefficient $P = J/C = 10^{-13}$ cm^3/s (where C=55 mol/L is the concentration of pure water) [176]. In our simulation, the water molecules permeate the membrane with a rate only one order of magnitude smaller (0.374 waters/ns going from the top bilayer to the bottom, and 0.376 waters/ns going the opposite direction). Thus, the average unidirectional single-pore permeability coefficient is $P \approx 10^{-14}$ cm^3/s. This value is on the same order of magnitude with the coefficient of a single-aquaporin channel, which is considered to be a highly water-permeable pore. Moreover the permeation coefficient of the PlnEF dimer is two orders of magnitude smaller than that of the octameric Protegrin-1 pore and of the hexameric Dermcidin pore, which are two very powerful broad spectrum AMPs that create pores with diameters ~4nm and kill their target cells by inducing an uncontrollable ion efflux [175,178].

Interestingly, the passive transport of ions through hydrophilic pores depends heavily on the size of the water channel; ions permeate small pores (diameter < 3nm) very slowly, while at higher diameters there is an enhanced transport of ions through the

pore [179]. Particularly, Tieleman et al. calculated that ions permeate small pores at a rate three orders of magnitude slower than water does [180]. If this is true for PlnEF, the time an ion requires to travel through the membrane is ~2.7μs, a length of time that exceeds our simulation. Nevertheless, during the 1 μs simulation, we did observe one ion crossing more than 3.5 nm of the 4 nm long membrane, and we established that there is a favorable interaction network for ion conduction to take place.

The opening of the pore in the top bilayer was more accessible to water and ion molecules, as there were more successful attempts to enter the inner hydrophobic area of the membrane. Thus, it was expected that there would be more water molecules crossing the membrane after they enter from the top. Surprisingly, though, the number of water molecules that ended up going through the pore was the same for both directions. This is a strange result, as it indicates that the limiting factor is probably the diameter of the narrowest part of the pore and how many molecules it will accommodate, rather than how many molecules are available at the beginning of the entrance of the pore. Another explanation is that the peak of the average residence time (Figure 5-9) is located closer to the bottom leaflet, and it therefore did not allow many water molecules to enter and reach the cutoff distance (0.75 nm from the center of the mass of the bilayer) to be considered a successful attempt. However, the possibility of surpassing the interactions around the area where the residence time peaks was the same going either direction.

Lastly, we analyzed the behavior of the water molecules that permeated the pore. Following an observation that some of these molecules spent more time in the pore than others, we performed clustering analysis on the residence time of the water molecules as they traversed the pore. This analysis revealed that there are three different water types that crossed the membrane, with average residence times of 24, 12.5, and 6.6 ns respectively. This is an interesting finding, because recently many studies have focused on the slow, ordered water molecules that are bound to the newly-solved crystal structures of transmembrane proteins. Particularly, over the last five years, there has been a significant effort to understand what is the functional role of ultraslow waters on the activation of G-protein-coupled receptors (GPCRs) [181,182]. Lee et al. simulated such a system and found that the residence time of water molecules in the active state of a specific GPCR was at the order 10^2 ns (an order of magnitude longer than the ones observed in the PlnEF simulation), while in the inactive state of the GCPR, the residence

time was three times shorter than in the active state [181]. They also found, that in the active state the water molecules are located around activity hotspots, while key residues control the flow of the water channel. Even though we do not suggest that there are similarities between the activation of GPCRs and the MOA of PlnEF, we wish to point out that slow water molecules and the interactions in which they participate could be of importance and might constitute a criterion for designing optimized peptides.

5.4. Conclusions

Plantaricin EF is a class IIb bacteriocin. Similarly, to other bacteriocins, its mechanism of action is associated with the dissipation of the transmembrane potential. However, it has been suggested that bacteriocins act through a receptor-mediated mechanism of action and do not induce pore formation and ion conduction by themselves. In this chapter, we demonstrated for the first time that contrary to this canonical, widely accepted model, a class IIb bacteriocin can create a small toroidal pore (diameter 0.5-2nm) in the bacterial cell membrane that leads to water permeation and, possibly, ion conduction.

The size and morphology of the pore are relevant to pores formed by some other broad spectrum AMPs. Water permeates the pore at a rate only one order of magnitude smaller that of aquaporin, whose key role is to transfer water across the bacterial membrane, and two orders of magnitude smaller than very powerful, large pore-forming AMPs. This indicates that the presence of pores induced by PlnEF will have a considerable impact on the solute transport across the cell membrane. We evaluated the time needed for an ion to travel through the pore and realized it is about three times longer than our simulation. Possibly computationally-demanding, longer atomistic MD simulations or enhanced sampling techniques would allow the ion transport through the dimer-induced pore. This hypothesis is strengthened by the fact that we observed an ion going about 90% through the membrane and we recognized a polar-interaction network that could lead the path for ion transfer.

Additionally, we analyzed the interactions and motifs that allow the two peptides, PlnE and PlnF, to associate and form a dimer. We witnessed that electrostatic and cation-π interactions create a network of polar attractors, allowing ions, lipids headgroups, and water to be present in the otherwise hydrophobic core. We believe that

some of these interactions might act as “microswitches” that control the structure of the dimer and the space it occupies. We also observed the presence of “slow” water molecules in the pore that might be important for the activity of the bacteriocin, as “ultraslow” water molecules have shown to mediate the activity of some GPCRs.

We are confident that the results presented in this Chapter could be of importance to the designing of new antibiotic agents, as it would steer the search for better bacteriocins toward peptides that form stable pores and develop optimal interaction networks that enhance the water or ion transfer. Furthermore, we believe that the work presented here extends beyond the benefit of understanding the mechanism of action of bacteriocins and adds important observations to the literature of transmembrane dimers in general.

One question that is raised in our research is that if we suggest that the mechanism of action of PlnEF (and bacteriocins in general) involves direct poration of the membrane, then how are these AMPs so selectively active against their target? The selectivity of the bacteriocins implies that there is some recognition process that enhances their activity. Moreover, it was shown experimentally that the presence of specific transmembrane proteins was important for the bactericidal action of some class II bacteriocins. Two possibilities among many are that these bacteriocins have multiple mechanisms of action, or that the receptors are required for the insertion of the peptides in the membrane. Without a detailed structure of the receptors or of the receptor-bacteriocin complex, we cannot assess any of these potential scenarios. In the next chapter, we present our efforts to construct a class II bacteriocin-receptor system and to evaluate their suggested interaction.

Chapter 6

A first look at a class II bacteriocin-receptor complex

6.1. Introduction

The examination of the mechanism of action (MOA) of antimicrobial peptides (AMPs) has attracted considerable scientific interest, because, in principle, elucidating their MOA could allow for the optimization and better control of their activity. However, the MOA of the class II bacteriocins in particular has remained quite enigmatic. The activity of most class II bacteriocins has been associated with membrane permeabilization and deadly solute efflux. Due to their narrow activity spectrum, it has been presumed that some type of interaction with a receptor at the target cell is responsible for their high sensitivity [183]. However, significantly less is known about their detailed, fundamental mechanism of action.

The only receptor-class II bacteriocin MOA that has been studied in more detail is the case of class IIa bacteriocins and their suggested receptor, a major sugar transporter system (Man-PTS) [184]. As described in Figure 1-3, it is hypothesized that class IIa bacteriocins do not form pores on their own, rather they interact with transmembrane extracellular loops of Man-PTS inducing some conformational change on the receptor that in turn leads to uncontrollable leakage of the cell contents [68]. This hypothesis cannot be further evaluated though, because we are missing an atomistic level description of the system.

Furthermore, different transmembrane proteins have been identified as possible receptors for other class II bacteriocins. Resistant mutants to the class IIb bacteriocins Lactococcin G and its homologous, Enterocin 1071, had an alteration in the uppP gene, encoding for the undecaprenyl pyrophosphate phosphatase (UppP), while an APC transporter was recently associated with the activity of class IIb bacteriocin Plantaricin JK [78,79]. Similarly, YvjB, a transmembrane Zinc-Metallopeptidase was identified as an interaction partner and possible receptor for the class-IId bacteriocin, LsbB [39]. In spite

of these developments, the lack of atomistic structure of the receptors hinders the thorough investigation of the MOA of bacteriocins, as is the case with many other membrane proteins.

The determination of membrane protein (MP) structure is one of the most challenging endeavors in the field of structural biology, yet exceptional progress is being made in that field. MPs are encoded by more than 30% of the human genome and is estimated that over 50% of all drugs target them [185].. However, the number of solved MP structures is considerably smaller than the number of solved globular protein structures, due to difficulties in the expression of the former and their required reconstruction in membrane mimetics. Indeed, MPs comprise only 2-3% of submitted structures in the protein databank (PDB) [185].

Astonishing progress in crystallography, NMR spectroscopy, and in cryo-electron microscopy has significantly increased the frequency and resolution of new MP structure being successfully solved [185]. Nevertheless, the next best alternative to an experimentally-solved structure is a good prediction using computational methods, and this is the method that we will explore in this chapter.

6.2. Computational protein structure prediction

Computational MP structure prediction has evolved remarkably over the last fifteen years, with different methods and software emerging regularly (a great recent review can be found at [185]). In the next paragraphs, we are going to provide a brief overview of the current methods.

The first step of structure prediction is assigning a possible secondary structure to a protein. Initially, this was done based on database-derived statistics, however, the introduction of multiple sequence alignment and machine learning techniques (such as artificial neural networks) have improved the quality of the prediction.

The second important aspect of MP structure prediction is the identification of their topology, i.e. the transmembrane domain-span and the periplasmatic or cytoplasmic orientation of those domains. Hydrophobic scales (based on the partitioning energies of different amino acids from water to a hydrophobic solvent) were originally used, while later evolutionary information, neural network, and hidden Markov model methods were incorporated to the topology prediction tools. Nevertheless, sequence-based structure

prediction cannot yield detailed information of the structure of MPs because these methods are insufficient to predict the contacts between the different structure elements and, thus, their tertiary structure. For this purpose, homology-based modelling techniques, threading methods, or ab initio protein structure prediction methods are employed.

In the case of homology modelling, the target sequence is aligned with a highly similar sequence, whose structure is known; the higher the similarity between the two molecules, the more accurate the prediction will be. Therefore, the availability of structures of high sequence similarity to the query sequence determines the limitations of this method. Threading, or fold recognition, methods rely on constructing the predicted structure by recognizing similar folds with solved structures, even in the absence of sequence similarity and evolutionary relationship. For sequences with low similarity, *ab initio* folding and *de novo* structure prediction is employed. In this case, fragments (of the sequence of interest) of different lengths are paired with different folding states and then undergo Monte-Carlo simulations with a knowledge-based potential.

Different softwares and platforms have been developed over the years, employing one or more of the above methods. These software are evaluated biannually and presented at the CASP (Critical Assessment of protein Structure Prediction) meeting, where a worldwide scientific experiment takes place [183]. Participants in CASP are given the sequence of a recently experimentally-determined structure (which was not previously available to them) to test their structure prediction methods. RosettaMP is one of the earliest and most reliable packages, while MEDELLER has demonstrated remarkable prediction quality of structures with high similarity homologues in the PDB database [186,187]. One of the best performing packages, acording to the the CASP ranking, that merges secondary structure assignment, homology modelling, fold recognition, and ab initio protein prediction, is the I-Tasser suite [188].

We have attempted to use the above methods to predict the structure of a possible receptor of class II bacteriocins. In each case of the class II receptors identified so far (the Man-PTS, the UppP, the APC transporter, and YvjB), the structure prediction methods yielded low-quality predictions of whole proteins, because homologues or proteins with similar folds have not been solved experimentally and the receptor sequences are too long for *ab initio* structure prediction.

However, we were able to suggest a topology and a partial structure of the Zn metallopeptidase YvjB. YvjB is significantly smaller than all the other receptors, making it a better target for structure prediction. In the next section, we provide an overview of all the experimental research available for LsbB and YvjB that are relevant to our work.

6.3. LsbB, a class IId bacteriocin and its hypothesized receptor, the Zn Metallopeptidase YvjB

LsbB is a 30 amino acid long, leaderless, non-pediocin-like bacteriocin that was first isolated from *Lactococcus lactis* subsp. *lactis* BGMN1-5. It exhibits a narrow activity, mostly targeting other *lactococcal* strains [189]. LsbB, whose sequence can be found at **Table 6-1** is relatively hydrophilic with a highly cationic C-terminus.

The gene that encodes for LsbB is located in a gene cluster that also produces LsbA, a hydrophobic unclassified bacteriocin that has not been further studied, and LmrB, a transporter that renders the producer cells resistant to both LsbA and LsbB [85]. Through experimental studies, it was realized that the two peptides do not act synergistically against a number of tested targets, as their combined activity was just the sum of the individual activities of the peptides, therefore they cannot be considered class IIb bacteriocins [85].

Table 6-1: Amino acid sequence of the class IId bacteriocin LsbB

LsbB	**MKTIL RFVAG YDIAS HKKKT GGYPW ERGKA**

In 2013, Uzelak et al. identified YvjB, a Zn metallopeptidase, as a possible receptor for LsbB through constructing a cosmic library of an LsbB-sensitive strain [39]. The cosmic library method relies on breaking down the chromosomal DNA of the sensitive target bacterium (BGMN1-596) and inserting the DNA pieces in Lambda phages to create a clone plasmid that next will be introduced to resistant bacteria. If, subsequently, some of the resistant bacteria become sensitive, then the plasmid clone that they contain, must encode for a receptor of the bacteriocin. After repeating this procedure multiple times, Uzelak et al. pinned down the gene that confers sensitivity to the cells. This gene, named yvjB, codes for a 428-residue, Zn-dependent membrane bound, metallopeptidase, which is named YvjB (Table 6-2).

YvjB is a highly-conserved Zn protease of the M50 family. Proteins of this family are

involved in gene regulation in other species, however the function of YvjB in *lactococci* is yet unclear [190]. Uzelak et al. also performed whole genome sequencing of a few spontaneously resistant BGMN1-596 cells and found that these bacteria contained alterations at specific residues of YvjB [39]. A G188S mutation was included in five mutants, while two mutants had a G414L, a V415G, and an N428K/M mutation, and in some cases yvjB had an earlier stop codon.

They then tested if another function of the bacteria was altered due to the mutations and thus hindered the growth of the cells. They introduced cells in an LsbB-free medium and observed that both the sensitive and the mutant BGMN1-596 cells had similar growth. Finally, they showed that heterologous expression of YvjB in otherwise resistant species, such as *Lactobacillus paracasei* and *Enterococcus faecalis*, rendered these bacteria sensitive to LsbB. In the same study, they examined whether the activity of LsbB is associated with Man-PTS or other sugar transporters, and they demonstrated that it has no such associations.

Table 6-2: Amino acid sequence of the Zn Metallopeptidase, YvjB

1	MIETL ITFII IFGII VAIHE YGHLW WAKRS GILVR EYAVG MGPKI FAHQA
51	KDGTL YTIRI LPLGG YVRLA GWGDD KTEIK KGQAA SLVVS KSEVV NPEAE
101	NSVSN IVRRI NLSEH VELEE AIPML ITEYD FEKEL FIEGE VFGEI KRYSV
151	DHDAT IIEED GTEVR IAPLD VQYQS AGVFH KMLTN FGGPL NNFIL GIIAF
201	IVLTF VQGGV PSTTN AIGQV EKGTP AYNAG LKAGD KIEAV NGTKT ADWNN
251	VVTEI SGSKG KELKL EVSRS GKSET LSVTP KKMDG SYRVG IMQSM KTGFF
301	DKITG GFVQA GQSAT AIFKA LGSLI ARPSL DKLGG PVAIY QLSGQ AARAG
351	LFPAIV LLAM LSINL GIVNL FPIPV LDGGK IVLNI IEAIR GKALS QEKES
401	IITMV GVVFM LVLFV AVTWN DILRA FVN

One year after the Uzelak et al. publication, Ovchinnikov et al. determined the 3D structure of LsbB and highlighted its possible binding domains through comparative activity essays of a series of truncated LsbB peptides, as well as Alanine substitution [87].

Similar to other bacteriocins, LsbB was unstructured in water but that changed in TFE and DPC environments. The N-terminus of LsbB forms an amphiphilic α-helix, about 18 amino acids long, which contains a series of basic amino acids (HKKK). The C-

terminus remains unstructured in both water and organic solvents. They found that only the last ten C-terminal residues are responsible for the specific activity of LsbB, however, they concluded that the basic amino acids series (HKKK) is vital for the initial unspecific interaction of the peptide with the membrane. The residues that were found (through Alanine scanning) to be crucial for the specificity of LsbB were A30, E26 and most significantly W25. Nevertheless, no further conclusion about the mechanism of action of LsbB could be made without the detailed atomistic description of its interaction with YvjB.

Lastly, in 2016, Miljkovic et al. investigated further the possible interaction domains of both YvjB and LsbB [190]. They performed site-directed mutagenesis on LsbB that further confirmed the importance of Tryptophan 25 and Alanine 30 for the activity of the peptides. Then, they performed a comparative study between the YvjB produced by a sensitive strain (YvjBMN) and a resistant strain (YvjBMG), which had different amino acids at 31 positions. *In vitro* experiments revealed that LsbB interacts with both YvjBMN and YvjBMG, however, the interaction with the latter are significantly less potent. In contrast, *in vivo* experiments with immunofluorescently-labeled antibodies showed that LsbB interacts specifically only with bacteria having YvjBMN.

Miljkovic et al. created hybrid proteins of YvjBMN and YvjBMG and expressed them in otherwise insensitive cells, in order to identify the domains that are important for LsbB-receptor interaction [190]. This experiment revealed that the last ¾ section of YvjBMN is what renders the cells sensitive, and thus is most likely responsible for the interaction with LsbB. Six residues are different between YvjBMN and YvjBMG in this section; residues Phe351, Ala353, Val354, Tyr356, Gln396, and Met404 in YvjBMN change to Leu351, Thr353, Ile354, Gln356, Pro396, and Leu404 in YvjBMG.

They performed site-directed mutagenesis where they mutated each of these six residues of YvjBMG to the respective amino acid of YvjBMN to examine which residue will deliver sensitivity to the target cells. They observed that a single mutation on Tyr356 was sufficient to make cells sensitive, however, the LsbB activity was lower in that mutation than it was against the wild type YvjBMN. Then they tried different combinations of mutations, that matched (and with some even improving) the activity of LsbB, however, clear conclusions could not be drawn.

Finally, they used a transmembrane domain prediction tool, which predicted that

YvjB has four transmembrane helices: 5 to 27, 188 to 210, 354 to 376, and 401 to 423. Thus, they conclude that YvjB interacts with LsbB through its third transmembrane helix, because Tyr356 is located there.

Interestingly, in their work, Miljkovic et al. revealed that the domain that contains Glycine 188 does not seem to be an important factor for the activity. The location of this Gly is in a domain of YjvB whose structure we could not successfully predict. As such, the previous computational investigation of the LsbB-YvjB complex had necessarily been halted. However, with the emergence of the data of the Miljkovic et al., we were able to move further and design a model of LsbB interacting with a partial structure of YvjB, using protein prediction tools, molecular dynamics simulations and docking.

6.4. Methods

6.4.1. Topology recognition and structure protein prediction

For the structure prediction, we used the online version of the I-TASSER suite [191]. Moreover, for the topology recognition we extensively employed the PSSred subroutine included in the suite [191].

We started with the sequence of YvjB that can be found at Table 6-2, and we then used domains of the protein of different lengths as well as truncated sequences as described in the results section. We considered a structure prediction to be successful if their TM-Score, calculated by I-TASSER, was larger than 0.5. The TM-score was proposed by Zhang et al. in order to quantify the structural similarity between two structures, and it is used by I-TASSER as an indication of how similar the prediction would be to the solved structure of the protein, if that existed. A TM-score larger than 0.5 indicates a correct topology prediction, while TM<0.17 indicates that the protein prediction of the model is random.

6.4.2. Design of the Transmembrane YvjB$_T$ models

After we concluded that the best model was YvjB$_T$, we had to determine the orientation of the protein with respect to a membrane-mimicking model. For this we used the structure of the Site-2 Protease (pdbid:3b4r) - that has a 42% similarity with YvjB$_T$ - embedded in a bilayer, that was obtained by the MemProtMD server [192,193]. MemProtMD is an online server where one can find the structures of all the membrane proteins (solved experimentally so far) inserted in an explicit bilayer. The membrane-

protein complexes in the MemProtMD server have undergone coarse-grained and atomistic MD simulation to allow the protein structure to relax in the membrane environment.

It is important to note that the crystallization of mjS2P, which is a Zn metalloprotease of an archaea, revealed that two molecules of mjS2P associate and form an antiparallel homodimer [192]. However, it is not clear if this is the state in which the protein exists on the cell membrane, or if this is a pseudo-dimer that was created as a crystal-packing artifact. Biochemical studies of different intramembrane metalloproteases support the hypothesis that they form dimers [194]. Due to this uncertainty, we modelled structures of both a monomer and a dimer. In the case of the $YvjB_T$ monomer, we aligned it to the structure of the chain A of the mjS2P dimer.

We performed the 3D structure alignments of the $YvjB_T$ monomer and dimer to the mjS2P-bilayer, using the VMD software and the Multiseq plugin [115,195]. We moved the center of the mass of the bilayer (of the mjS2P-bilayer complex) to the center of the axis in order to retain the relevant placement of the $YvjB_T$ molecule to a bilayer.

We then inserted the aligned $YvjB_T$ model in a POPG and POPE lipid bilayer at a 3:1 ratio, using the CHARMM-Gui server [119]. In the case of the $YvjB_T$ monomer, the upper leaflet of the bilayer had a total of 140 lipids, while the bottom had 144, because $YvjB_T$ occupied more space close to the top bilayer. The bilayer is symmetrical and includes the $YvjB_T$ dimer, which had 180 lipid molecules on each leaflet. The $YvjB_T$-bilayer complexes were solvated and ionized using the VMD solvator and autoionize plugin [115]. The ion concentration of the systems was set to 0.15 M NaCl, and additional ions were introduced to electroneutralize the systems.

6.4.3. Design of the surface LsbB model

The structure of LsbB has previously been solved and deposited on the PDB database with accession id 2MLU [87]. In order to define the orientation of LsbB on the membrane, we used the PPM Server [196]. PPM predicts the position of a protein with respect to a membrane surface, taking into account possible hydrophobic, electrostatic, and hydrogen bond interactions, and implicitly representing the water-lipid environment. We aligned the output of the PPM server to a pre-equilibrated bilayer that contains POPG and POPE lipids at a 3:1 ratio and 120 lipids per leaflet (created by the CHARMM-Gui server), using the VMD software. Finally, we solvated and autoionized the

LsbB-bilayer system with a similar protocol to what was described above for the $YvjB_T$ models.

6.4.4. Molecular dynamics and docking

The atomistic molecular dynamics simulation was conducted with the NAMD 2.11 simulation engine [115] using the CHARMM 36 force field [142] under constant pressure and temperature (NPT ensemble). Each part of the simulation was carried out on the Stampede supercomputer through the XSEDE portal. The MD protocol is identical to the one we used for the simulation of the PlnEF transmembrane dimer in Chapter 5 (see paragraph 5.1.2). The only difference is that the simulation of the $YvjB_T$ monomer and dimer systems were run for 200 ns, while the LsbB simulation was run for 100ns

Finally, we performed a simple docking calculation using the HADDOCK server, which employs rigid-body energy minimization and a semi-flexible refinement in the torsion angle space. HADDOCK is experimentally knowledge-driven and requires the user to input the residues that might act as binding hotspots. Based on the previous experimental studies described in paragraph 0, we used W25 of LsbB and Y356 of YvjB (or Y146 of $YvjB_T$) as possible interaction surfaces.

6.5. Results and Discussion

We started our effort to investigate the interaction between a class II bacteriocin, LsbB, with its receptor, YvjB, by employing structure prediction methods. After numerous iterations, we were able to identify a detailed topology of YvjB and determine the structure of its N- and C-termini - the latter is proposed by experiments to be the region of interaction with LsbB.

We then inserted YvjB (which is a membrane-bound protein) in a model lipid bilayer and performed molecular dynamics (MD) simulations in order to allow the protein to relax in an environment closer to its natural state. For the same reason, we performed MD simulations of LsbB on a surface bilayer. Finally, we docked LsbB on YvjB to identify the best LsbB-YvjB complex. We hope this project will be continued in the future by other students who can better refine the LsbB-YvjB complex and study in detail the interaction between these two partners.

6.5.1. Topology and structure prediction of YvjB

Initially, we attempted to perform 3D structure prediction of the whole sequence of YvjB on the I-TASSER server. The TM-score of the best predicted model was 0.47±0.15, which indicates a successfully predicted topology. However, after visual inspection, we noticed that pieces of the structure had unnatural-looking folds, i.e. extended long coils connecting two well-defined regions. In order to avoid this problem, we proceeded to dismantle the sequence of YvjB into distinct structural sub-domains through a detailed secondary structure prediction with PSSred and by comparison with the current literature and available homologous structures in the PDB database. We then performed 3D structure prediction for each subdomain. The results are detailed in Table 6-3. We then combined this information into a suggested topology that is illustrated in Figure 6-1 which is significantly improved when compared to the one suggested by Miljkovic et al. [190].

Figure 6-1: Suggested topology of YvjB

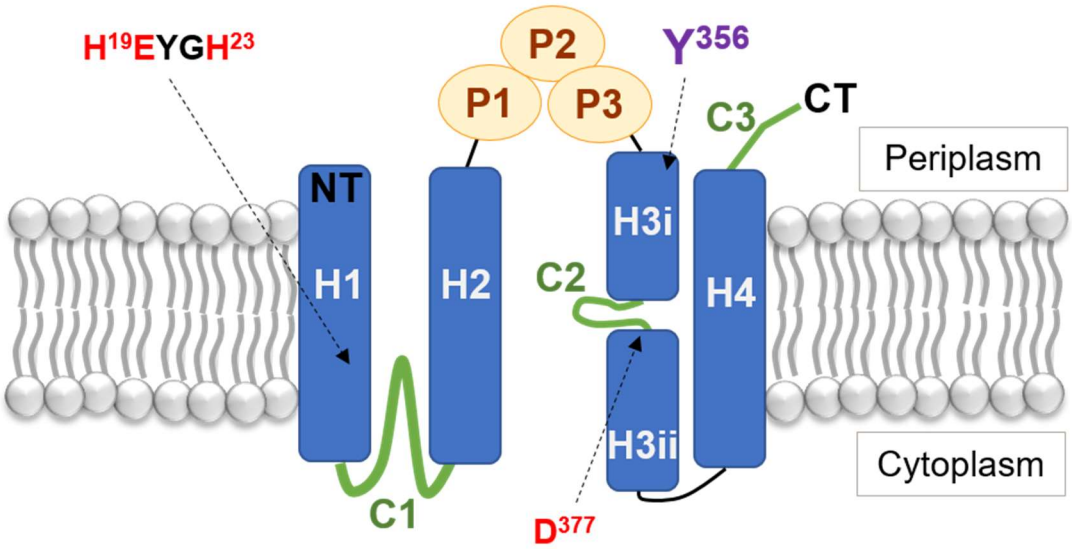

According to the domain analysis presented in **Table 6-3**, we create the topology of YvjB. The transmembrane helices are colored blue, while the intramembrane stretches are colored green and the PDZ domains are yellow. The location of the Zn binding residues is marked red. In purple, we point to the location of Y356 that was suggested to be the binding site of LsbB. NT and CT denote the N- and C- terminai, respectively

Table 6-3: Domain analysis of the Zn metallopeptidase YvjB

Sub-domains	*Res #*	*Sec. Structure*	*Conf.*	*Function*
Domain I: N-terminal TM domain				TM core of Zn metalloprotease
H1	1-30	TM helix (oi)	8-9	
C1	30-90	TM beta sheet and coil (i)	8-9	
H2	90-120	TM helix (io)	6-9	
Domain II: Possible extracellular PDZ domains				PDZ domains of intramembrane proteases
P1	120-220	beta sheet & helix (o)	2-5	
P2	220-280	beta sheet & helix (o)	9	
P3	290-350	unknown	0	
Domain III: C' terminal TM domain				TM core of Zn metalloprotease
H3i	350-370	TM helix (oi)	8-9	
C2	370-380	Coil (i)	8-9	
H3ii	380-390	TM helix (oi)	8-9	
H4	395-420	TM helix (io)	8-9	
C3	420-428	Coil (o)	5-8	

The names of the individual sub-domains are located in the first column, and the residues that they approximately include are in the second. The predicted secondary structure of each sub-domain can be found on column three. In parenthesis, we note the orientation of each segment: i=intramembrane, oi= starting from the periplasm (out of the cell) and ending at the cytoplasm (in the cell) while io denotes the opposite orientation. The confidence level of each prediction can be found in column four, and it ranges from 0 to 9. Finally, in the fifth column we suggested the possible function of each domain.

This analysis revealed that YvjB is an M50, Zinc Metallopeptidase. In general, peptidases (otherwise called proteinases or proteases) are enzymes that cleave the N-terminal domains of other proteins by hydrolyzing a peptide bond [194]. In the case of metalloproteases, the hydrolytic reaction is catalyzed by a metal (Zinc, in the majority of

cases). The domain I of YvjB is the characteristic N-terminal catalytic domain found in metalloproteases that contains the catalytic zinc-binding motif HExxH. Similarly to other Zn metalloproteases, this motif is found on a transmembrane helix (H1) that is followed by a hydrophobic stretch (C1) and a second transmembrane helix (H2). The orientation (whether the structural elements begin at the periplasmic or cytoplasmic side of the membrane) of these helices is conserved in all metalloproteases.

Domain II contains 3 subdomains that could possibly be classified as PDZs, which are extracellular parts of membrane enzymes that are abundant in all cells and serve as recognition domains [195]. Finally, domain III is the C-terminal conserved domain of Zn metallopeptidase, and it is comprised of H3i and H3ii, two transmembrane helical parts that are separated by an intramembrane coil region C2. This is followed by the last transmembrane helix H4, while the final few amino acids of the C-terminus are possibly located outside the membrane, in the periplasmatic space. In the HExxH motif found in H1, the two Histidine residues are ligands of the Zinc ion while the Glutamic acid activates a water molecule that is considered to be a third ligand. However, the Aspartic acid (D77) (located in the H3ii intramembrane helix) is also required as a fourth ligand.

Domains I and II have highly-conserved features of intramembrane proteases and their individual structure prediction was successful. The template that was used most for the prediction was the crystallized structure of another Zn metalloprotease, mjS2P, isolated from the archaea species, *Methanocaldococcus jannaschii* [192]. The similarity between domains I and II of YvjB and mjS2P is ~42%, while the identity is ~24%. MjS2P has one more N-terminal and one more C-terminal helices, while it contains no PDZ domains. Out of the three hypothesized PDZ subdomains, only the structure prediction of the second (P2) was successful, due to its high similarity to two available PDZ structures - one of them being isolated from another intramembrane protease RseP [195]. Additionally, the structure of P1 was predicted to an extent with the ab initio folding subroutine of I-Tasser, while similar calculation on the structure of P3 yielded no valuable results.

Since the structure of large pieces of YvjB could not be predicted, we decided to create numerous truncated protein sequences where subdomains of the YvjB were removed. In all cases, we needed to include domain III because it was concluded from experiments that domain III possibly interacts with LsbB, as described in paragraph 6.3.

$YvjB_T$, was the longer sequence that produced a successfully predicted structure (TM-score 0.56±0.15), and it includes only domains I and III (residues 1 to 213 and 334 to 423), which are the transmembrane core of YvjB. More of the last five residues of YvjB are missing in $YvjB_T$, because they were disturbing the structure prediction and they are not expected to contribute to the interaction with LsbB. The sequence of YvjBT can be found in Table 6-4 and its predicted 3D structure in Figure 6-2a.

Table 6-4: Amino acid sequence of the truncated protein, $YvjB_T$

1	MIETL ITFII IFGII VAIHE YGHLW WAKRS GILVR EYAVG MGPKI FAHQA
51	KDGTL YTIRI LPLGG YVRLA GWGDD KTEIK KGQAA SLVVS KSEVV NPEAE
101	NSVSN IVRRI NLSEH VELEE AIP^{123}G^{334}G PVAIY QLSGQ AARAG DKITG GFVQA
151	GQSAT AIFKA LGSLI ARPSL LFPAIV LLAM LSINL GIVNL FPIPV LDGGK
201	IVLNI IEAIR GKALS QEKES IITMV GVVFM LVLFV AVTWN DIL^{423}

With superscript, we note the residue number of amino acids at the cut sites

Figure 6-2: 3D structure of $YvjB_T$ and insertion in the membrane.

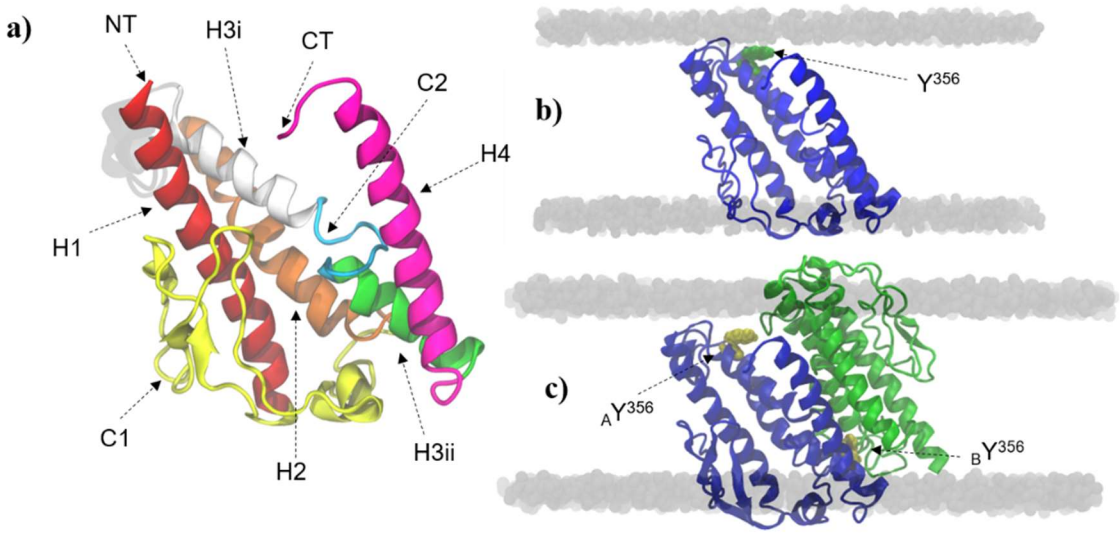

The 3D structure of YvjBT, as predicted by the I-TASSER server, is pictured with a cartoon representation in a. Each color indicates a different sub-domain: H1-red, C1-yellow, H2-orange, H3i-white, C2-cyan, H3ii-green, H4-pink, and the residues that linked H2 and H3i are transparent grey. In b, the transmembrane YvjBT monomer is shown in blue, while the antiparallel dimer is shown in c (monomer A is colored blue, while monomer B is colored green). The headgroup atoms of the lipids of the bilayer are shown as grey spheres. Tyrosine 356 is green in b and yellow in c, based on the VDW radii of its atoms.

We then inserted $YvjB_T$ in a model lipid bilayer as described in paragraph 6.4.2. Previous structural and biochemical studies suggested that Zn metalloproteases might be packed as antiparallel homodimers in the membrane. Therefore, we designed both a monomer and a dimer $YvjB_T$ transmembrane structure, Figure 6-2b and c respectively. Interestingly, in both models, Y356 is close to the membrane and as such it might be easily accessible to LsbB.

6.5.2. MD simulations and docking

In order to create a possible structure of the $YvjB_T$-LsbB complex, we first performed atomistic molecular dynamics simulation on each component (LsbB and $YvjB_T$) individually, with the intention to allow the molecules to relax in a membrane environment. We performed 200 ns of MD simulations of both the monomer and dimer YvjBT inserted in a lipid bilayer (Figure 6-3), while we performed only 100 ns of LsbB on the surface of a lipid bilayer (Figure 6-4).

Figure 6-3: Snapshot of the transmembrane $YvjB_T$ after 200 ns of MD simulations.

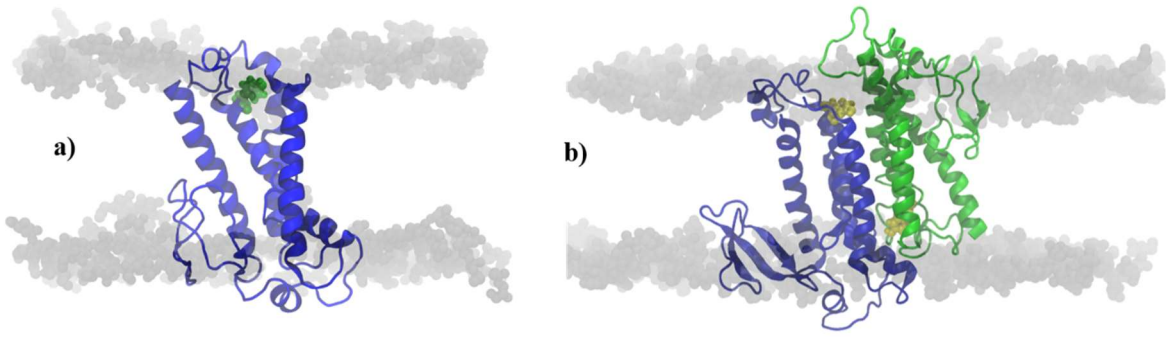

Final snapshots after 200 ns of atomistic MD simulation of the YvjBT monomer (a) and dimer (b). The monomer YvjBT is colored blue in a, while in b monomer A is colored blue and monomer B is green. The headgroup atoms of the lipids of the bilayer are shown as grey spheres. Tyrosine 356 (that is hypothesized to interact with the bacteriocin) is green in a and yellow in b, based on the VDW radii of its atoms.

The structure of both the monomer and dimer $YvjB_T$ did not diverge significantly from their initial structure. The backbone RMSD of the monomer was 0.65±0.07 nm, with most deviation being around the coil regions; the backbone RMSD of the helical regions was ~0.3 nm. However, visual inspection revealed that the relevant positon between the helices changed and, in fact, H3ii became almost perpendicular to the z-axis, which suggests that in future simulation, it might get expelled from the membrane.

In contrast, the structure of the dimer seems more stable - the whole dimer backbone RMSD was 0.48±0.09 nm, while the backbone RMSD of monomer A was 0.51±0.1 nm, and that of monomer B was 0.38±0.08 nm. The two monomers did not translocate in the membrane significantly, as they were anchored in the bilayer and they approached each other closely.

LsbB exhibited an α-helical structure through the whole 100 ns simulation. Interestingly, LsbB adopts a perpendicular orientation to the surface of the bilayer, even though it starts from a parallel one. Structural analysis of the trajectory revealed that there was a bend around G11 that did not disrupt the continuity of the α-helix. This may have happened because there is a cluster of cation-π interactions among Tryptophan 25, Tyrosine 23 and 11, and Phenylalanine 7. The backbone RMSD of LsbB was 0.35±0.12 nm.

Figure 6-4: MD simulation of LsbB on the surface of a bilayer.

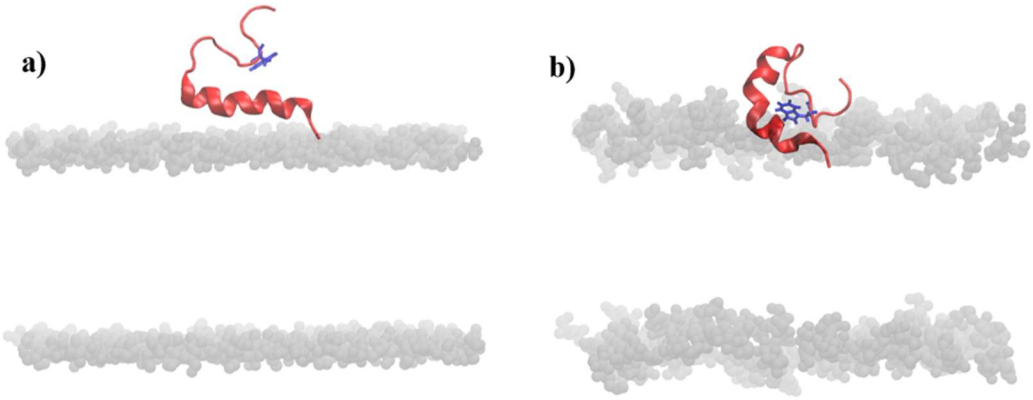

Initial (a) and final (b, after 100 ns) snapshots of the MD simulation of LsbB on the surface of a lipid bilayer. LsbB is colored red and is pictured in cartoon representation. W25 (believed to interact with the receptor) is shown in blue. The headgroup atoms of the lipids of the bilayer are shown as grey spheres.

Finally, we employed the HADDOCK server to dock LsbB to both the $YvjB_T$ monomer and dimer. As input structures, we used the final frame of the respective MD simulation. The possible binding sites, i.e. W25 of LsbB and Y356 of YvjB, were provided to the server so as to guide the docking calculations. The complexes that were produced are pictured in Figure 6-5. In both cases, LsbB penetrated the bilayer and was able to come in close proximity to the Tyrosine 356 of the receptor.

Figure 6-5: Suggested LsbB-YvjB$_T$ complex based on docking

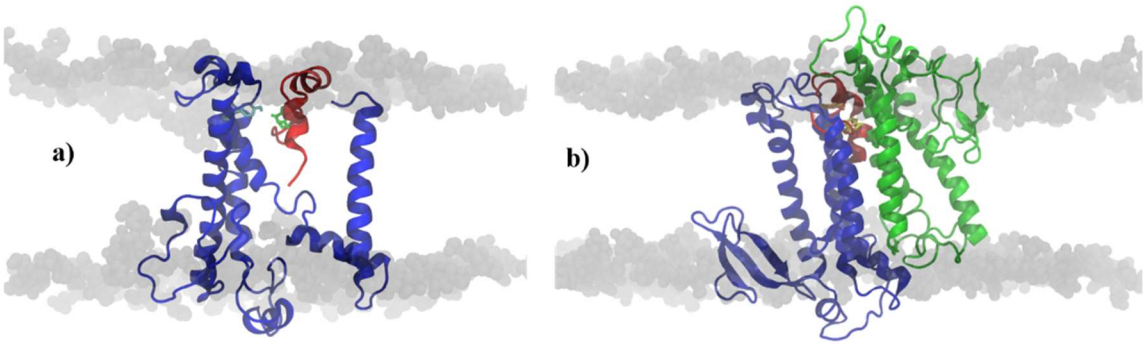

Docking results of LsbB on the YvjB$_T$ monomer (a) and dimer (b). LsbB is colored red. YvjB$_T$ in a and the YvjB$_T$-monomer A in b are colored blue, while the YvjB$_T$-monomer B in b is colored green. The hypothesized important residues for the interaction between LsbB (W25) and YvjB (Y356) are colored green in a and yellow in b. The headgroup atoms of the lipids of the bilayer are shown as grey spheres.

6.6. Conclusions and future directions

The bactericidal activity of some class II bacteriocins has been associated with the presence of specific proteins in the target cells. This, alongside the fact that most bacteriocins have high selectivity, leads to the hypothesis that class II bacteriocins could act through a receptor-mediated mechanism of action (MOA).

Even though there are experimental studies that describe to an extent the key elements of this MOA, its thorough examination is not possible. In this chapter, we attempted, for the first time, to design a class II bacteriocin-receptor complex and to propose that computational structure prediction and molecular simulations can be powerful tools in the endeavor of unravelling the MOA of class II bacteriocins.

We started by reviewing the current literature about the membrane-protein structure-prediction options and the available experimental data that suggest a relationship between class II bacteriocins and their receptors. We then evaluated which receptor-bacteriocin system might have the best potential for computational structure prediction. We concluded that the Zn metallopeptidase, YvjB, which is considered a hypothetical receptor for the class IId bacteriocin LsbB, was a good candidate to proceed with because it had decent initial prediction scores and a relatively smaller size, compared to similar systems. In addition, there is a significant amount of data indicating

the binding sites between the two interaction partners, YvjB and LsbB.

We first analyzed the sequence of YvjB in detail and broke it down into sub-domains. We identified the possible structure and function of each sub-domain, and thus we were able to propose a detailed topology for the protein that was different than what had been previously proposed. Then we truncated parts of YvjB for which we could not obtain a satisfactory 3D structure prediction and that we knew from previous studies are not required for the interaction with LsbB. We named the truncated protein $YvjB_T$.

Next, we introduced $YvjB_T$ in a model lipid bilayer based on the structure of S2P, a different metallopeptidase. Interestingly S2P is packed into antiparallel homodimers in its crystal structure, and it is unclear if this is the biological assembly of metallopeptidases or just an artifact of crystallization. We therefore concluded that we should examine both a $YvjB_T$ monomer and a dimer. We then performed atomistic molecular dynamics (MD) simulation of the system in order to allow YvjB to relax in the membrane environment. Similarly, we positioned LsbB, which has a structure that was previously solved experimentally, on the surface of a model bilayer and performed atomistic MD simulations. Finally, we obtained the ultimate structure of each system and subsequently fed them to a docking server that in turn produced possible structures of the $YvjB_T$-LsbB complex. In both the monomer and dimer cases, LsbB approaches $YvjB_T$ around the suggested interaction surfaces.

Creating a bacteriocin-receptor complex structure was a significant first step in elucidating the mechanism of action of these interesting antimicrobial peptides. Nevertheless, there is a lot more that can be investigated in the future. To begin with, it would be of great interest to investigate in greater detail which of the YvjB monomer or dimer is more stable, and what exactly is the function of this protein. Then an extended atomistic MD simulation of the LsbB-$YvjB_T$ complex could verify if these two proteins do, in fact, interact and if so, which residues are important for this interaction. A study similar to the one conducted in Chapter 3 (where we compare the biophysical image of different systems with known experimental activity) could provide a better understanding of the structure-activity relationship of LsbB and its interaction with YvjB. Moreover, experimental mutation on residues that are deemed important through our model could exam the accuracy of our prediction. Lastly, the structure of the receptor could further improve with more detailed structure prediction and a more thorough docking protocol.

Chapter 7

Summary and concluding remarks

The discovery of antibiotics in the mid-20th century revolutionized modern medicine, improved our quality of life, and increased longevity. However, bacteria would soon fight back and develop resistance. Different government issued reports warn that we are quickly approaching a “post-antibiotic era”, where even minor bacterial infections could be deadly. As the number of cases of antibiotic resistance is increasing, the effective utilization of conventional antibiotics is rapidly decreasing. Therefore, there is an urgent need to identify and take advantage of sources of new antibiotic drugs.

Antimicrobial peptides (AMPs) are a promising alternative to conventional antibiotics, and they may provide a solution to the emerging problem of antibiotic resistant infections. Class II bacteriocins are bacteria-produced AMPs that do not contain post-translational modifications. These bacteriocins show great potential as novel antibiotic agents because they are active against different microorganisms with high specificity and they are amenable to bioengineering.

Two decades ago, researchers entered a race to understand and optimize the bactericidal activity of bacteriocins in general. However, before the full potential of bacteriocins can be unlocked, it is imperative that we gain a detailed understanding of their mechanism of action (MOA). The great potential for future use of bacteriocins motivated us to explore the mechanism of action of class II bacteriocins through atomistic molecular dynamics simulations.

Information is limited regarding the mechanism(s) by which class II bacteriocins kill their target. It has been shown that their bactericidal activity is associated with ion or solute efflux, which ultimately leads to the death of the target organism. Our primary goal in this work was to investigate the interaction of class II bacteriocins with model membranes and determine the likelihood of pore formation that leads to an ion efflux. However, due to their narrow target spectrum, it has also been suggested that class II bacteriocins might act instead through a receptor-mediated MOA. It became apparent that it would be impossible to build a complete and accurate picture of the MOA of class II bacteriocins without having a detailed understanding of the bacteriocin-receptor

complex – specifically, without possessing an accurate, 3-Dimensional structure of a receptor. In response to missing that piece of the puzzle, and with the goal of coming to a more holistic conclusion, we continued our research by examining the hypothesized class II bacteriocin receptors.

We began by exploring the mechanism of action of Plantaricin EF (or PlnEF). PlnEF is a class IIb, two-peptide bacteriocin comprised of peptides Plantaricin E (PlnE) and Plantaricin F (PlnF). As is the case with other class IIb bacteriocins, the two peptides are hypothesized to former a dimer. Previous experiments have demonstrated that PlnE and PlnF are unstructured in water, while they form α-helical structures in membrane-mimicking environments, such as DPC micelles. We performed atomistic MD simulations of PlnE and PlnF both in water and in a DPC micelle environment. We observed that in water, each individual peptide had significant loss of structure only when interacting with the complimentary peptide, which seemingly indicates that more than 85 ns are required to reproduce the unfolding dynamics of these peptides. We observed that the two peptides interacted with each other through amino acids in their middle sections. These simulations provided a first insight of the regions of the peptides that interact with a membrane, and suggested that the amphiphilic nature of these peptides would probably not allow them to get inserted individually in a membrane.

Although bacteriocins are hypothesized to act through a receptor-mediated MOA, there is speculation that an initial, unspecified interaction with the target membrane takes place that is facilitated by electrostatic interactions. To test this theory, we simulated PlnEF on the surface of a model lipid bilayer. The relevant orientation of the two peptides on the surface of the membrane is unclear, so we examined both a parallel and an antiparallel surface dimer. The simulations revealed that the peptides associated with each other through their middle section in both models, while they interacted with the membrane through their terminal residues. Interestingly, we observed that in the parallel model there are stronger peptide-peptide interactions than there were in the antiparallel model. Such interactions are prerequisite for a bacteriocin's antimicrobial activity. Therefore, we concluded that a parallel orientation is more probable for the two peptides when they are on the surface of a membrane. To connect the atomistic behavior of PlnEF to its experimentally-observed activity, we performed a series of MD simulation of PlnEF mutants of known activity. There was an apparent tendency for

decreasing peptide-membrane interactions in systems of higher activity, in favor of interactions between the peptides. This seems to suggest that a parallel dimer model is not associated with insertion in the membrane.

New experiments indicated that PlnEF forms an antiparallel transmembrane dimer, and that the two peptides that comprise PlnEF associate through a GxxxG motif (a common motif found in abundance in the sequence of transmembrane proteins), located at the C-terminal of PlnF and N-terminal of PlnE. Using these conclusions, we were able to design a transmembrane dimer of PlnEF and position it successfully inside a model lipid bilayer. We subsequently performed MD simulation on this system. That simulation revealed that in addition to the GxxxG motif, the peptides' association can be attributed to a polar "clamp" of interactions between the middle sections of the peptides, and to cation-π interactions that also anchor the dimer in the membrane.

We furthered the analysis of the transmembrane PlnEF dimer through a 1μs long atomistic MD simulation. We observed that the cation-π and polar interactions not only assist the peptide-peptide interaction, but also create a network of polar attractors that lures water molecules, ions, and lipid headgroups in the otherwise hydrophobic membrane core. This leads to the formation of a toroidal pore, which is comparable to pores created by other AMPs that exhibit broader activity. This is the first time that it has been demonstrated that a class II bacteriocin can form a pore independent of a receptor.

It could be hypothesized that PlnEF (and by extension other class II bacteriocins) has a dual MOA: it forms pores on a membrane, irrepressibly increasing the permeation by water and ions, while it also interacts with a receptor, hindering some vital function for the cell. This would explain why in many cases, bacteriocins are highly active against some microorganisms (that possibly have a receptor), while much higher concentrations of the bacteriocin are required to kill different microorganisms (where only the poration MOA is effective). Alternatively, the receptor could act as a trojan horse, enabling the insertion of the class II bacteriocin in the membrane, which can then form pores. Yet another possible scenario is that the receptor enables the enlargement of the dimer-formed pore or the oligomerization of several dimers, which in turn might increase the permeability of solutes, leading to the cell death.

In order to evaluate these hypotheses, knowledge of the receptor, or ideally the receptor-bacteriocin complex structure, is required. Lacking this foundation of

information, we used protein structure prediction methods to design the topology and predict the partial 3D structure of YvjB (a Zn, metallopeptidase), which has been identified as a possible receptor to LsbB (a class IId bacteriocin). We then employed atomistic MD simulation and docking calculation to create a receptor-bacteriocin complex. In the future, this complex can be studied to elucidate the role that a receptor plays in the MOA of class II bacteriocins. Ideally, we would have studied the receptor of PlnEF or another class IIb bacteriocin, however, in the former case no receptor has yet been identified, and in the latter, the structure of receptors of other class IIb bacteriocins could not be successfully predicted.

In conclusion, we set out with this work to employ different computational methods, with the goal of shedding light into the mechanism of action of class II bacteriocins. We believe that the insights provided by our research may enable the optimization of bacteriocin-based antibiotic drugs that will exhibit potent activity against specific pathogens. Such drugs will indisputably attract the interest of the pharmaceutical industry, ultimately leading to commercial bacteriocin-based applications that will go on to assist in the fight against antimicrobial resistance.

References

[1] C. a Arias, B.E. Murray, The rise of the Enterococcus: beyond vancomycin resistance., Nat. Rev. Microbiol. 10 (2012) 266–78.

[2] C.L. Ventola, The antibiotic resistance crisis: part 1: causes and threats., P T. 40 (2015) 277–83.

[3] M.F. Anjum, N.A. Duggett, M. AbuOun, L. Randall, J. Nunez-Garcia, R.J. Ellis, et al., Colistin resistance in Salmonella and Escherichia coli isolates from a pig farm in Great Britain, J. Antimicrob. Chemother. 71 (2016) 2306–2313.

[4] Y. Wang, G.-B. Tian, R. Zhang, Y. Shen, J.M. Tyrrell, X. Huang, et al., Prevalence, risk factors, outcomes, and molecular epidemiology of mcr-1-positive Enterobacteriaceae in patients and healthy adults from China: an epidemiological and clinical study, Lancet Infect. Dis. (2017).

[5] Antimicrobial Resistance: Tackling a Crisis for the Future Health and Wealth of Nations, in: Rev. Antimicrob. Resist. Chaired by Jim O'Neill, 2014.

[6] CDC, Antibiotic resistance threats, (2013).

[7] WHO, Antimicrobial resistance: global report on surveillance 2014, (n.d.).

[8] S. Reardon, WHO warns against "post-antibiotic" era, Nature. (2014).

[9] S. Hernando-Amado, F. Sanz-García, P. Blanco, J.L. Martínez, Fitness costs associated with the acquisition of antibiotic resistance, Essays Biochem. 61 (2017) 37–48.

[10] S. Baker, A return to the pre-antimicrobial era?, Science (80-.). 347 (2015) 1064–1066.

[11] T.J. Centner, Recent government regulations in the United States seek to ensure the effectiveness of antibiotics by limiting their agricultural use, Environ. Int. 94 (2016) 1–7.

[12] M.K. Chattopadhyay, Use of antibiotics as feed additives: a burning question., Front. Microbiol. 5 (2014) 334.

[13] T.F. Landers, B. Cohen, T.E. Wittum, E.L. Larson, A review of antibiotic use in food animals: perspective, policy, and potential., Public Health Rep. 127 (2012) 4–22.

[14] T. Hiltunen, M. Virta, A.-L. Laine, Antibiotic resistance in the wild: an eco-evolutionary perspective, Philos. Trans. R. Soc. B Biol. Sci. 372 (2017) 20160039.

[15] P. Courvalin, Why is antibiotic resistance a deadly emerging disease?, Clin. Microbiol. Infect. 22 (2016) 405–407.

[16] D.I. Andersson, D. Hughes, Antibiotic resistance and its cost: is it possible to reverse resistance?, Nat. Rev. Microbiol. 8 (2010) 260–71.

[17] A.P. Health, C. Brews, Bad Bugs , No Drugs About IDSA, (2004).

[18] J.G. Bartlett, D.N. Gilbert, B. Spellberg, Seven Ways to Preserve the Miracle of Antibiotics, Clin. Infect. Dis. 56 (2013) 1445–1450.

[19] M. Perros, A sustainable model for antibiotics, Science (80-.). 347 (2015) 1062–1064.

[20] J. Li, J.-J. Koh, S. Liu, R. Lakshminarayanan, C.S. Verma, R.W. Beuerman, Membrane Active Antimicrobial Peptides: Translating Mechanistic Insights to Design., Front. Neurosci. 11 (2017) 73.

[21] D.H. Lloyd, Alternatives to conventional antimicrobial drugs: a review of future prospects.,

Vet. Dermatol. 23 (2012) 299–304, e59-60.

[22] G. Wang, X. Li, Z. Wang, APD3: the antimicrobial peptide database as a tool for research and education, Nucleic Acids Res. 44 (2016) D1087–D1093.

[23] H. Jenssen, P. Hamill, R.E.W. Hancock, Peptide antimicrobial agents., Clin. Microbiol. Rev. 19 (2006) 491–511.

[24] Z. Wang, G. Wang, APD: the Antimicrobial Peptide Database, Nucleic Acids Res. 32 (2004) 590D–592.

[25] J. Nissen-Meyer, I.F. Nes, Ribosomally synthesized antimicrobial peptides: their function, structure, biogenesis, and mechanism of action, Arch. Microbiol. 167 (1997).

[26] M. Masuda, H. Nakashima, T. Ueda, H. Naba, R. Ikoma, A. Otaka, et al., A novel anti-HIV synthetic peptide, T-22 ([Tyr5,12,Lys7]-polyphemusin II)., Biochem. Biophys. Res. Commun. 189 (1992) 845–50.

[27] J. Wiesner, A. Vilcinskas, Antimicrobial peptides: The ancient arm of the human immune system, Virulence. 1 (2010) 440–464.

[28] A.M. McDermott, Defensins and other antimicrobial peptides at the ocular surface., Ocul. Surf. 2 (2004) 229–47.

[29] Y. Ge, D.L. MacDonald, K.J. Holroyd, C. Thornsberry, H. Wexler, M. Zasloff, In vitro antibacterial properties of pexiganan, an analog of magainin., Antimicrob. Agents Chemother. 43 (1999) 782–8.

[30] S.A. Baltzer, M.H. Brown, Antimicrobial Peptides – Promising Alternatives to Conventional Antibiotics, J Mol Microbiol Biotechnol. 20 (2011) 228–235.

[31] J.L. Fox, Antimicrobial peptides stage a comeback, Nat. Biotechnol. 31 (2013) 379–382.

[32] J.L. Fox, Rare-disease drugs boosted by new Prescription Drug User Fee Act, Nat. Biotechnol. 30 (2012) 733–734.

[33] D.I. Andersson, D. Hughes, J.Z. Kubicek-Sutherland, Mechanisms and consequences of bacterial resistance to antimicrobial peptides, Drug Resist. Updat. 26 (2016) 43–57.

[34] F. Guilhelmelli, N. Vilela, P. Albuquerque, L. da S. Derengowski, I. Silva-Pereira, C.M. Kyaw, Antibiotic development challenges: the various mechanisms of action of antimicrobial peptides and of bacterial resistance., Front. Microbiol. 4 (2013) 353.

[35] F. Porcelli, A. Ramamoorthy, G. Barany, G. Veglia, Membrane Proteins, 1063 (2013).

[36] D. Bolintineanu, E. Hazrati, H.T. Davis, R.I. Lehrer, Y.N. Kaznessis, Antimicrobial mechanism of pore-forming protegrin peptides: 100 pores to kill E. coli, Peptides. 31 (2010) 1–8.

[37] H.H. Hauge, D. Mantzilas, V.G. Eijsink, J. Nissen-Meyer, Membrane-mimicking entities induce structuring of the two-peptide bacteriocins plantaricin E/F and plantaricin J/K., J. Bacteriol. 181 (1999) 740–7.

[38] N. Sitaram, R. Nagaraj, Interaction of antimicrobial peptides with biological and model membranes: structural and charge requirements for activity., Biochim. Biophys. Acta. 1462 (1999) 29–54.

[39] G. Uzelac, M. Kojic, J. Lozo, T. Aleksandrzak-Piekarczyk, C. Gabrielsen, T. Kristensen, et al., A Zn-dependent metallopeptidase is responsible for sensitivity to LsbB, a class II leaderless bacteriocin of Lactococcus lactis subsp. lactis BGMN1-5., J. Bacteriol. 195 (2013) 5614–5621.

[40] M. Kjos, I.F. Nes, D.B. Diep, Mechanisms of resistance to bacteriocins targeting the

mannose phosphotransferase system., Appl. Environ. Microbiol. 77 (2011) 3335–42.

[41] R.E.W. Hancock, A. Rozek, Role of membranes in the activities of antimicrobial cationic peptides., FEMS Microbiol. Lett. 206 (2002) 143–9.

[42] Y. Héchard, H.-G. Sahl, Mode of action of modified and unmodified bacteriocins from Gram-positive bacteria, Biochimie. 84 (2002) 545–557.

[43] S. Duquesne, D. Destoumieux-Garzón, J. Peduzzi, S. Rebuffat, Microcins, gene-encoded antibacterial peptides from enterobacteria, Nat. Prod. Rep. 24 (2007) 708.

[44] M.A.R.B. Castanho, M.X. Fernandes, Lipid membrane-induced optimization for ligand-receptor docking: recent tools and insights for the “membrane catalysis” model., Eur. Biophys. J. 35 (2006) 92–103.

[45] A.T.R. Mattick, A. Hirsch, N.J. Berridge, Further observations on inhibitory substance (nisin) from lactic streptococci, Lancet. 250 (1947) 5–8.

[46] E.M. Balciunas, F.A. Castillo Martinez, S.D. Todorov, B.D.G.D.M. Franco, A. Converti, R.P.D.S. Oliveira, Novel biotechnological applications of bacteriocins: A review, Food Control. 32 (2013) 134–142.

[47] R. Kemperman, A. Kuipers, H. Karsens, A. Nauta, O. Kuipers, J. Kok, Identification and characterization of two novel clostridial bacteriocins, circularin A and closticin 574., Appl. Environ. Microbiol. 69 (2003) 1589–97.

[48] R.H. Perez, T. Zendo, K. Sonomoto, Novel bacteriocins from lactic acid bacteria (LAB): various structures and applications, Microb. Cell Fact. 13 (2014) S3.

[49] H.B. HAWLEY, THE DEVELOPMENT AND USE OF NISIN, J. Appl. Bacteriol. 18 (1955) 388–395.

[50] Http://oralpeace.wixsite.com/lang-en, ORALPEACE,

[51] J.W. Hegarty, C.M. Guinane, R.P. Ross, C. Hill, P.D. Cotter, Bacteriocin production: a relatively unharnessed probiotic trait?, F1000Research. 5 (2016) 2587.

[52] G. Vukotic, N. Mirkovic, B. Jovcic, M. Miljkovic, I. Strahinic, D. Fira, et al., Proteinase PrtP impairs lactococcin LcnB activity in Lactococcus lactis BGMN1-501: New insights into bacteriocin regulation, Front. Microbiol. 6 (2015) 92.

[53] P.D. Cotter, R.P. Ross, C. Hill, Bacteriocins - a viable alternative to antibiotics?, Nat. Rev. Microbiol. 11 (2013) 95–105.

[54] A. Gálvez, H. Abriouel, R.L. López, N. Ben Omar, Bacteriocin-based strategies for food biopreservation, Int. J. Food Microbiol. 120 (2007) 51–70.

[55] S. Kaur, S. Kaur, Bacteriocins as Potential Anticancer Agents., Front. Pharmacol. 6 (2015) 272.

[56] J. Borrero, Y. Chen, G.M. Dunny, Y.N. Kaznessis, Modified lactic acid bacteria detect and inhibit multiresistant enterococci., ACS Synth. Biol. 4 (2015) 299–306.

[57] K. Geldart, J. Borrero, Y.N. Kaznessis, Chloride-inducible expression vector for delivery of antimicrobial peptides targeting antibiotic-resistant Enterococcus faecium, Appl. Environ. Microbiol. 81 (2015) 3889–3897.

[58] B. Forkus, S. Ritter, M. Vlysidis, K. Geldart, Y.N. Kaznessis, Antimicrobial Probiotics Reduce Salmonella enterica in Turkey Gastrointestinal Tracts, Sci. Rep. 7 (2017) 40695.

[59] M.C. Rea, R.P. Ross, P.D. Cotter, C. Hill, Classification of Bacteriocins from Gram-Positive Bacteria, in: Prokaryotic Antimicrob. Pept., Springer New York, New York, NY, 2011: pp. 29–53.

[60] N.C.K. Heng, P.A. Wescombe, J.P. Burton, R.W. Jack, J.R. Tagg, The Diversity of Bacteriocins in Gram-Positive Bacteria, in: Bacteriocins, Springer Berlin Heidelberg, Berlin, Heidelberg, 2007: pp. 45–92.

[61] A.C.-Y. Lai, S. Tran, R.S. Simmonds, Functional characterization of domains found within a lytic enzyme produced by Streptococcus equi subsp. zooepidemicus., FEMS Microbiol. Lett. 215 (2002) 133–8.

[62] Y. Belguesmia, K. Naghmouchi, N.-E. Chihib, D. Drider, Class IIa Bacteriocins: Current Knowledge and Perspectives, in: Prokaryotic Antimicrob. Pept., Springer New York, New York, NY, 2011: pp. 171–195.

[63] M. Kjos, J. Borrero, M. Opsata, D.J. Birri, H. Holo, L.M. Cintas, et al., Target recognition, resistance, immunity and genome mining of class II bacteriocins from Gram-positive bacteria, Microbiology. 157 (2011) 3256–3267.

[64] G. Fimland, L. Johnsen, B. Dalhus, J. Nissen-Meyer, Pediocin-like antimicrobial peptides (class IIa bacteriocins) and their immunity proteins: biosynthesis, structure, and mode of action., J. Pept. Sci. 11 (2005) 688–96.

[65] C. Richard, R. Cañon, K. Naghmouchi, D. Bertrand, H. Prévost, D. Drider, Evidence on correlation between number of disulfide bridge and toxicity of class IIa bacteriocins, Food Microbiol. 23 (2006) 175–183.

[66] P.C. A, H.S. Haugen, G. Fimland, J. Nissen-meyer, P.E. Kristiansen, Three-Dimensional Structure in Lipid Micelles of the Pediocin-like Antimicrobial, (2005) 16149–16157.

[67] K. Kaur, L.C. Andrew, D.S. Wishart, J.C. Vederas, § Kamaljit Kaur, ‖ Lena C. Andrew, et al., Dynamic relationships among type IIa bacteriocins: temperature effects on antimicrobial activity and on structure of the C-terminal amphipathic alpha helix as a receptor-binding region., Biochemistry. 43 (2004) 9009–20.

[68] D.B. Diep, M. Skaugen, Z. Salehian, H. Holo, I.F. Nes, Common mechanisms of target cell recognition and immunity for class II bacteriocins., Proc. Natl. Acad. Sci. U. S. A. 104 (2007) 2384–9.

[69] C. Oppegård, G. Fimland, L. Thorbaek, J. Nissen-Meyer, Analysis of the two-peptide bacteriocins lactococcin G and enterocin 1071 by site-directed mutagenesis., Appl. Environ. Microbiol. 73 (2007) 2931–8.

[70] J. Nissen-Meyer, C. Oppegård, P. Rogne, H.S. Haugen, P.E. Kristiansen, The Two-Peptide (Class-IIb) Bacteriocins: Genetics, Biosynthesis, Structure, and Mode of Action, in: Prokaryotic Antimicrob. Pept., Springer New York, New York, NY, 2011: pp. 197–212.

[71] J. Nissen-Meyer, C. Oppegård, P. Rogne, H.S. Haugen, P.E. Kristiansen, Structure and Mode-of-Action of the Two-Peptide (Class-IIb) Bacteriocins., Probiotics Antimicrob. Proteins. 2 (2010) 52–60.

[72] C.T. Lohans, K.M. Towle, M. Miskolzie, R.T. McKay, M.J. van Belkum, L.M. McMullen, et al., Solution structures of the linear leaderless bacteriocins enterocin 7A and 7B resemble carnocyclin A, a circular antimicrobial peptide., Biochemistry. 52 (2013) 3987–94.

[73] G.N. Moll, E. Van Den Akker, H.H. Hauge, I.F. Nes, W.N. Konings, J. Arnold, et al., Complementary and Overlapping Selectivity of the Two-Peptide Bacteriocins Plantaricin EF and JK Complementary and Overlapping Selectivity of the Two-Peptide Bacteriocins Plantaricin EF and JK, (1999) 1–6.

[74] P. Rogne, P.E. Kristiansen, J. Nissen-meyer, Structure analysis of the two-peptide bacteriocin lactococcin G by introducing D -amino acid residues, (2010) 1883–1889.

[75] C. Oppegård, J. Schmidt, P.E. Kristiansen, J. Nissen-Meyer, Mutational analysis of

putative helix-helix interacting GxxxG-motifs and tryptophan residues in the two-peptide bacteriocin lactococcin G., Biochemistry. 47 (2008) 5242–9.

[76] R.F.S. Walters, W.F. DeGrado, Helix-packing motifs in membrane proteins., Proc. Natl. Acad. Sci. U. S. A. 103 (2006) 13658–63.

[77] A. Senes, M. Gerstein, D.M. Engelman, Statistical analysis of amino acid patterns in transmembrane helices: the GxxxG motif occurs frequently and in association with β-branched residues at neighboring positions, J. Mol. Biol. 296 (2000) 921–936.

[78] M. Kjos, C. Oppegård, D.B. Diep, I.F. Nes, J.-W. Veening, J. Nissen-Meyer, et al., Sensitivity to the two-peptide bacteriocin lactococcin G is dependent on UppP, an enzyme involved in cell-wall synthesis., Mol. Microbiol. (2014).

[79] C. Oppegård, M. Kjos, J.-W. Veening, J. Nissen-Meyer, T. Kristensen, A putative amino acid transporter determines sensitivity to the two-peptide bacteriocin plantaricin JK, Microbiologyopen. 5 (2016) 700–708.

[80] W.P. Russ, D.M. Engelman, The GxxxG motif: A framework for transmembrane helix-helix association, J. Mol. Biol. 296 (2000) 911–919.

[81] L.A. Martin-Visscher, M.J. van Belkum, J.C. Vederas, Class IIc or Circular Bacteriocins, in: Prokaryotic Antimicrob. Pept., Springer New York, New York, NY, 2011: pp. 213–236.

[82] I.F. Nes, D.A. Brede, D.B. Diep, Class II Non-Lantibiotic Bacteriocins, Second Edi, Elsevier Inc., 2013.

[83] M. Sánchez-Hidalgo, M. Montalbán-López, R. Cebrián, E. Valdivia, M. Martínez-Bueno, M. Maqueda, AS-48 bacteriocin: close to perfection, Cell. Mol. Life Sci. 68 (2011) 2845–2857.

[84] S. Iwatani, T. Zendo, K. Sonomoto, Class IId or Linear and Non-Pediocin-Like Bacteriocins, in: Prokaryotic Antimicrob. Pept., Springer New York, New York, NY, 2011: pp. 237–252.

[85] O. Gajic, G. Buist, M. Kojic, L. Topisirovic, O.P. Kuipers, J. Kok, Novel Mechanism of Bacteriocin Secretion and Immunity Carried Out by Lactococcal Multidrug Resistance Proteins, J. Biol. Chem. 278 (2003) 34291–34298.

[86] F. Yoneyama, Y. Imura, K. Ohno, T. Zendo, J. Nakayama, K. Matsuzaki, et al., Peptide-lipid huge toroidal pore, a new antimicrobial mechanism mediated by a lactococcal bacteriocin, lacticin Q., Antimicrob. Agents Chemother. 53 (2009) 3211–7.

[87] K. V. Ovchinnikov, P.E. Kristiansen, G. Uzelac, L. Topisirovic, M. Kojic, J. Nissen-Meyer, et al., Defining the structure and receptor binding domain of the leaderless bacteriocin LsbB, J. Biol. Chem. 289 (2014) 23838–23845.

[88] D.W. Borhani, D.E. Shaw, The future of molecular dynamics simulations in drug discovery., J. Comput. Aided. Mol. Des. 26 (2012) 15–26.

[89] M.P. Allen, D.J. Tildesley, Computer Simulation of Liquids, Oxford University Press, USA, 1989.

[90] P.J. Bond, S. Khalid, Antimicrobial and cell-penetrating peptides: structure, assembly and mechanisms of membrane lysis via atomistic and coarse-grained molecular dynamics simulations., Protein Pept. Lett. 17 (2010) 1313–27.

[91] C.-W. Tsai, N.-Y. Hsu, C.-H. Wang, C.-Y. Lu, Y. Chang, H.-H.G. Tsai, et al., Coupling Molecular Dynamics Simulations with Experiments for the Rational Design of Indolicidin-Analogous Antimicrobial Peptides, J. Mol. Biol. 392 (2009) 837–854.

[92] D.P. Tieleman, M.S.P. Sansom, Molecular dynamics simulations of antimicrobial peptides:

From membrane binding to trans-membrane channels, Int. J. Quantum Chem. 83 (2001) 166–179.

[93] A. Langham, Y.N. Kaznessis, Molecular Simulations of Antimicrobial Peptides, in: Methods Mol. Biol., 2010: pp. 267–285.

[94] A. Prince, P. Sandhu, P. Kumar, E. Dash, S. Sharma, M. Arakha, et al., Lipid-II Independent Antimicrobial Mechanism of Nisin Depends On Its Crowding And Degree Of Oligomerization., Sci. Rep. 6 (2016) 37908.

[95] A. Chugunov, D. Pyrkova, D. Nolde, A. Polyansky, V. Pentkovsky, R. Efremov, Lipid-II forms potential “landing terrain” for lantibiotics in simulated bacterial membrane, Sci. Rep. 3 (2013) 749–56.

[96] S. Mulholland, E.R. Turpin, B.B. Bonev, J.D. Hirst, Docking and molecular dynamics simulations of the ternary complex nisin2:lipid II., Sci. Rep. 6 (2016) 21185.

[97] S.-T.D. Hsu, E. Breukink, E. Tischenko, M.A.G. Lutters, B. de Kruijff, R. Kaptein, et al., The nisin-lipid II complex reveals a pyrophosphate cage that provides a blueprint for novel antibiotics., Nat. Struct. Mol. Biol. 11 (2004) 963–7.

[98] § Kamaljit Kaur, ‖ Lena C. Andrew, ‖ and David S. Wishart, § John C. Vederas*, Dynamic Relationships among Type IIa Bacteriocins: Temperature Effects on Antimicrobial Activity and on Structure of the C-Terminal Amphipathic α Helix as a Receptor-Binding Region‡, (2004).

[99] W. Soliman, S. Bhattacharjee, K. Kaur, Molecular dynamics simulation study of interaction between a class IIa bacteriocin and its immunity protein, Biochim. Biophys. Acta - Proteins Proteomics. 1774 (2007) 1002–1013.

[100] W. Soliman, L. Wang, S. Bhattacharjee, K. Kaur, Structure-activity relationships of an antimicrobial peptide plantaricin s from two-peptide class IIb bacteriocins, J. Med. Chem. 54 (2011) 2399–2408.

[101] G.C.A. da Hora, N.L. Archilha, J.L.S. Lopes, D.M. Müller, K. Coutinho, R. Itri, et al., Membrane negative curvature induced by a hybrid peptide from pediocin PA-1 and plantaricin 149 as revealed by atomistic molecular dynamics simulations, Soft Matter. 12 (2016) 8884–8898.

[102] P.K. Kyriakou, B. Ekblad, P.E. Kristiansen, Y.N. Kaznessis, Interactions of a class IIb bacteriocin with a model lipid bilayer, investigated through molecular dynamics simulations., Biochim. Biophys. Acta - Biomembr. 1858 (2016) 824–35.

[103] B. Ekblad, P.K. Kyriakou, C. Oppegård, J. Nissen-Meyer, Y.N. Kaznessis, E. Kristiansen, et al., Structure–Function Analysis of the Two-Peptide Bacteriocin Plantaricin EF, Biochemistry. 55 (2016) 5106–5116.

[104] E.L. Anderssen, D.B. Diep, I.F. Nes, V.G. Eijsink, J. Nissen-Meyer, Antagonistic activity of Lactobacillus plantarum C11: two new two-peptide bacteriocins, plantaricins EF and JK, and the induction factor plantaricin A., Appl. Environ. Microbiol. 64 (1998) 2269–72.

[105] A.Z. Mustopa, Kusdianawati, Fatimah, R.N. Umami, Budiarto, H. Danuri, Cloning and expression of plantaricin E and F genes of Lactobacillus Plantarum S34 isolated from Indonesia traditional-fermented meat, Int. Food Res. J. 23 (2016) 762–769.

[106] N. Ben Omar, H. Abriouel, R. Lucas, M. Martínez-Cañamero, J.-P. Guyot, A. Gálvez, Isolation of bacteriocinogenic Lactobacillus plantarum strains from ben saalga, a traditional fermented gruel from Burkina Faso, Int. J. Food Microbiol. 112 (2006) 44–50.

[107] M.A. Daeschel, M.C. Mckenney, L.C. Mcdonald, Bacteriocidal activity ofLactobacillus plantarum C-11, Food Microbiol. 7(2) (1990) 91–98.

[108] G. Pal, S. Srivastava, Inhibitory effect of plantaricin peptides (Pln E/F and J/K) against Escherichia coli, World J. Microbiol. Biotechnol. 30 (2014) 2829–2837.

[109] V. Nallala, V. Sadishkumar, K. Jeevaratnam, Molecular characterization of antimicrobial *Lactobacillus* isolates and evaluation of their probiotic characteristics *in vitro* for use in poultry, Food Biotechnol. 31 (2017) 20–41.

[110] X.X. Zhang, Y. Wang, L. Liu, Y. Wei, N. Shang, X.X. Zhang, et al., Two-peptide bacteriocin PlnEF causes cell membrane damage to Lactobacillus plantarum, Biochim. Biophys. Acta - Biomembr. 1858 (2016) 274–280.

[111] M. Schiffer, A.B. Edmundson, Use of Helical Wheels to Represent the Structures of Proteins and to Identify Segments with Helical Potential, Biophys. J. 7 (1967) 121–135.

[112] N. Fimland, P. Rogne, G. Fimland, J. Nissen-Meyer, P.E. Kristiansen, Three-dimensional structure of the two peptides that constitute the two-peptide bacteriocin plantaricin EF, Biochim. Biophys. Acta - Proteins Proteomics. 1784 (2008) 1711–1719.

[113] S. Bobone, G. Bocchinfuso, Y. Park, A. Palleschi, K.-S. Hahm, L. Stella, The importance of being kinked: role of Pro residues in the selectivity of the helical antimicrobial peptide P5., J. Pept. Sci. 19 (2013) 758–69.

[114] H.H. Hauge, J. Nissen-Meyer, I.F. Nes, V.G. Eijsink, Amphiphilic alpha-helices are important structural motifs in the alpha and beta peptides that constitute the bacteriocin lactococcin G--enhancement of helix formation upon alpha-beta interaction., Eur. J. Biochem. 251 (1998) 565–72.

[115] J.C. Phillips, R. Braun, W. Wang, J. Gumbart, E. Tajkhorshid, E. Villa, et al., Scalable molecular dynamics with NAMD, J. Comput. Chem. 26 (2005) 1781–1802.

[116] J.B. Klauda, R.M. Venable, J.A. Freites, J.W. O'Connor, D.J. Tobias, C. Mondragon-Ramirez, et al., Update of the CHARMM All-Atom Additive Force Field for Lipids: Validation on Six Lipid Types, J. Phys. Chem. B. 114 (2010) 7830–7843.

[117] W. Humphrey, A. Dalke, K. Schulten, VMD - Visual Molecular Dynamics, J. Molec. Graph. 14 (1996) 33–38.

[118] W.Z. Pierce BG, Wiehe K, Hwang H, Kim BH, Chen R, Zheng Y, ZDOCK Server: Docking and Visualization of Protein Complexes and Multimers., (In Prep. (n.d.).

[119] X. Cheng, S. Jo, H.S. Lee, J.B. Klauda, W. Im, CHARMM-GUI micelle builder for pure/mixed micelle and protein/micelle complex systems, J. Chem. Inf. Model. 53 (2013) 2171–2180.

[120] M.K. B. R. Brooks, C. L. Brooks III, A. D. Mackerell, L. Nilsson, R. J. Petrella, B. Roux, Y. Won, G. Archontis, C. Bartels, S. Boresch A. Caflisch, L. Caves, Q. Cui, A. R. Dinner, M. Feig, S. Fischer, J. Gao, M. Hodoscek, W. Im, K. Kuczera, T. Lazaridis, J. M, CHARMM: The Biomolecular simulation Program, J. Comp. Chem. 30 (2009) 1545–1615.

[121] D. Frishman, P. Argos, Knowledge-based protein secondary structure assignment., Proteins. 23 (1995) 566–79.

[122] J.J. Lopez Cascales, A. Garro, R.D. Porasso, R.D. Enriz, The dynamic action mechanism of small cationic antimicrobial peptides., Phys. Chem. Chem. Phys. 16 (2014) 21694–705.

[123] R.M. Epand, H.J. Vogel, Diversity of antimicrobial peptides and their mechanisms of action., Biochim. Biophys. Acta. 1462 (1999) 11–28.

[124] Y. Shai, Mode of action of membrane active antimicrobial peptides., Biopolymers. 66 (2002) 236–48.

[125] D.S. Bolintineanu, Y.N. Kaznessis, Computational studies of protegrin antimicrobial

peptides: a review., Peptides. 32 (2011) 188–201.

[126] M.A. McCloskey, M.M. Poo, Rates of membrane-associated reactions: reduction of dimensionality revisited., J. Cell Biol. 102 (1986) 88–96.

[127] R.M. Epand, R.F. Epand, Lipid domains in bacterial membranes and the action of antimicrobial agents, Biochim. Biophys. Acta - Biomembr. 1788 (2009) 289–294.

[128] D.P. Tieleman, S.J. Marrink, H.J. Berendsen, A computer perspective of membranes: molecular dynamics studies of lipid bilayer systems., Biochim. Biophys. Acta. 1331 (1997) 235–70.

[129] J. Nissen-Meyer, H. Holo, L.S. Håvarstein, K. Sletten, I.F. Nes, A novel lactococcal bacteriocin whose activity depends on the complementary action of two peptides., J. Bacteriol. 174 (1992) 5686–92.

[130] K. Sikic, S. Tomic, O. Carugo, Systematic comparison of crystal and NMR protein structures deposited in the protein data bank., Open Biochem. J. 4 (2010) 83–95.

[131] C. Nick Pace, J. Martin Scholtz, A Helix Propensity Scale Based on Experimental Studies of Peptides and Proteins, Biophys. J. 75 (1998) 422–427.

[132] S. Yohannan, S. Faham, D. Yang, J.P. Whitelegge, J.U. Bowie, The evolution of transmembrane helix kinks and the structural diversity of G protein-coupled receptors., Proc. Natl. Acad. Sci. U. S. A. 101 (2004) 959–63.

[133] X. Deupi, M. Olivella, C. Govaerts, J.A. Ballesteros, M. Campillo, L. Pardo, Ser and Thr residues modulate the conformation of pro-kinked transmembrane alpha-helices., Biophys. J. 86 (2004) 105–15.

[134] M. Weber, L. Tome, D. Otzen, D. Schneider, A Ser residue influences the structure and stability of a Pro-kinked transmembrane helix dimer., Biochim. Biophys. Acta. 1818 (2012) 2103–7.

[135] J.A. Ballesteros, X. Deupi, M. Olivella, E.E. Haaksma, L. Pardo, Serine and threonine residues bend alpha-helices in the chi(1) = g(-) conformation., Biophys. J. 79 (2000) 2754–60.

[136] J. Li, M. Garg, D. Shah, R. Rajagopalan, Solubilization of aromatic and hydrophobic moieties by arginine in aqueous solutions., J. Chem. Phys. 133 (2010) 54902.

[137] N. Schmidt, A. Mishra, G.H. Lai, G.C.L. Wong, Arginine-rich cell-penetrating peptides., FEBS Lett. 584 (2010) 1806–13.

[138] K. Knoblich, S. Park, M. Lutfi, L. van 't Hag, C.E. Conn, S.A. Seabrook, et al., Transmembrane Complexes of DAP12 Crystallized in Lipid Membranes Provide Insights into Control of Oligomerization in Immunoreceptor Assembly., Cell Rep. 11 (2015) 1184–1192.

[139] L. Carlier, P. Joanne, L. Khemtémourian, C. Lacombe, P. Nicolas, C. El Amri, et al., Investigating the role of GXXXG motifs in helical folding and self-association of plasticins, Gly/Leu-rich antimicrobial peptides., Biophys. Chem. 196 (2015) 40–52.

[140] G.N. Moll, E. van den Akker, H.H. Hauge, J. Nissen-Meyer, I.F. Nes, W.N. Konings, et al., Complementary and overlapping selectivity of the two-peptide bacteriocins plantaricin EF and JK., J. Bacteriol. 181 (1999) 4848–52.

[141] P. Güntert, C. Mumenthaler, K. Wüthrich, Torsion angle dynamics for NMR structure calculation with the new program Dyana, J. Mol. Biol. 273 (1997) 283–298.

[142] J.B. Klauda, R.M. Venable, J.A. Freites, J.W. O'Connor, D.J. Tobias, C. Mondragon-Ramirez, et al., Update of the CHARMM All-Atom Additive Force Field for Lipids:

Validation on Six Lipid Types, J. Phys. Chem. B. 114 (2010) 7830–7843.

[143] L. Adamian, J. Liang, Interhelical hydrogen bonds and spatial motifs in membrane proteins: polar clamps and serine zippers., Proteins. 47 (2002) 209–18.

[144] K.M. Sanchez, G. Kang, B. Wu, J.E. Kim, Tryptophan-Lipid Interactions in Membrane Protein Folding Probed by Ultraviolet Resonance Raman and Fluorescence Spectroscopy, Biophys. J. 100 (2011) 2121–2130.

[145] N.A. Berglund, T.J. Piggot, D. Jefferies, R.B. Sessions, P.J. Bond, S. Khalid, Interaction of the Antimicrobial Peptide Polymyxin B1 with Both Membranes of E. coli: A Molecular Dynamics Study, PLOS Comput. Biol. 11 (2015) e1004180.

[146] J. Li, S. Liu, R. Lakshminarayanan, Y. Bai, K. Pervushin, C. Verma, et al., Molecular simulations suggest how a branched antimicrobial peptide perturbs a bacterial membrane and enhances permeability, Biochim. Biophys. Acta - Biomembr. 1828 (2013) 1112–1121.

[147] Y. Wang, D.E. Schlamadinger, J.E. Kim, J.A. McCammon, Comparative molecular dynamics simulations of the antimicrobial peptide CM15 in model lipid bilayers., 1818 (2012).

[148] Y. Wang, T. Zhao, D. Wei, E. Strandberg, A.S. Ulrich, J.P. Ulmschneider, How reliable are molecular dynamics simulations of membrane active antimicrobial peptides?, Biochim. Biophys. Acta - Biomembr. 1838 (2014) 2280–2288.

[149] P.D. Cotter, An “Upp”-turn in bacteriocin receptor identification, Mol. Microbiol. 92 (2014) 1159–1163.

[150] K. Egan, D. Field, M.C. Rea, R.P. Ross, C. Hill, P.D. Cotter, Bacteriocins: Novel solutions to age old spore-related problems?, Front. Microbiol. 7 (2016) 461.

[151] V.L. Cruz, J. Ramos, M.N. Melo, J. Martinez-Salazar, Bacteriocin AS-48 binding to model membranes and pore formation as revealed by coarse-grained simulations, Biochim. Biophys. Acta - Biomembr. 1828 (2013) 2524–2531.

[152] N. Fimland, P. Rogne, G. Fimland, J. Nissen-Meyer, P.E. Kristiansen, Three-dimensional structure of the two peptides that constitute the two-peptide bacteriocin plantaricin EF, Biochim. Biophys. Acta - Proteins Proteomics. 1784 (2008) 1711–1719.

[153] N.M. Glykos, Software News and Updates Carma: A Molecular Dynamics Analysis Program, J Comput Chem. 27 (2006) 1765–1768.

[154] R. Guixa-Gonzalez, I. Rodriguez-Espigares, J.M. Ramirez-Anguita, P. Carrio-Gaspar, H. Martinez-Seara, T. Giorgino, et al., MEMBPLUGIN: studying membrane complexity in VMD, Bioinformatics. 30 (2014) 1478–1480.

[155] D. Sengupta, H. Leontiadou, A.E. Mark, S.-J. Marrink, Toroidal pores formed by antimicrobial peptides show significant disorder, Biochim. Biophys. Acta - Biomembr. 1778 (2008) 2308–2317.

[156] J.L. Adelman, Y. Sheng, S. Choe, J. Abramson, E.M. Wright, J.M. Rosenberg, et al., Structural determinants of water permeation through the sodium-galactose transporter vSGLT., Biophys. J. 106 (2014) 1280–9.

[157] G. Kleiger, R. Grothe, P. Mallick, D. Eisenberg, GXXXG and AXXXA: Common R-Helical Interaction Motifs in Proteins, Particularly in Extremophiles, (n.d.).

[158] M.G. Teese, D. Langosch, Role of GxxxG Motifs in Transmembrane Domain Interactions, Biochemistry. 54 (2015) 5125–5135.

[159] J.U. Bowie, Understanding membrane protein structure by design, Nat. Struct. Biol. 7 (2000) 91–94.

[160] H. Mohammadiarani, H. Vashisth, All-Atom Structural Models of the Transmembrane Domains of Insulin and Type 1 Insulin-Like Growth Factor Receptors., Front. Endocrinol. (Lausanne). 7 (2016) 68.

[161] Y. Wang, P. Barth, Evolutionary-guided de novo structure prediction of self-associated transmembrane helical proteins with near-atomic accuracy., Nat. Commun. 6 (2015) 7196.

[162] N. Flinner, E. Schleiff, Dynamics of the Glycophorin A Dimer in Membranes of Native-Like Composition Uncovered by Coarse-Grained Molecular Dynamics Simulations., PLoS One. 10 (2015) e0133999.

[163] M. Chavent, A.P. Chetwynd, P.J. Stansfeld, M.S.P. Sansom, Dimerization of the EphA1 Receptor Tyrosine Kinase Transmembrane Domain: Insights into the Mechanism of Receptor Activation, Biochemistry. 53 (2014) 6641–6652.

[164] M. Nishizawa, K. Nishizawa, Potential of mean force analysis of the self-association of leucine-rich transmembrane α-helices: Difference between atomistic and coarse-grained simulations, J. Chem. Phys. 141 (2014) 75101.

[165] E. Psachoulia, D.P. Marshall, M.S.P. Sansom, Molecular Dynamics Simulations of the Dimerization of Transmembrane α-Helices, Acc. Chem. Res. 43 (2010) 388–396.

[166] S.J. Marrink, D.P. Tieleman, Perspective on the Martini model, Chem. Soc. Rev. 42 (2013) 6801.

[167] T.E. Decoursey, Voltage-Gated Proton Channels and Other Proton Transfer Pathways, Physiol. Rev. 83 (2003).

[168] E. V Bocharov, Y.E. Pustovalova, K. V Pavlov, P.E. Volynsky, M. V Goncharuk, Y.S. Ermolyuk, et al., Unique dimeric structure of BNip3 transmembrane domain suggests membrane permeabilization as a cell death trigger., J. Biol. Chem. 282 (2007) 16256–66.

[169] J.R. Herrmann, A. Fuchs, J.C. Panitz, T. Eckert, S. Unterreitmeier, D. Frishman, et al., Ionic Interactions Promote Transmembrane Helix–Helix Association Depending on Sequence Context, J. Mol. Biol. 396 (2010) 452–461.

[170] D. Langosch, J.R. Herrmann, S. Unterreitmeier, A. Fuchs, Helix-helix interaction patterns in membrane proteins, in: Struct. Bioinforma. Membr. Proteins, Springer Vienna, Vienna, 2010: pp. 165–186.

[171] K.E. Norman, H. Nymeyer, Indole localization in lipid membranes revealed by molecular simulation., Biophys. J. 91 (2006) 2046–54.

[172] C.-Y. Lee, A possible biological role of the electron transfer between tyrosine and tryptophan, FEBS Lett. 299 (1992) 119–123.

[173] J.K. Williams, Y. Zhang, K. Schmidt-Rohr, M. Hong, pH-Dependent Conformation, Dynamics, and Aromatic Interaction of the Gating Tryptophan Residue of the Influenza M2 Proton Channel from Solid-State NMR, Biophys. J. 104 (2013) 1698–1708.

[174] D.L. Beene, K.L. Price, H.A. Lester, D.A. Dougherty, S.C.R. Lummis, Cellular/Molecular Tyrosine Residues That Control Binding and Gating in the 5-Hydroxytryptamine 3 Receptor Revealed by Unnatural Amino Acid Mutagenesis, (n.d.).

[175] A.A. Langham, A.S. Ahmad, Y.N. Kaznessis, On the nature of antimicrobial activity: a model for protegrin-1 pores., J. Am. Chem. Soc. 130 (2008) 4338–4346.

[176] H. Leontiadou, A. Alan E. Mark, Siewert J. Marrink, Antimicrobial Peptides in Action, (2006).

[177] S.A. Kirsch, R.A. Böckmann, Membrane pore formation in atomistic and coarse-grained simulations, Biochim. Biophys. Acta - Biomembr. 1858 (2016) 2266–2277.

[178] C. Song, C. Weichbrodt, E.S. Salnikov, M. Dynowski, B.O. Forsberg, B. Bechinger, et al., Crystal structure and functional mechanism of a human antimicrobial membrane channel., Proc. Natl. Acad. Sci. U. S. A. 110 (2013) 4586–91.

[179] S.J. Marrink, A.H. de Vries, D.P. Tieleman, Lipids on the move: Simulations of membrane pores, domains, stalks and curves, Biochim. Biophys. Acta - Biomembr. 1788 (2009) 149–168.

[180] A. D. Peter Tieleman*, S.-J. Marrink*, Lipids Out of Equilibrium: Energetics of Desorption and Pore Mediated Flip-Flop, (2006).

[181] Y. Lee, S. Kim, S. Choi, C. Hyeon, Ultraslow Water-Mediated Transmembrane Interactions Regulate the Activation of A2A Adenosine Receptor, Biophys. J. 111 (2016) 1180–1191.

[182] S. Yuan, S. Filipek, K. Palczewski, H. Vogel, G. Groenhof, Activation of G-protein-coupled receptors correlates with the formation of a continuous internal water pathway, Nat. Commun. 5 (2014) 4733.

[183] G.N. Moll, W.N. Konings, A.J.M. Driessen, Bacteriocins: mechanism of membrane insertion and pore formation, Antonie Van Leeuwenhoek. 76 (1999) 185–198.

[184] M. Kjos, Z. Salehian, I.F. Nes, D.B. Diep, An extracellular loop of the mannose phosphotransferase system component IIC is responsible for specific targeting by class IIa bacteriocins, J. Bacteriol. 192 (2010) 5906–5913.

[185] J. Koehler Leman, M.B. Ulmschneider, J.J. Gray, Computational modeling of membrane proteins, Proteins Struct. Funct. Bioinforma. 83 (2015) 1–24.

[186] S. Kelm, J. Shi, C.M. Deane, MEDELLER: homology-based coordinate generation for membrane proteins., Bioinformatics. 26 (2010) 2833–40.

[187] J. Koehler Leman, B.K. Mueller, J.J. Gray, Expanding the toolkit for membrane protein modeling in Rosetta, Bioinformatics. 109 (2016) btw716.

[188] J. Yang, R. Yan, A. Roy, D. Xu, P. J, Y. Zhang, The I-TASSER Suite: Protein structure and function prediction, Nat. Methods. 12 (2015) 7–8.

[189] O. Gajic, M. Kojic, A. Banina, L. Topisirovic, Characterization of natural isolate Lactococcus lactis subsp. lactis BGMN1-5, a strain producing two bacteriocins, cell wall-associated proteinase and showing, Arch. Biol. (1999).

[190] M. Miljkovic, G. Uzelac, N. Mirkovic, G. Devescovi, D.B. Diep, V. Venturi, et al., LsbB Bacteriocin Interacts with the Third Transmembrane Domain of the YvjB Receptor, Appl. Environ. Microbiol. 82 (2016) 5364–5374.

[191] Y. Zhang, J. Skolnick, Z. Feng, G. Gilliland, T. Bhat, H. Weissig, et al., I-TASSER server for protein 3D structure prediction, BMC Bioinforma. 2008 91. 59 (2008) 305–309.

[192] L. Feng, H. Yan, Z. Wu, N. Yan, Z. Wang, P.D. Jeffrey, et al., Structure of a site-2 protease family intramembrane metalloprotease., Science. 318 (2007) 1608–12.

[193] P.J. Stansfeld, J.E. Goose, M. Caffrey, E.P. Carpenter, J.L. Parker, S. Newstead, et al., MemProtMD: Automated Insertion of Membrane Protein Structures into Explicit Lipid Membranes, Structure. 23 (2015) 1350–1361.

[194] L. Kroos, Y. Akiyama, Biochemical and structural insights into intramembrane metalloprotease mechanisms, Biochim. Biophys. Acta - Biomembr. 1828 (2013) 2873–2885.

[195] E. Roberts, J. Eargle, D. Wright, Z. Luthey-Schulten, MultiSeq: unifying sequence and structure data for evolutionary analysis., BMC Bioinformatics. 7 (2006) 382.

[196] M.A. Lomize, I.D. Pogozheva, H. Joo, H.I. Mosberg, A.L. Lomize, OPM database and PPM web server: resources for positioning of proteins in membranes, Nucleic Acids Res. 40 (2012) D370–D376.

[197] L. Axelsson, A. Holck, The genes involved in production of and immunity to sakacin A, a bacteriocin from Lactobacillus sake Lb706., J. Bacteriol. 177 (1995) 2125–37.

[198] L. Axelsson, T. Katla, M. Bjørnslett, V.G. Eijsink, A. Holck, A system for heterologous expression of bacteriocins in Lactobacillus sake., FEMS Microbiol. Lett. 168 (1998) 137–43.

[199] S.N. Ho, H.D. Hunt, R.M. Horton, J.K. Pullen, L.R. Pease, Site-directed mutagenesis by overlap extension using the polymerase chain reaction., Gene. 77 (1989) 51–9.

[200] L. Edebo, A new press for the disruption of micro-organisms and other cells, J. Biochem. Microbiol. Technol. Eng. 2 (1960) 453–479.

[201] K.W. Miller, R. Schamber, Y. Chen, B. Ray, Production of active chimeric pediocin AcH in Escherichia coli in the absence of processing and secretion genes from the Pediococcus pap operon., Appl. Environ. Microbiol. 64 (1998) 14–20.

[202] C. Oppegård, P. Rogne, L. Emanuelsen, P.E. Kristiansen, G. Fimland, J. Nissen-Meyer, The Two-Peptide Class II Bacteriocins: Structure, Production, and Mode of Action, J. Mol. Microbiol. Biotechnol. 13 (2007) 210–219.

[203] W.-M. Yau, W.C. Wimley, K. Gawrisch, S.H. White, The Preference of Tryptophan for Membrane Interfaces †, Biochemistry. 37 (1998) 14713–14718.

[204] G. Fimland, V.G.H. Eijsink, J. Nissen-Meyer, Mutational analysis of the role of tryptophan residues in an antimicrobial peptide., Biochemistry. 41 (2002) 9508–15.

Appendix

A. Experimental material and methods related to Chapter 3

Peptide mutants with purity equal to or higher than 80% were purchased from GenScript. The peptides were dissolved in sterile dH2O containing 40% isopropanol. The absorption was measured spectrophotometrically at 280 nm and the concentration was determined based on the molar extinction coefficients of the amino acids Tyr and Trp (PlnE, ε_{280} = 1,200 M^{-1} cm^{-1} and PlnF, ε_{280} = 11,320 M^{-1} cm^{-1}).

The indicator strains used were *Lactobacillus curvatus* LTH1174, *Pediococcus pentosaceus* NCDO 990 and *Pediococcus acidilactici* NCDO 521. All strains were grown over night at 30 °C in MRS medium without agitation. The overnight cultures were diluted 1:50 and applied to microtiter plates containing MRS medium to a final volume of 200 µl together with wild type peptides in combination with its complementary mutated variants in a 1:1 molar ratio. The concentration of the peptide combinations was twofold dilution going from one well to the next. The microtiter plates were incubated for 5 hours at 30 ºC. The growth of the indicator cells was measured spectrophotometrically at 600 nm by use of a Sunrise™ Remote microplate reader (Tecan).

The minimum inhibitory concentration (MIC) value was defined as the total amount of peptide mutants together with the complementary wild type peptide that inhibited the growth of the indicator strain by 50%. The relative MIC value was quantitated in terms of fold increase or decrease in activity compared to the wild type combination.

B. Experimental material and methods related to Chapter 4

B.1 Bacterial strains and growth conditions

Lactobacillus plantarum C11 was grown overnight at 30 °C without agitation in de Man-Rogosa-Sharpe (MRS) medium (Oxoid). *Escherichia coli* DH5α and BL21(DE3) cells were used for plasmid amplification and production of fusion polypeptides, respectively. The cells were grown at 37 °C in Lysogeny Broth (LB) medium in baffled flasks with vigorous agitation. The medium contained either 150 µg/ml erythromycin for selection of the plasmids pPlnE100/pPlnF100 or 100 µg/ml ampicillin for selection of pET22b(+) and pGEM®-T Easy Vector derivatives. For growth of *E. coli* DH5α on agar plates, the LB medium was solidified with 1.5% (w/v) agar.

Lactobacillus sakei Lb790, containing pSAK20 and either pPlnE100 or pPlnF100, was used for production of, respectively, PlnE or PlnF and their mutated variants. The plasmids pSAK20 and pPlnE100/pPlnF100 contain a marker for chloramphenicol and erythromycin resistance, respectively, and the cells were consequently grown (30 °C without agitation) in MRS medium containing 10 µg/ml of each antibiotic.

The indicator strains used in the bacteriocin activity assays were *Lactobacillus viridescens* NCDO 1655, *Lactobacillus curvatus* LTH 1174, *Pediococcus pentosaceus* NCDO 990 and *Pediococcus acidilactici* NCDO 521. All strains were grown at 30 °C in MRS medium without agitation.

B.2 DNA isolation

Genomic DNA from *L. plantarum* C11 was isolated using the QIAGEN DNeasy® Tissue Kit according to protocol. Plasmids were isolated from *E. coli* DH5α cells using the Macherey-Nagel NucleoSpin® Plasmid Kit.

B.3 A two-plasmid expression system for production of bacteriocins

A two-plasmid expression system [197,198] consisting of pSAK20 and the pLPV111-derived plasmids pPlnE100 or pPlnF100 was used to produce wild type and mutant variants of PlnE and PlnF. The two plasmids were introduced into the bacteriocin deficient strain *L. sakei* Lb790. pSAK20 contains the *orf4-sapKRTE* operon needed for activation of the sakacin A promoter and processing and export of the bacteriocin [197,198]. pPlnE100 and pPlnF100 contain the genes encoding PlnE or PlnF, respectively, and PlnI (the plantaricin EF immunity protein) and the genes are placed under the control of the sakacin A promoter. The *plnE*- and *plnF*-genes are fused to the sakacin P leader sequence. Previous studies have demonstrated that the sakacin A secretion machinery encoded in pSAK20 recognizes both the sakacin A and sakacin P leader peptides equally efficient [198].

For construction of the pPlnF100 plasmid, the plasmid pLT100α (a pLPV111-derivate used for expression of lactococcin Gα [69]) was used as a template for amplification of the sakacin A promoter region and the sakacin P leader sequence using the primers PlnFA and SakPB. The resulting PCR product (Megaprimer 1F) contains the restriction site for *Mlu*I, the sakacin A promoter, the sakacin P leader sequence as well as a tail complementary to the beginning of the *plnF*-gene. In the following PCR reaction, genomic DNA from *L. plantarum* C11 was used as template to amplify the *plnF*- and

plnI-genes using the primers PlnEFimm and Megaprimer 1F. The PCR product (flanked by restriction sites for *Mlu*I and *Cla*I) was sub-cloned into the pGEM®-T Easy Vector due to incomplete restriction digestion and the restriction site for *Cla*I was changed into an *Xba*I restriction site by use of the QuikChange site-directed mutagenesis method and the primers PlnEFXbaIF and PlnEFXbaIR. The fragment was subsequently cloned into the *Mlu*I and *Xba*I sites of pLPV111, resulting in pPlnF100.

The pPlnE100 plasmid was constructed in a similar manner. Primers PlnEC and Megaprimer 1E (containing the sakacin A promoter, the sakacin P leader sequence and the beginning of *plnE*) were used to amplify the *plnE*-gene. The resulting PCR-product (Fragment 1) also contains the beginning of *plnI*. The *plnI*-gene and the end of the *plnE*-gene were amplified in a separate PCR reaction using primers PlnEFimmstart and PlnEFimm (Fragment 2). Fragment 1 and Fragment 2 were spliced by PCRSOEing [199]. The spliced PCR product was amplified by adding the two external primers PlnEFimm and SakPB. The final PCR product consists of the entire *plnI*-gene, the *plnE*-gene fused to the leader sequence of sakacin P and the sakacin A promoter region, flanked by the restriction sites *Mlu*I and *Cla*I. The PCR product was sub-cloned into the pGEM®-T Easy Vector due to incomplete restriction digestion. Finally, the fragment was cloned into the *Mlu*I and *Cla*I sites of pLPV111 resulting in pPlnE100.

B.4 Preparation of competent cells and cell transformation

E. coli cells were made competent by the CaCl2-method (protocol II), basically as described by Sambrook et al. 30 The plasmids were introduced into *E. coli* DH5α cells according to the QuikChange® site-directed mutagenesis protocol. Preparation of competent *L. sakei* Lb790/pSAK20 cells and transformation were performed as previously described by Aukrust *et al.* (procedure 2) [199].

B.5 Site-directed mutagenesis and DNA sequencing

In order to introduce point mutations in plnE and plnF, Quik Change site-directed mutagenesis was performed according to manufacturer's protocol.

The DNA sequences of all the mutated plasmids were verified by DNA sequencing using an ABI PRISM® 3730 DNA Analyzer and a BigDye® Terminator v3.1 Cycle Sequencing Kit.

Production and purification of peptides

The two-plasmid expression system described above was used for the production of wild type and mutant variants of PlnE and PlnF.

The peptides were purified from 1 L overnight cultures, basically as previously described. 33 The overnight cultures were applied directly to a cation exchange column equilibrated with 20 mM phosphate buffer (pH 6). The column was washed with 100 ml of the phosphate buffer before the peptides were eluted in 40 ml of 20 mM phosphate buffer (pH 6) containing 1 M NaCl and 20% (v/v) 2-propanol. The eluate was sterile-filtrated through a 0.20 µm non-pyrogenic sterile filter (Sarstedt) and subsequently diluted four-fold with H2O/0.1% (v/v) trifluoroacetic acid (TFA) and applied to a reverse phase column (3 ml RESOURCETM RPC, GE Healthcare). The peptides were eluted with a linear 2-propanol-gradient containing 0.1% TFA. The absorbance at 280 and 214 nm was recorded as a function of ml eluent. The molecular masses of the peptide variants were confirmed by MALDI-TOF mass spectrometry at the MS/Proteomics Core Facility at the Department of Chemistry, Biotechnology and Food Science, Norwegian University of Life Sciences. Due to the relatively weak absorbance at 280 nm (only one Tyr residue in the PlnE-peptide), the relative amount of peptides added to the bacteriocin activity measurements was estimated based on the absorbance peak at 214 nm obtained after purifying the peptides on a reverse phase column.

Some mutant peptides were ordered synthetically from GenScript. The synthetic peptides were ordered with a purity of >80 % and dissolved in 40% 2-propanol upon arrival. The absorption was measured spectrophotometrically at 280 nm and the concentration was estimated based on the molar extinction coefficients of the amino acids Tyr (ε280 = 1200 M^{-1} cm^{-1}) and Trp (ε280 = 5560 M^{-1} cm^{-1}).

B.6 Construction, production and purification of the PlnE and PlnF fusion polypeptides

Synthetic genes (from GenScript) encoding PlnE or PlnF fused to a hexahistidine (His6)-tag, the immunoglobulin-binding domain of streptococcal protein G (GB1-domain; 56 aa) and a non-helical linker of five consecutive Gly residues between the GB1-domain and the sequence encoding either of the two peptides were cloned into the *Nde*I and *Bam*HI sites of pET-22b(+). The fusion polypeptides were designed in such a way that the fusion-partner was either fused to the N- or C-terminus of the peptides. This

resulted in four different vectors. Cloning into pET-22b(+) was performed by GenScript.

The vectors were introduced into competent E. coli BL21 (DE3) cells from Invitrogen. Expression of the fusion polypeptides was induced with 1 mM isopropyl β-D-1-thiogalactopyranoside (IPTG) when the OD600 of the cell culture had reached approximately 1. The culture was then grown overnight at 250 rpm and 25 °C. Approximately 20 g of cells were harvested by centrifugation, frozen and lysed using an X-press [200]. The lysed cells were dissolved in 100 ml of 50 mM phosphate buffer, pH 7.4, containing a cocktail of protease inhibitors (cOmplete ULTRA Tablets, EDTA-free; Roche). DNA was removed from the solution with 2% streptomycin sulfate and the proteins were precipitated with ammonium sulfate (0.33 g/L). The pellet was dissolved in 20 mM phosphate buffer, pH 7.4, and desalted using a 5 ml Hi Trap Desalting column (GE Healthcare) using the ÄKTA chromatography system (GE Healthcare). NaCl and imidazole were added to the eluate to final concentrations of 0.5 M and 20 mM, respectively. The solution was applied to a 5 ml HisTrap HP column (GE Healthcare) equilibrated with 20 mM phosphate buffer (pH 7.4), 0.5 M NaCl and 20 mM imidazole. The fusion polypeptides were eluted using a linear gradient of 20 mM phosphate buffer, pH 7.4, 0.5 M NaCl and 0.5 M imidazole. Buffer exchange to 50 mM phosphate buffer, pH 7.4, and concentration of the fusion polypeptides were performed using Amicon Ultra-15 Centrifugal Filter Units with a molecular mass cut-off at 3 kDa (Millipore), at 4 °C. The correct molecular masses of the fusion polypeptides were confirmed by mass spectrometry at the Proteomics Facility at the Department of Biosciences, University of Oslo. The fusion polypeptides were digested with trypsin and the resulting peptide fragments were analyzed by high performance liquid chromatography-tandem mass spectrometry (HPLC-MS/MS).

The concentration of the fusion polypeptides was determined by UV absorption at 280 nm and calculated using molar extinction coefficients based on the Trp and Tyr residues. The extinction coefficients for the PlnE and PlnF fusion polypeptides were calculated to be 11,560 M^{-1} cm^{-1} and 18,320 M^{-1} cm^{-1}, respectively.

B.7 Bacteriocin activity assay

For detection of antimicrobial activity of the wild type and mutant variants of PlnE and PlnF as well as the fusion polypeptides, a microtiter plate assay system was used, essentially as described by Nissen-Meyer *et al.* [129]. Each well of the microtiter plate

contained MRS medium to a final volume of 200 µl, combinations of wild type and mutated variants of PlnE and PlnF (in 1:1 ratio), and one of the four indicator strains. The fusion polypeptides were added at a 10:1 molar ratio with respect to the concentration of the complementary wild type peptide. The dilution factor of the peptide combinations was two-fold going from one well to the next. Stationary phase cultures of indicator strains were diluted 1:50 and the microtiter plates were incubated for 5 hours at 30 °C. The growth of the indicator cells was measured spectrophotometrically at 600 nm by use of a Sunrise™ Remote microplate reader (Tecan).

The minimum inhibitory concentration (MIC) was defined as the total amount of wild type or peptide mutants of PlnE and PlnF, at a 1:1 ratio, that inhibited the growth of the indicator strain by 50%. The relative MIC value was quantitated in terms of fold increase or decrease in activity compared to the wild type combination.

C. Experimental results related to Chapter 4

The first set of experiments involved mutation of the Gly and Ser residues that are located in possible GxxxG and GxxxG-like motifs to evaluate which of these motifs are essential for the bactericidal activity of PlnEF. The residues were mutated into different small amino acids (Ala, Gly, Ser), large hydrophobic amino acids (Ile and/or Leu), or hydrophilic amino acids (Gln, Lys). Altogether, 39 and 26 mutated variants of PlnE and PlnF, respectively, were assayed against the indicator strain, *L. curvatus* LTH1174. The activity of the bacteriocins that contain single point mutations was compared with the wild-type PlnEF, and the results are shown as relative MIC values in Figure C-1. The activities of the peptides were tested against three more different strains [103]. Overall, the relative MIC values for all four strains were comparable, but the effects of mutations on relative MIC values are overall greater when using *L. curvatus* LTH1174 because of its higher sensitivity to wild-type Plantaricin EF.

C.1 The GxxxG and GxxxG-like motifs in PlnE

The effect the mutations had on the antimicrobial activity varied considerably between the two GxxxG motifs in PlnE; nearly all replacements of the glycine residues in the G_5xxxG_9 motif were detrimental, while nearly all similar replacements in the $G_{20}xxxG_{24}$ motif were tolerated.

Figure C-1: Relative MIC of the peptides with single-point mutations at the GxxxG and GxxxG-like motifs

The relative MIC values from activity measurements of four independent parallels of GxxxG and GxxxG-like mutant peptides together with the wild-type complementary peptide against the indicator strain L. *curvatus* LTH 1174. The activity is as good as or better than the wild-type peptide combination when the number is equal to or less than 1, respectively. Green illustrates mutant peptides with low or no reduction in activity compared to the wild-type bacteriocin. Red illustrates peptides where the mutation had a highly detrimental effect on activity (e.g. a value of 30 means a 30-fold reduction in activity).

The only mutations that were tolerated in the G_5xxxG_9 motif were the G5A and G5S mutations, as almost all activity was retained with these replacements (Figure C-1). In contrast, replacing this glycine residue with large hydrophilic (G5K and G5Q) or hydrophobic (G5I and G5L) residues reduced the activity 10 to 200-fold. Replacement of the other glycine residue, Gly9, in the G_5xxxG_9 motif was not tolerated at all. Even replacements with small residues (G9A and G9S) caused a 30 to 200-fold reduction in the activity, while replacements with large hydrophilic (G9Q and G9K) or hydrophobic (G9I and G9L) residues reduced the activity 100- to 1000-fold. This indicates that these two Gly residues are in a structurally restricted environment, possibly needed for close interhelical contact with the complementary peptide.

In contrast, the glycine residues in the $G_{20}xxxG_{24}$ motif in PlnE tolerated nearly all substituents quite well. Individual replacements of these glycine residues with small (Ala

and Ser) and large hydrophobic (Ile and Leu) and hydrophilic (Gln) residues resulted in similar or somewhat higher activity than the wild-type combination (Figure C-1). Introducing a positive charge at positions 20 and 24 was, however, detrimental. The G20K and G24K mutations resulted in approximately a 50-fold reduction in activity. These results indicate that Gly20 and Gly24 (in contrast to Gly5 and Gly9) are not in a structurally restricted environment, nor in a strictly hydrophobic or hydrophilic environment, and that the $G_{20}xxxG_{24}$ region is not in close interhelical contact with the complementary peptide.

The same tendency is also seen for the two GxxxG-like motifs, $A_{23}xxxG_{27}$ and $G_{27}xxxS_{31}$. Substituting the small residues with other amino acids such as small large hydrophilic or large hydrophobic residues did not seem to greatly affect the antimicrobial activity (Figure C-1).

Except for the A21S mutation, which was well tolerated, all replacements of the two alanine residues in the GxxxG-like motif $A_{17}xxxA_{21}$ in PlnF were unfavorable. Even replacements with a small glycine residue were detrimental, as the A17G and A21G mutations reduced the activity 30-to-60-fold and 15-to-30-fold, respectively (Figure C-1). Notably, replacing these alanine residues with a large hydrophobic residue (Leu) was somewhat less detrimental than replacement with a glycine residue, as the A17L and A21L mutations reduced the activity only 10-to-30-fold. Replacements with a large hydrophilic residue were more detrimental than replacement with a leucine residue, as the A17K and A21Q mutations reduced the activity 30-to-60-fold and the A17Q and A21K mutations reduced the activity 60-to-130-fold. The fact that replacements with leucine residues were less detrimental than replacements with glycine residues indicate that the $A_{17}xxxA_{21}$ region is not in close interhelical contact with the complementary peptide. However, the detrimental effect of the glycine substitutions does indicate that the increased flexibility induced in the helix is non-beneficiary for the function of the bacteriocin, thus the helix in this region of the peptide is important for function.

The OH-group in Ser26, which is part of the GxxxG-like motif $S_{26}xxxG_{30}$, is apparently involved in hydrogen bonding, since replacement with a threonine residue – which also contains an OH-group – resulted in only a 4-to-15-fold reduction in the activity and was the substitution that was best tolerated (Figure C-1). Replacement of Ser26 with a glycine or alanine residue reduced the activity about 15-to-30-fold, while

replacement with a large hydrophilic (Lys and Gln) or a large hydrophobic residue (Leu) caused, respectively, a 30-to-130-fold and 60-to-250-fold reduction in the activity. A small residue with hydrogen bonding properties seems to be preferred in position 26.

All the replacements of Gly30, which is in both the $S_{26}xxxG_{30}$ and $G_{30}xxxG_{34}$ motifs, were detrimental, indicating that Gly30 is in a structurally-restricted environment. Substituting Gly30 with small residues such as Ala and Ser were the least detrimental replacements, causing a 15-to-30- and 60-to-130-fold reduction in activity, respectively (Figure C-1). The other mutations, G30K, G30Q and G30L were highly detrimental, causing more than a 500-fold reduction in the activity (Figure C-1). The other glycine residue, Gly34, in the $G_{30}xxxG_{34}$ motif was, however, less restricted, as replacement with Ser resulted in wild-type or better than wild-type activity and replacement with Ala and the larger hydrophilic Gln residue reduced the activity 2-to-15-fold (Figure C-1). Replacement with a hydrophobic leucine residue (G34L) and a hydrophilic-charged lysine residue (G34K) reduced the activity, respectively, 10-to-30-fold and 15-to-130-fold (Figure C-1). The greater flexibility of Gly34 in PlnF compared to Ser26 and Gly30 in PlnF and to Gly5 and Gly9 in PlnE is possibly due to the fact that Gly34 is the last residue in PlnF, and this enables the residue to fluctuate to a greater extent than internal residues. The highly-restricted environment of Gly30 suggests that Gly30, as part of the $S_{26}xxxG_{30}$ or $G_{30}xxxG_{34}$ motif in PlnF, might be in close interhelical contact - in either a parallel or antiparallel orientation - with the G_5xxxG_9 motif in PlnE.

C.2 Orientation of Plantaricin EF in Target-Cell Membranes

In order to determine the orientation of PlnE and PlnF in target-cell membranes and whether the two peptides interact in a parallel or anti-parallel manner, we constructed four fusion polypeptides in which the hydrophilic GB1-domain was fused to either the N- or C-terminal ends of PlnE and PlnF. The two fusion polypeptides in which the GB1-domain is attached to the ends of the Pln-peptides that enter into or traverse the target-cell membrane are expected to be inactive. In contrast, the two fusion polypeptides in which the GB1-domain is attached to the ends of the Pln-peptides that do not enter into the hydrophobic part of the membrane may still have some antimicrobial activity. The activity may, however, be greatly reduced compared to the wild type peptides due to possible steric interference by the GB1-domain. The penta-Gly linker between the GB1-domain and the Pln-peptides was included in order to increase the structural flexibility

and thus reduce steric obstructions. The indicator strain, L. *curvatus* LTH 1174, that is most sensitive to plantaricin EF was used when assaying the activity of the four fusion polypeptides. A similar approach has earlier been successfully used to study the orientation in membranes of the class-IIa bacteriocin pediocin PA-1 and the class IIb bacteriocin Lactococcin G [201,202].

The four fusion polypeptides were named according to the side of the peptide to which the GB1-domain was attached; for N-PlnE and N-PlnF the GB1-domain is attached at the N-terminus of PlnE and PlnF, respectively, and for C-PlnE and C-PlnF the GB1-domain is attached at their C-termini. When applied together with the complementary wild-type peptide, PlnF, the C-PlnE fusion polypeptide displayed bacteriocin activity at 0.2 μM concentrations and higher, whereas the N-PlnE fusion polypeptide showed no significant activity even at concentrations up to 20 μM. The N-PlnF fusion polypeptide together with its complementary wild wild-type, PlnE, displayed bacteriocin activity at 10 μM concentrations and higher, whereas the C-PlnF fusion polypeptide showed no significant activity at concentrations up to 20 μM. These results indicate that the C-terminus of PlnE and the N-terminus of PlnF are located on the outer part of the target-cell membrane, and that the two peptides thus interact in an antiparallel manner when integrated in the membrane. The two active fusion polypeptides, C-PlnE and N-PlnF, resulted in greatly reduced activity compared to the wild-type peptides; whereas the latter display activity at nM concentrations, the former were only active at concentrations in the μM range. In view of the possibility for steric interactions between the GB1-domain and either the membrane, the complementary peptide, or (possibly) a transmembrane receptor, this result is not unexpected.

C.3 Effects of aromatic substitutions

It is known that the aromatic residues Tyr and especially Trp prefer to position themselves in the membrane interface and may therefore be important contributors to the anchoring of the peptides in the membrane [144,203,204]. To test the role of these residues, Trp and Tyr were substituted with either a large hydrophobic residue (Leu), a large, positively charged residue (Arg), the hydrophobic aromatic residue Phe, as well as either Trp or Tyr.

Replacement of Tyr at position 6 in PlnE with a Leu or Arg (Y6L and Y6R) resulted in a 15-to-60-fold reduction in activity (Figure C-2). All activity was retained when

substituting Tyr with the aromatic residues Phe and Trp (Y6F and Y6W). The preference for an aromatic residue at this location in PlnE indicates a positioning in the membrane interface, possibly on the inner part of the membrane, since the results obtained with the fusion polypeptides suggests that the C-terminus of PlnE is on the outer part of the membrane.

Figure C-2: The relative MIC values of aromatic substitution

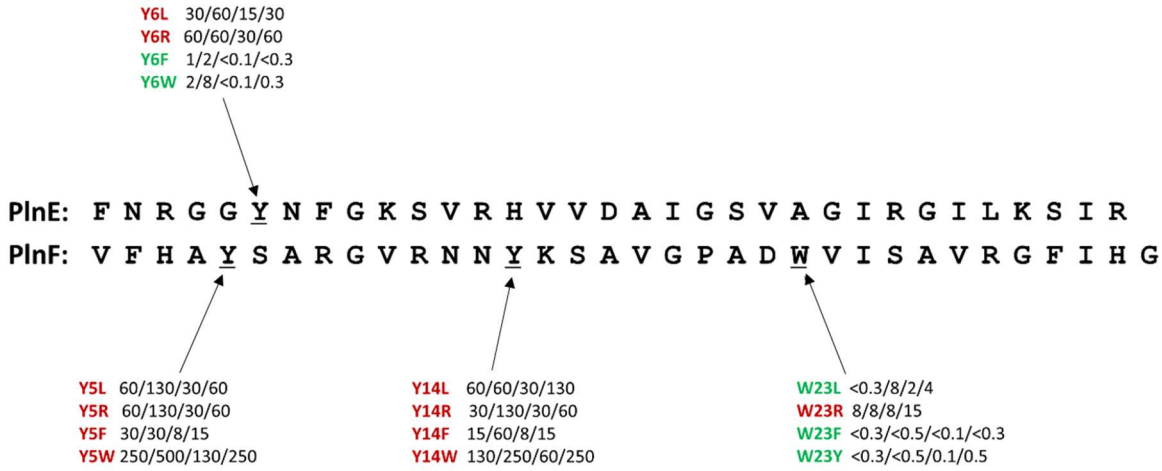

The relative MIC values from activity measurements of aromatic mutant peptides complemented with the wild-type peptide against the indicator strain L. *curvatus* LTH1174. The activity is as good as or better than the wild-type peptide combination when the number is equal to or less than 1, respectively. Green illustrates mutant peptides with low or no reduction in activity compared to the wild-type bacteriocin. Red illustrates peptides where the mutation had a highly detrimental effect on antimicrobial activity.

Substituting the two Tyr residues in PlnF at positions 5 and 14 with either a Leu or an Arg reduced the activity 30-to-130-fold, whereas replacing it with Phe caused a 10-to-50-fold reduction in activity (Figure C-2). Replacing these Tyr residues with a Trp, however, was very detrimental to the activity, reducing it 100-to-300-fold, implicating a spatial restriction on these sites and possibly also hydrogen bonding opportunities mediated by the OH-group of Tyr.

The Trp residue at position 23 in PlnF did not seem to have any specific preferences for an aromatic side chain, since replacing it with either Leu, Phe, or Tyr resulted in equal or better than wild-type activity. The positively charged Arg residue (W23R) resulted in an 8-to-15-fold decrease in activity, suggesting a preference for hydrophobicity and a possible positioning in or near the hydrophobic core of the

membrane.

The Trp residue at position 23 in PlnF did not seem to have any specific preferences for an aromatic side chain since replacing it with either Leu, Phe or Tyr resulted in equal or better than wild type activity. The positively charged Arg residue (W23R) resulted in 8- to 15-fold decrease in activity, suggesting a preference for hydrophobicity and a possible positioning in or near the hydrophobic core of the membrane.